TEMPORAL VARIABILITY IN FLUVIAL DEPOSITION AND THE IMPLICATIONS FOR STATIC RESERVOIR CONNECTIVITY: JOHN HENRY MEMBER, STRAIGHT CLIFFS FORMATION (CRETACEOUS, UTAH)

by

Alexandre Marcel Turner

A thesis submitted to the faculty of
The University of Utah
in partial fulfillment of the requirements for the degree of

Master of Science

In

Geology

Department of Geology and Geophysics

The University of Utah

May 2014

The University of Utah Graduate School

STATEMENT OF THESIS APPROVAL

The thesis of **Alexandre Marcel Turner**

has been approved by the following supervisory committee members:

Lisa Stright	, Chair	**February 19, 2014** Date Approved
Cari Johnson	, Member	**February 19, 2014** Date Approved
Lauren Birgenheier	, Member	**February 19, 2014** Date Approved

and by **John Bartley** , Chair/Dean of

the Department/College/School of **Geology and Geophysics**

and by David B. Kieda, Dean of The Graduate School.

ABSTRACT

Accurately predicting hydrocarbon recovery from fluvial reservoirs is challenging due to uncertainties associated with alluvial architecture. Fluvial deposits exhibit rapid lateral and vertical facies changes that result in discontinuous and disconnected sand bodies. Subsurface interpretations are further limited due to the scarcity and indirect nature of subsurface data. Accurate predictions of alluvial architecture, and thus sand body connectivity, are essential for good reservoir management practices. When used as analogs for subsurface reservoirs, outcrop-based studies can provide useful data for more informed predictions of subsurface fluvial organization. Exposures of the Upper Cretaceous John Henry Member along the flanks of the Kaiparowits Plateau of southern Utah offer an opportunity to study variability in alluvial architecture and address its impact on reservoir connectivity.

A detailed study of the fluvial strata of the John Henry Member was conducted at Bull Canyon (southwestern Kaiparowits Plateau). This study leveraged a wealth of digital outcrop data as well as an integrated paleomorphodynamic workflow that estimates paleochannel morphology and formative paleohydraulic conditions. Outcrop observations and results of the paleomorphodynamic workflow were combined to build 3-D conceptual models of

river system morphology in the John Henry Member. The conceptual models were then used to constrain model input parameters for object-based facies simulation. Static reservoir connectivity at four well configurations was calculated on 30 facies model realizations.

The results of this study show that outcrops of the John Henry Member at Bull Canyon exhibit significant variability in fluvial style over a 180-meter (591-feet) thick interval. The lower John Henry Member (DUs 1, 2, and 3) was influenced by backwater hydraulics at the time of deposition, resulting in a stratigraphic architecture characterized by straight, narrow, and dispersive channel belts. Results of the static reservoir connectivity analysis show that, in 40% of model realizations, reservoir connectivity in at least one unit of the lower John Henry Member is 0%. This implies that backwater hydraulic effects may induce a reservoir dimensionality that negatively impacts static reservoir connectivity. This study highlights the importance of integrating paleomorphodynamic workflows along with more traditional outcrop observations to conceptually characterize fluvial systems and constrain model input parameters.

TABLE OF CONTENTS

APPENDICES

LIST OF FIGURES

INTRODUCTION

It is estimated that hydrocarbons contained in fluvial reservoirs account for 20% of the world's remaining hydrocarbon reserves (Keogh et al., 2007). Maximizing hydrocarbon recovery from fluvial reservoirs is a technical challenge because (1) fluvial deposits exhibit rapid lateral and vertical facies changes (Miall, 1988; Bridge, 2004) and (2) fluvial successions show significant variability in depositional style (North, 1996; Blum and Törnqvist, 2000). Spatial and temporal variations in fluvial architecture govern sand body distribution and control reservoir connectivity and hydrocarbon recovery efficiency (Larue and Yue, 2003; Larue and Friedmann, 2005; Larue and Hovadik, 2006). The Pilong Formation (Pliocene–Pleistocene) in the Malay Basin is an example of a fluvial interval that exhibits wide variability in fluvial style and irregular sand body distribution (Miall, 2002). Shallow seismic time-slices through the Pilong Formation reveal the presence of five types of fluvial styles with highly variable cross-sectional dimensions (30 m to 10 km wide and 3 m to 20 m thick) (98 ft to 6 mi wide and 10 ft to 66 ft thick) in a volume of rock that measures 70 m (230 ft) in thickness and 2,800 km^2 (1,081 mi^2) aerially (Miall, 2002). Unfortunately, the scarcity of well data and the limited resolution of seismic surveys at reservoir depths inhibits our ability to adequately characterize the subsurface reservoir architecture of ancient fluvial successions. For this reason, 3-D studies of

outcrop exposures are invaluable resources to support subsurface reservoir characterization and modeling (Bryant and Flint, 1993; Grammer et al., 2004). A detailed study of the fluvial strata of the John Henry Member (Upper Cretaceous Straight Cliffs Formation) at Bull Canyon is presented here to show how temporal variability in fluvial style can affect reservoir connectivity.

A number of authors have undertaken outcrop-based studies of ancient and modern fluvial strata with the purpose of collecting data that can be used to assist in subsurface reservoir characterization and modeling (see Cuevas Gozalo and Martinius, 1993; Dreyer et al., 1993; Robinson and McCabe, 1997; Visser and Chessa, 2000; Gibling, 2006). These studies often result in a 2-D characterization of the analog because traditional field methods, such as photomosaics, are ill-suited for accurately recording and interpreting the spatial and temporal variability in alluvial architecture over reservoir-scale areas. As Labourdette and Jones (2007) state, a significant challenge exists in capturing the full 3-D geometry of fluvial deposits from outcrop analogs. Fortunately, the recent proliferation of digital techniques for the study of outcrops, such as LiDAR and high-precision GPS, as well as the ease of access to sophisticated reservoir modeling software packages have opened a new door in the realm of outcrop analog studies (see Martinsen et al., 2011 and authors therein). Using digital data collection methods, field geologists are better equipped to quickly and accurately quantify such things as channel sand body dimensions and spatial and temporal facies relationships across multiple outcrop exposures.

Another recent addition to the geologists' toolbox is the application of integrated paleomorphodynamic workflows. Paleomorphodynamic workflows, employed by a number of recent studies including Hajek and Wolinsky (2012) and Hampson et al. (2013), utilize a series of scaling relationships and empirical equations to estimate bankfull channel dimensions and paleohydraulic conditions. These workflows help bridge the gap between 2-D and 3-D outcrop characterization by estimating formative hydraulic conditions, such as discharge and slope, which are known to be first order controls on fluvial style (Bridge, 2003). Paleomorphodynamic workflows, when used in conjunction with lithofacies models, provide a method for interpreting the depositional style and river planform of ancient fluvial systems (Lunt et al., 2004; Lynds, 2005). A combination of traditional methods, digital data collection and paleomorphodynamic workflows enables geoscientists to define 3-D conceptual models to build 3-D geocellular models from outcrop datasets. This workflow can lead to more quantitative 3-D characterization of outcrop analogs and, as is the case in this study, result in definitive implications for subsurface reservoir characterization.

The John Henry Member of the Straight Cliffs Formation, an Upper Cretaceous siliciclastic succession that outcrops in the Kaiparowits Plateau of southern Utah, is the ideal target for a 3-D digital outcrop analog study. The outcrop exposures of the Kaiparowits Plateau showcase a thick, well-exposed section of fluvial stratigraphy (Figure 1). Shanley and McCabe (1991, 1993) and Little (1995, 1997) first analyzed the genetic stratigraphy of the John Henry

Member by examining potential allogenic controls on alluvial architecture. More recently, Gooley (2010) and Pettinga (2013) added to the geologic framework of the proximal fluvial strata of the John Henry Member by focusing on two specific areas: Rock House Cove and Bull Canyon. These two authors defined lithofacies and facies associations, split the stratigraphic interval into seven depositional units (DUs), and documented large-scale trends in grain-size and channel belt amalgamation. Aside from this work however, little has been done to define the plan-view morphology of the river systems and build 3-D conceptual models. Furthermore, outcrop data has not been used to build 3-D facies models as a quantitative analysis of the controls on static connectivity for analogous subsurface deposits.

This study utilizes a differential GPS (dGPS) device to construct a digital outcrop model of Bull Canyon which enables accurate measurements of net-to-gross and channel belt width-to-thickness ratios. Additionally this study employs a paleomorphodynamic workflow that estimates paleochannel morphology (bankfull depth, sinuosity, etc.) and paleohydraulic conditions (bankfull discharge, slope, etc.) from data collected at the outcrop. The paleomorphodynamic workflow assists in defining a 3-D conceptual model of river system morphology at Bull Canyon. This conceptual model feeds directly into 3-D stochastic facies models built using object-based simulation. The purpose of this study is to bridge the gap between a largely qualitative outcrop characterization of the fluvial strata of the John Henry Member at Bull Canyon and full 3-D geological modeling for analog reservoir purposes. The primary goal of this study is to use traditional

field methods combined with digital outcrop measurements and paleomorphodynamic calculations to define 3-D conceptual models that capture the variability in fluvial style expressed in the outcrops at Bull Canyon. The statistics derived from the digital data are coupled with the robust conceptual model to build equiprobable 3-D facies models, measure the static reservoir connectivity at a four unique well spacing patterns, and determine how connectivity varies with changes in alluvial architecture.

Figure 1 – Paleogeographic reconstruction of the southwest United States and map of the Kaiparowits Plateau region. (1) Inset map of the southwest United States. (2) Paleogeographic reconstruction of the southwest United States during Late Cretaceous time (Szwarc, 2014). The reconstruction shows the location of the Kaiparowits Plateau (dark shade) and Bull Canyon (red dot) in relation to the three principle source terranes of the Straight Cliffs Formation; the Sevier Thrust Belt, Cordilleran Volcanic Arc, and Mogollon Highlands. (3) Map of the Kaiparowits Plateau region showing the location of this study, Bull Canyon. Colored regions represent present day exposures of the four members of the Straight Cliffs Formation (modified from Doelling and Willis, 2006).

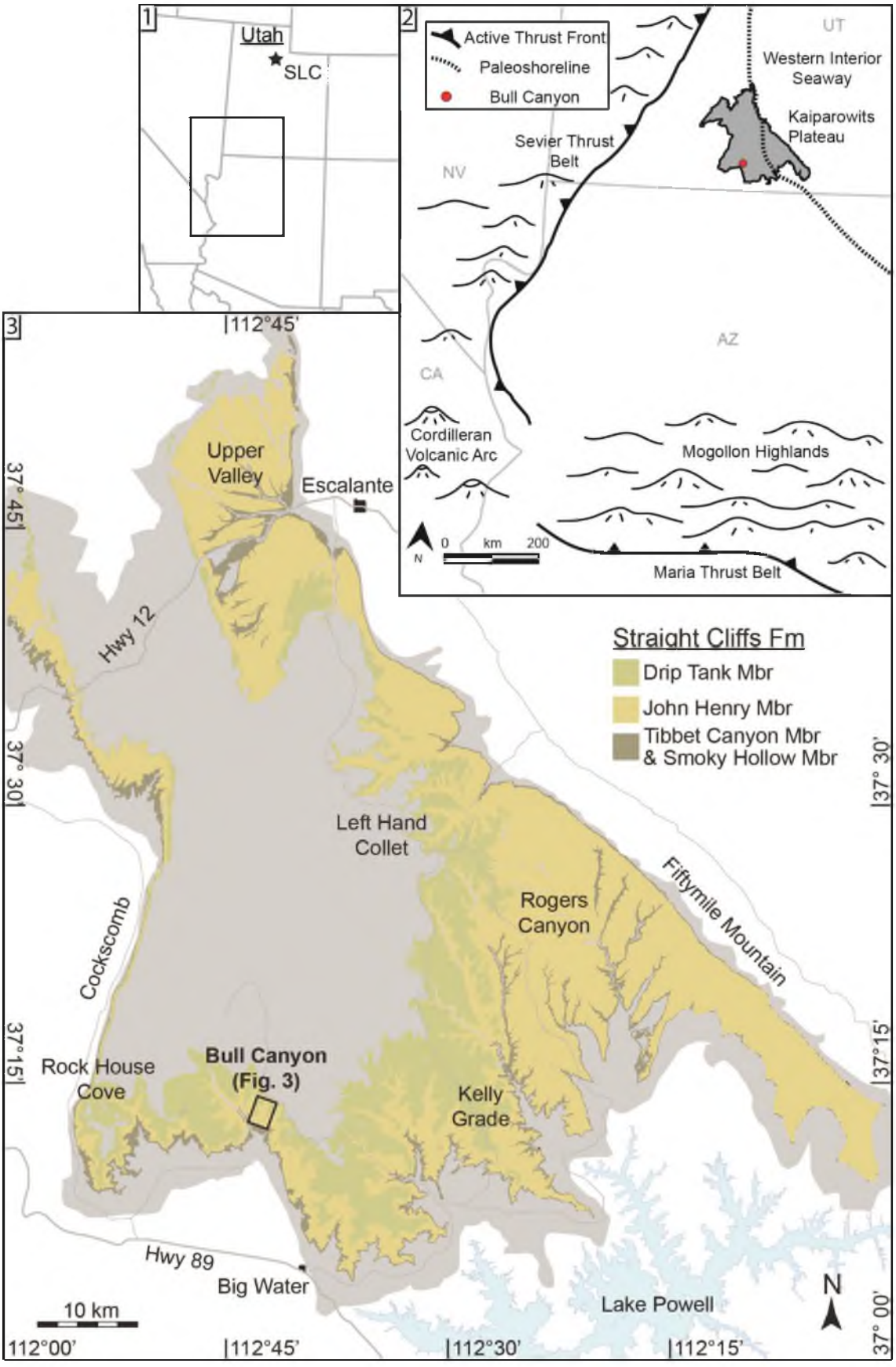
1
Utah
SLC
2
Active Thrust Front
Paleoshoreline
Bull Canyon
UT
Western Interior Seaway
Kaiparowits Plateau
Sevier Thrust Belt
NV
AZ
CA
Cordilleran Volcanic Arc
Mogollon Highlands
Maria Thrust Belt
N
0 km 200
3
112°45'
37° 45'
37° 30'
37°15'
Upper Valley
Escalante
Hwy 12
Straight Cliffs Fm
Drip Tank Mbr
John Henry Mbr
Tibbet Canyon Mbr & Smoky Hollow Mbr
Left Hand Collet
Rogers Canyon
Fiftymile Mountain
Cockscomb
Rock House Cove
Bull Canyon (Fig. 3)
Kelly Grade
Hwy 89
Big Water
Lake Powell
10 km
N
112°00'
112°45'
112°30'
112°15'
37° 00'

GEOLOGIC BACKGROUND

Tectonic and Paleogeographic Setting

The Kaiparowits Plateau of south-central Utah provides uninterrupted exposures of the Upper Cretaceous (Santonian–Campanian) Straight Cliffs Formation (Figure 1). The study area sits on the southwestern corner of the Colorado Plateau and is bounded by the Escalante River valley to the east, the Colorado River to the south, and the East Kaibab Monocline to the west (Doelling and Willis, 2006). Strata of the plateau, although locally deformed, are generally flat-lying with a gentle overall dip (<5°) to the north (Peterson, 1969; Doelling and Blackett, 2000).

In the Late Cretaceous, the area was situated in an extensive asymmetrical foreland basin (Figure 1). The basin formed, at least in part, by tectonic loading from the Sevier fold and thrust belt to the west (Kauffman and Caldwell, 1993; Liu and Nummedal, 2004). East-west shortening and uplift caused by subduction of the Farallon plate along the west coast of Laurentia and the resulting dynamic subsidence kept the foreland basin active through the Late Cretaceous and into the Paleogene (Kauffman, 1977; Kauffman and Caldwell, 1993; DeCelles and Coogan, 2006; Liu et al., 2011). The siliciclastic sediments that make-up the Upper Cretaceous strata of the Kaiparowits Plateau, including the Straight Cliffs Formation, were shed from three principle source terranes: the

Sevier fold and thrust belt to the west, the Cordilleran Volcanic Arc to the southwest, and the Mogollon Highlands to the south (Figure 1) (Peterson, 1969; Eaton, 1991; Hettinger et al., 1993; Lawton et al., 2003; Szwarc, 2014). The sediments were transported east-northeastward and deposited within the Kaiparowits Basin along the western margin of the Western Interior Seaway (Vaninetti, 1979; Kauffman and Caldwell, 1993; Szwarc, 2014). As the tectonic regime changed, the Upper Cretaceous strata were exhumed with uplift of the Colorado Plateau (Spencer, 1996). Today, the Straight Cliffs Formation exposed on the Kaiparowits Plateau sits roughly 1500 meters (5000 ft) above sea level.

Straight Cliffs Formation

Gregory and Moore (1931) were the first to study the Upper Cretaceous strata of the Kaiparowits Plateau. They named the Straight Cliffs Sandstone for the thick and continuous exposures of caramel-colored sandstone along Fifty Mile Mountain southeast of Escalante, Utah. Peterson and Waldrop (1965) redefined this unit as the Straight Cliffs Formation to include the coals and mudstones beyond the type area at Fifty Mile Mountain.

Peterson (1969) established a detailed correlation of the Straight Cliffs Formation throughout the Kaiparowits Plateau. Peterson divided the formation into four formal units. These units are, from oldest to youngest, the Tibbet Canyon Member, marked by cliff-forming marine sandstones; the Smoky Hollow Member, marked by slope- and ledge- forming coastal plain deposits; the John Henry Member, marked by alluvial, paralic, and marine deposits; and lastly the

Drip Tank Member marked by cliff-forming alluvial sandstones (Figure 2). Peterson (1969) also noted a gradual transition from proximal fluvial to shallow marine facies within the John Henry Member from west to east across the plateau. In the area immediately surrounding Fifty Mile Mountain he identified seven shoreface intervals (A through G) and further to the west he mapped four major coal zones, all of these within the John Henry Member. Because of their economic importance, the coal-bearing facies became the subject of many early studies (Robison, 1966; Doelling and Graham, 1972; Vaninetti, 1979).

Eaton (1987, 1991) was able to place age-date constraints on deposition of the Straight Cliffs Formation by establishing a biostratigraphic framework for the Upper Cretaceous strata of the Kaiparowits Plateau. He placed an early Coniacian age on the lower John Henry Member based on the presence of inoceramid bivalves, *Volviceramus involutus*. He also suggested a late Santonian age for the upper John Henry Member based on assemblages of inoceramid bivalves and the presence of the ammonite *Desmoscaphites*. Eaton's early work is in general agreement with more recent studies including that of Szwarc (2014), which focuses on evidence from outside the marine realm, specifically detrital zircon U–Pb geochronologic data.

The work of Shanley and McCabe (1991, 1993) and Little (1995, 1997) marks a shift in focus to the fluvial portions of the Straight Cliffs Formation. These authors applied concepts in genetic stratigraphy to the alluvial architecture of the John Henry Member. The work of Shanley and McCabe (1991) has translated into a very well-cited sequence stratigraphic model of alluvial

architecture. They identified four unconformity-bounded sequences in the marginal-marine section and traced these surfaces into coeval terrestrial strata. The resulting model establishes three stages of alluvial basin fill that are tied to changes in base level. Little (1995, 1997) investigated the proximal alluvial architecture of the John Henry Member in the northwestern portion of the Kaiparowits Plateau. Little suggested the depositional architecture he observed was likely influenced by hinterland tectonics and, to a lesser extent, eustatic sea level.

Allen (2009), Allen and Johnson (2010), and Dooling (2013) investigated the marginal marine strata of the John Henry Member in Rogers Canyon and Left Hand Collet (Figures 1, 2). These studies suggest that high accommodation rates and high sediment supply contributed to the preservation of the A through G shorefaces. Furthermore, these studies suggest that shorefaces A–G record seven transgressive-regressive cycles (T–R cycles 0–6). Allen (2009) constructed a coastal onlap curve for the John Henry Member near Rogers Canyon. It has been proposed that this onlap curve correlates with varying levels of channel belt clustering up dip (Benhallam, 2014).

Gallin et al. (2010) shifted focus to the west of the paleoshoreline and investigated paralic and alluvial facies within the John Henry Member near Kelly Grade (Figure 1). In correlating paralic and alluvial facies to shifts in marine shoreface architecture Gallin made a number of key observations. Most notably, Gallin reported no evidence of an unconformable surface correlative to the A-sequence boundary of Shanley and McCabe (1991, 1993), which they concluded

marked the early lowstand systems tract. Additionally, in partial contrast to the findings of Shanley and McCabe (1991, 1993), Gallin concluded that the John Henry Member is characterized by an upward increase in grain size, channel belt amalgamation, and downstream accretion as well as an upward decrease in tidal influence.

Gooley (2010), Pettinga (2013), and Szwarc (2014) presented studies focusing on the nonmarine portions of the John Henry Member. Analyzing trends in detrital zircon U–Pb geochronologic data, Szwarc (2014) concluded that the axial fluvial system depositing Straight Cliffs alluvial strata was fed by distributive fluvial systems draining the Mogollon highlands, Sevier thrust belt, and Cordilleran volcanic arc. His findings shed light on the provenance of the Straight Cliffs Formation and add confidence to the understanding of the regional depositional setting. Gooley (2010) and Pettinga (2013), working at Rock House Cove and Bull Canyon respectively, divided the proximal fluvial strata of the John Henry Member into seven depositional units, named DU-0 through DU-6. Both authors were in general agreement as to the characteristics of each depositional unit, and they are summarized as, in ascending order, (DU-0) tidally-influenced channel belt complex; (DU-1) single story, laterally-isolated, tidally-influenced channels; (DU-2) moderately laterally extensive, laterally accreting channel belts; (DU-3) single story, laterally isolated channels; (DU-4) laterally extensive channel belts; (DU-5) laterally extensive channel belt complexes; and (DU-6) highly amalgamated channel belt complexes. Additionally, both authors documented two characteristic large scale trends: (1) an upward decrease in grain size,

channel belt frequency, and lateral extent in depositional units 0 through 3 and (2) an upward increase in grain size, channel belt frequency, and lateral extent in depositional units 4 through 6. The specific attributes of each depositional unit are summarized in Table 1. This study builds and expands on the work of Pettinga (2013) at Bull Canyon by using the proximal fluvial strata of the John Henry Member as an outcrop analog for deriving insights into subsurface reservoir characterization.

Figure 2 – Late Cretaceous stratigraphy of south-central Utah and stratigraphic framework of the Straight Cliffs Formation. A. Late Cretaceous (Cenomanian–Campanian) stratigraphy of south-central Utah. B. Stratigraphic framework of the Straight Cliffs Formation depicting the southwest-northeast transition from fluvial-dominated deposition to shallow marine-dominated deposition. Highlights the work of Gooley (2010) at Rock House Cove, Pettinga (2013) at Bull Canyon, Gallin (2010) at Kelly Grade, Allen (2010) at Rogers Canyon and Dooling (2010) at Left Hand Collet. Displays the coastal onlap curve of Allen and Johnson (2010) and the sequence stratigraphic framework as proposed by Shanley and McCabe (1991).

A. Regional Stratigraphy

B. Straight Cliffs Formation, Kaiparowits Plateau

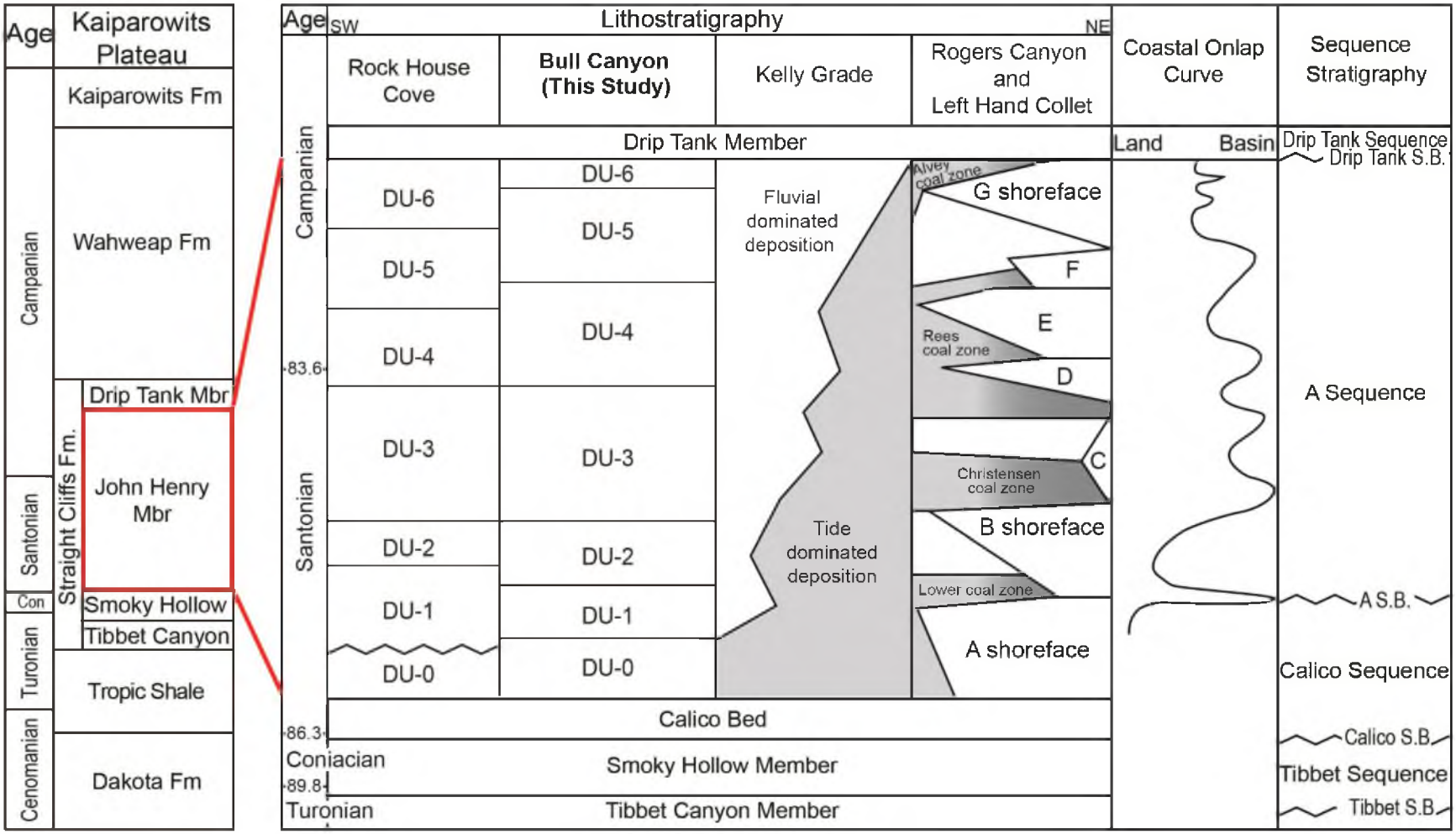

Table 1

Depositional Unit Summary. Summarized from Gooley (2010) and Pettinga (2013).

Depositional Unit	Lithofacies	Notable Elements	Sandbody Descriptions	Average Bedload Grain Size (mm)	Average Thickness (m)	Net-to-Gross
DU-6	Trough cross-bedded sandstone; Planar cross-bedded sandstone; Mud-rip up clast conglomerate; Trough cross-stratified matrix supported conglomerate	Numerous gravel lags; devoid of fine-grained material	Multistory, highly amalgamated channel belt complexes	0.625 Coarse Sand	14	1.000
DU-5	Massive siltstones; Trough cross-bedded sandstone; Planar cross-bedded sandstone; Convoluted sandstone	Abundant trace fossils; gravel lags	Multistory, thick, and laterally extensive channel belts and channel belt complexes	0.516 Coarse Sand	33	0.400
DU-4	Massive siltstones; Trough cross-bedded sandstone; Planar cross-bedded sandstone; Convoluted sandstone	*Skolithos* burrows; bone fragments	Multistory, thick, and laterally extensive channel belts	0.3385 Medium Sand	70	0.325

Table 1 Continued

Depositional Unit	Lithofacies	Notable Elements	Sandbody Descriptions	Average Bedload Grain Size (mm)	Average Thickness (m)	Net-to-Gross
DU-3	Coal; Carbonaceous mud; Rooted mud and silt; Trough cross-bedded sandstone; Convoluted sandstone	Soil development; coal beds up to one meter thick	Thin and laterally isolated channel stories	0.2125 Fine Sand	40	0.125
DU-2	Trough cross-bedded sandstone; Planar cross-bedded sandstone; Ripple cross-laminated sandstone; Rooted mud and silt; Massive mudstone	*Skolithos* and *Planolities* trace fossils	Single and multistory, laterally isolated channel belts	0.2635 Medium Sand	20	0.300
DU-1	Coal; Carbonaceous mud; Rooted mud and silt; Flaser bedded sandstone; Trough cross-bedded sandstone; Convoluted sandstone	Inclined heterolithic strata; shell material; diverse suite of trace fossils	Single story and laterally isolated channel belts	0.301 Medium Sand	10	0.225

Table 1 Continued

Depositional Unit	Lithofacies	Notable Elements	Sandbody Descriptions	Average Bedload Grain Size (mm)	Average Thickness (m)	Net-to-Gross
DU-0	Trough cross-bedded sandstone; Planar cross-bedded sandstone	Little fine-grained material; large-scale, high angle dune foresets	Multistory, highly amalgamated channel belt complexes	0.53 Coarse Sand	13	0.750

METHODOLOGY

A three step methodology is employed to define 3-D conceptual models that adequately capture the variability in fluvial style expressed in the outcrops at Bull Canyon and show how this variability affects static reservoir connectivity.

Step 1 is an alluvial architecture characterization. This step builds heavily on the work of Pettinga (2013) and establishes the architectural framework at Bull Canyon. The alluvial architecture characterization relies on outcrop data to establish the size, stratigraphic arrangement, and stacking density of channel belt sand bodies as well as the dominant grain-size, lithofacies, and paleoflow direction of each depositional unit.

Step 2 is a paleomorphodynamic workflow. This step bridges the gap between the 2-D alluvial architecture characterization and the development of 3-D conceptual models of river system morphology. The paleomorphodynamic workflow estimates paleohydraulic conditions as well as paleochannel geometry in each depositional unit. Formative hydraulic conditions such as discharge and slope are known to be first order controls on fluvial style and therefore are invaluable in defining the plan view morphology of ancient river systems.

Step 3 is facies modeling and static reservoir connectivity analysis. This step utilizes 3-D object-based modeling to analyze how temporal variability in fluvial style impacts reservoir connectivity in the John Henry Member.

Alluvial Architecture Characterization

Five detailed stratigraphic sections were measured in Bull Canyon (two from this study and three from Pettinga, 2013; Figure 3). Each vertical section logs over 165 meters (541 ft) of stratigraphy within the John Henry and Drip Tank Members of the Straight Cliffs Formation. All sections begin at the canyon floor and continue through the uppermost cliff-forming sandstone of the Drip Tank Member. Lithology, grain size, sedimentary structures, and body and trace fossil descriptions were recorded for each section as outlined by Miall (2000).

Four high-resolution composite photographs of Bull Canyon, which cover approximately 4 km (2.5 mi) of continuous outcrop, were interpreted and examined for channel belt sand body frequency and stacking pattern. The interpretations reflect a sand versus nonsand lithofacies scheme. Lateral and vertical facies distributions mapped on the composite photographs provide a visual estimate of the ratio of net sandstone to gross sediment (net-to-gross) within each depositional unit (Figure 4).

A total of 2,725 paleocurrents and accretion sets were measured throughout the John Henry Member to determine flow directions and mode of accretion. Paleocurrents were measured predominantly from trough cross-stratification, ripple cross-lamination, and planar cross-stratification; however, a small fraction of the measurements were taken from wood fragments, flute casts, and imbricated mud clasts. Accretion sets were measured predominantly from truncated macroscale barforms and were evaluated in relation to paleocurrent direction in order to determine the dominant mode of barform accretion.

Additionally, a total of 2,360 cross-set thickness measurements were collected from mesoscale structures including trough cross-stratification and planar cross-stratification.

The dimensions and distributions of channel belt sand bodies in Bull Canyon were documented and mapped using a differential GPS device paired with a laser rangefinder. Over 20,000 positions were collected corresponding to 196 channel belt sand bodies. Using the position data, in combination with a Digital Elevation Model (DEM) of Bull Canyon, a digital outcrop model was generated that captures lateral and vertical facies variability (Figure 3). The digital outcrop model enabled accurate calculations of channel belt thickness and apparent width within each depositional unit. Outcrop orientation, mean paleocurrent direction and apparent channel belt width were used to solve for true, cross-channel belt width (Fabuel-Perez et al., 2009). The differential GPS device was also used to record the path of each stratigraphic section, enabling the sections to be included in the digital outcrop model and resulting in a robust digital database.

Paleochannel Reconstruction and Paleohydraulic Analysis

Cross-set height (S_m) measurements in combination with median (d50) bedload grain size measurements (Pettinga, 2013; this study) were used for a paleomorphodynamic workflow to reconstruct paleochannel morphology and analyze paleohydraulic conditions in each depositional unit of the John Henry Member at Bull Canyon. The seven parameters estimated for the paleochannel

reconstruction were mean dune height (h_m), bankfull depth (H), bankfull channel width (B), sinuosity (P), meander wavelength (L), and channel belt width (B_{cb}) (Figure 5). The six parameters estimated for the paleohydraulic analysis were paleoslope (S), backwater length (L_w), flow velocity (V), bankfull discharge (Q), drainage area (A), and distance from source (L) (Figure 5). Both the paleochannel reconstruction and paleohydraulic analysis rely on a number of scaling relationships that reflect how specific parameters relate to one another. These scaling relationships are predominantly derived from laboratory flume studies and/or observations from modern river systems and are presented in the form of empirical equations. Ranges of error are established when calculating mean dune height, bankfull depth, and flow velocity. These error ranges are carried through when estimating each additional parameter. The equations used to estimate each parameter are presented along with the results. Observations from the alluvial architecture characterization along with results of the paleomorphodynamic workflow are together used to define 3-D conceptual models of river system morphology.

Facies Modeling and Static Reservoir Connectivity Analysis

To test the impact of temporal variability in alluvial architecture on static reservoir connectivity at Bull Canyon, 3-D facies models were built using an object-based approach. The model framework consists of a geocellular grid with seven distinct zones, a zone corresponding to each depositional unit. Individual cells measure 10 x 10 x 0.5 m (33 x 33 x 1.6 ft) in the x, y, and z dimensions

respectively. This cell size provides adequate resolution to simulate the smallest channel belt sand bodies. The model grid contains ~15 million cells and measures 1,740 m (5,709 ft) in the x-direction, 2,240 m (7,349 ft) in the y-direction, and 232 m (761 ft) in the z-direction.

Channel belt orientation, channel belt form, and target net-to-gross are derived from the conceptual model of river system morphology (presented in the discussion). Statistical distributions of channel belt orientation, channel belt width, channel belt thickness, meander wavelength, and meander amplitude reflect observations and results from the alluvial architecture characterization and paleomorphodynamic workflow. Five upscaled facies logs derived from five measured sections (Westside #1, #2, and Bull Canyon #1–3 from Pettinga [2013]) were used not only as hard conditioning data but also to derive a vertical facies proportion curve (Figure 6).

Thirty stochastically-generated facies models were produced and each model realization was validated by testing to see if it (1) reproduced facies proportions and mimicked the vertical proportion curve (Figure 6), (2) reproduced paleochannel form and orientation, (3) matched all available measured section (pseudo-well) data, and (4) passed an objective visual comparison with the digital outcrop model (Figure 3). Model realizations were then subjected to a static connectivity analysis to assess how reservoir connectivity is affected by variability in alluvial architecture. Static reservoir connectivity herein is defined as the portion of channel belt sand bodies that are connected to the well bore. This metric can be presented as a reservoir rock volume or as a percentage of

total reservoir rock volume (Larue and Hovadik, 2006). Static reservoir connectivity was measured at four unique well spacing patterns (Figure 7). Results were analyzed by examining average reservoir connectivity per depositional unit (%), cumulative gross connected sandstone rock volume (km^3), and total sandstone volume per depositional unit (km^3).

Figure 3 – Digital outcrop model and map of Bull Canyon. (1) Digital outcrop model of Bull Canyon showing channel belt sand bodies (yellow) and the location of stratigraphic sections. This model, which is spatially referenced in 3-Dimensions, was constructed using a workflow that involved over 20,000 dGPS position measurements from this study and Pettinga (2013). (2) Map of Bull Canyon with differential Global Positioning System (dGPS) data collection locations as well as the locations of measured sections and composite photographs. The red box denotes the boundary polygon of the geocellular grid that was constructed for the area.

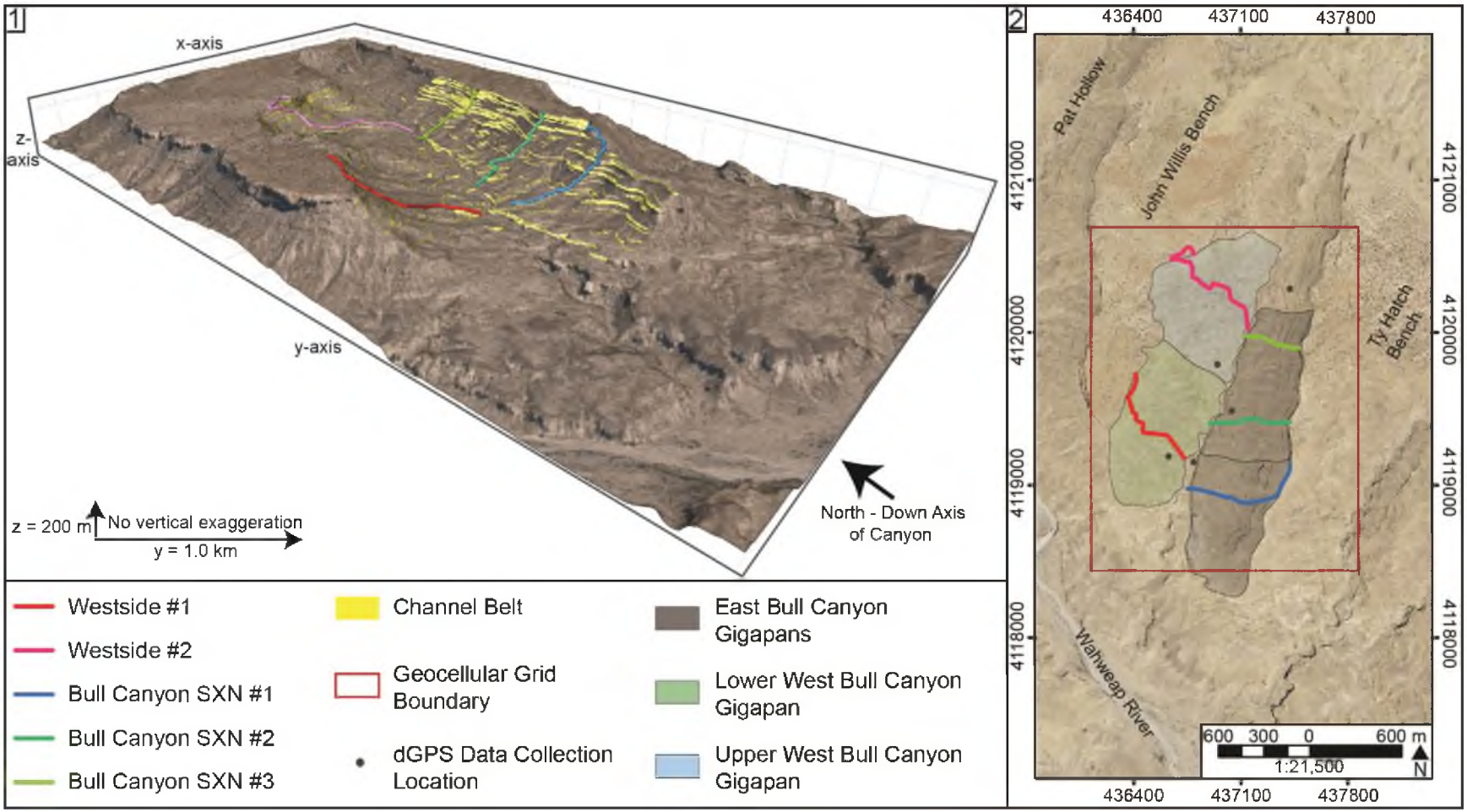
1
x-axis
z-axis
y-axis
z = 200 m
No vertical exaggeration
y = 1.0 km
North - Down Axis of Canyon
Westside #1
Westside #2
Bull Canyon SXN #1
Bull Canyon SXN #2
Bull Canyon SXN #3
Channel Belt
Geocellular Grid Boundary
dGPS Data Collection Location
East Bull Canyon Gigapans
Lower West Bull Canyon Gigapan
Upper West Bull Canyon Gigapan
2
436400
437100
437800
4121000
4120000
4119000
4118000
Pat Hollow
John Willis Bench
Ty Hatch Bench
Wahweap River
600 300 0 600 m
1:21,500
N

Figure 4 – Composite photograph and interpretation of the John Henry and Drip Tank Members at the southwestern portion of Bull Canyon along with a simplified stratigraphic section (Westside #1). The interpretation shows sandstone bodies (yellow) distributed throughout floodplain silts and muds (light brown). Depositional unit boundaries one through six are interpreted from changes in fluvial architecture. These boundaries are denoted by green lines. The red line shows the approximate location of measured section Westside #1. The boundary with the Drip Tank Member is denoted by the blue line. The red fill that caps the canyon wall is the Drip Tank Member.

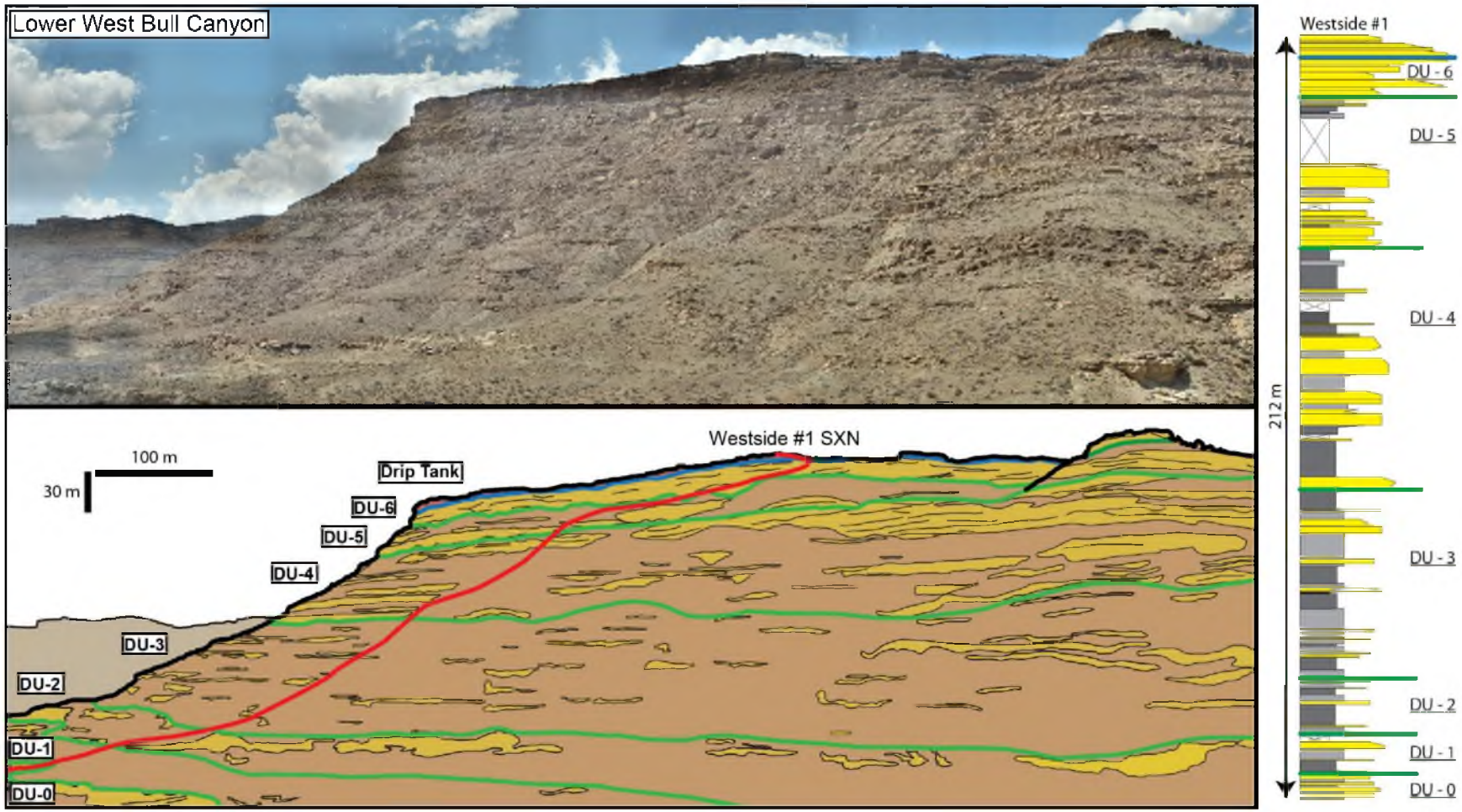
Lower West Bull Canyon
Westside #1 SXN
100 m
30 m
Drip Tank
DU-6
DU-5
DU-4
DU-3
DU-2
DU-1
DU-0
Westside #1
212 m
DU - 6
DU - 5
DU - 4
DU - 3
DU - 2
DU - 1
DU - 0

Figure 5 – Flowchart that depicts the sequential steps taken in reconstructing paleochannel form and analyzing paleohydraulic conditions. Cross-set height measurements (n = 2360) and d50 grain size measurements form the basis of the workflow. Ranges of error are initially established when calculating mean dune height and subsequently expanded when calculating bankfull depth and determining flow velocity. These error ranges are carried through when estimating each additional parameter. The equations used to calculate each parameter along with key references are found in the results portion of this study.

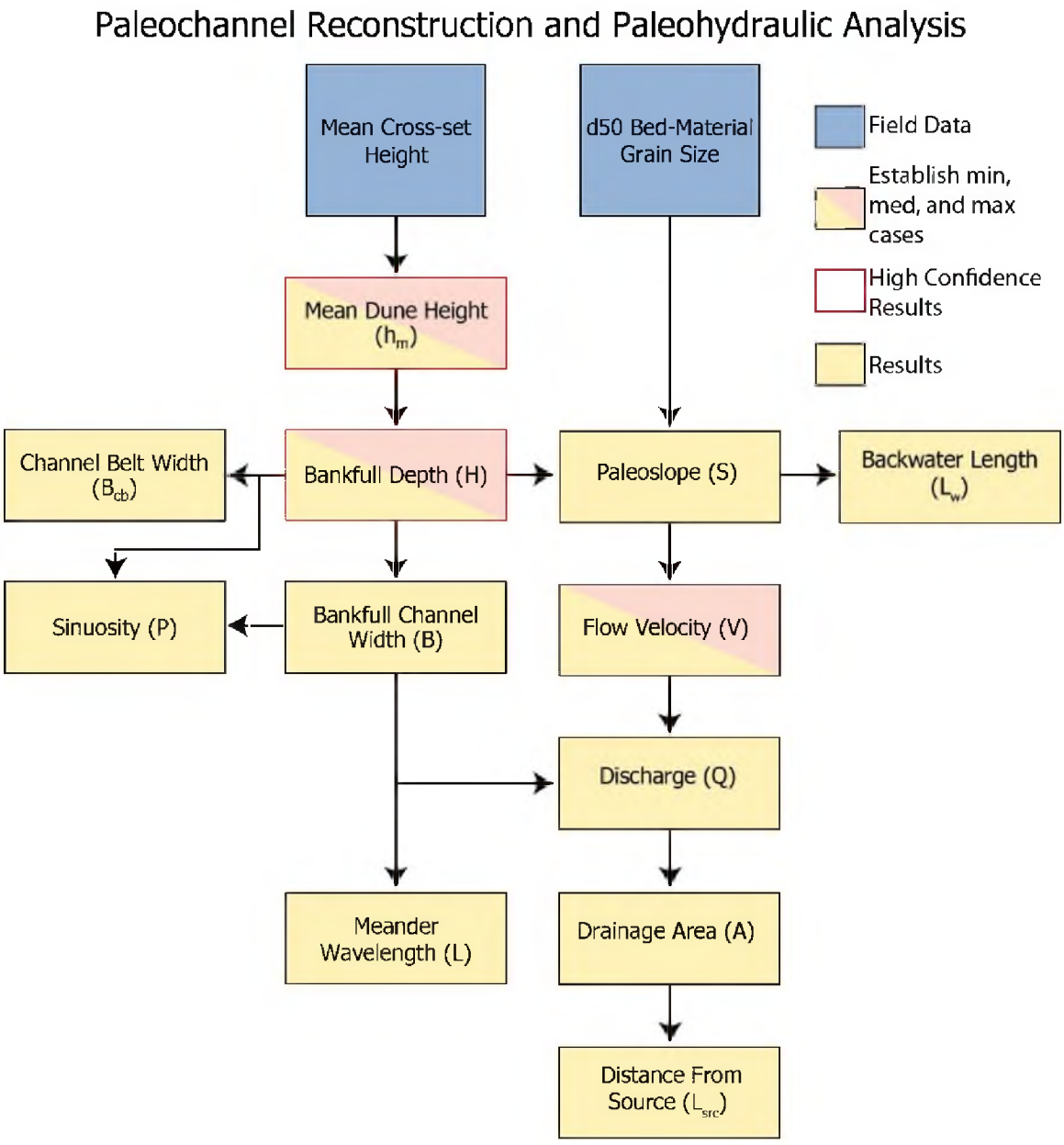
Paleochannel Reconstruction and Paleohydraulic Analysis
Mean Cross-set Height
d50 Bed-Material Grain Size
Field Data
Establish min, med, and max cases
High Confidence Results
Results
Mean Dune Height (h_m)
Channel Belt Width (B_{cb})
Bankfull Depth (H)
Paleoslope (S)
Backwater Length (L_w)
Sinuosity (P)
Bankfull Channel Width (B)
Flow Velocity (V)
Discharge (Q)
Meander Wavelength (L)
Drainage Area (A)
Distance From Source (L_{src})

Figure 6 – Vertical proportion curve for channel belt fill and background overbank facies. The curve shows the probability of a channel body being present at a given model layer (stratigraphic horizon). Depositional unit boundaries are marked by red dashed lines. The curve is derived from five upscaled facies logs (measured sections; Westside #1, #2, and Bull Canyon #1–3 from Pettinga [2013]).

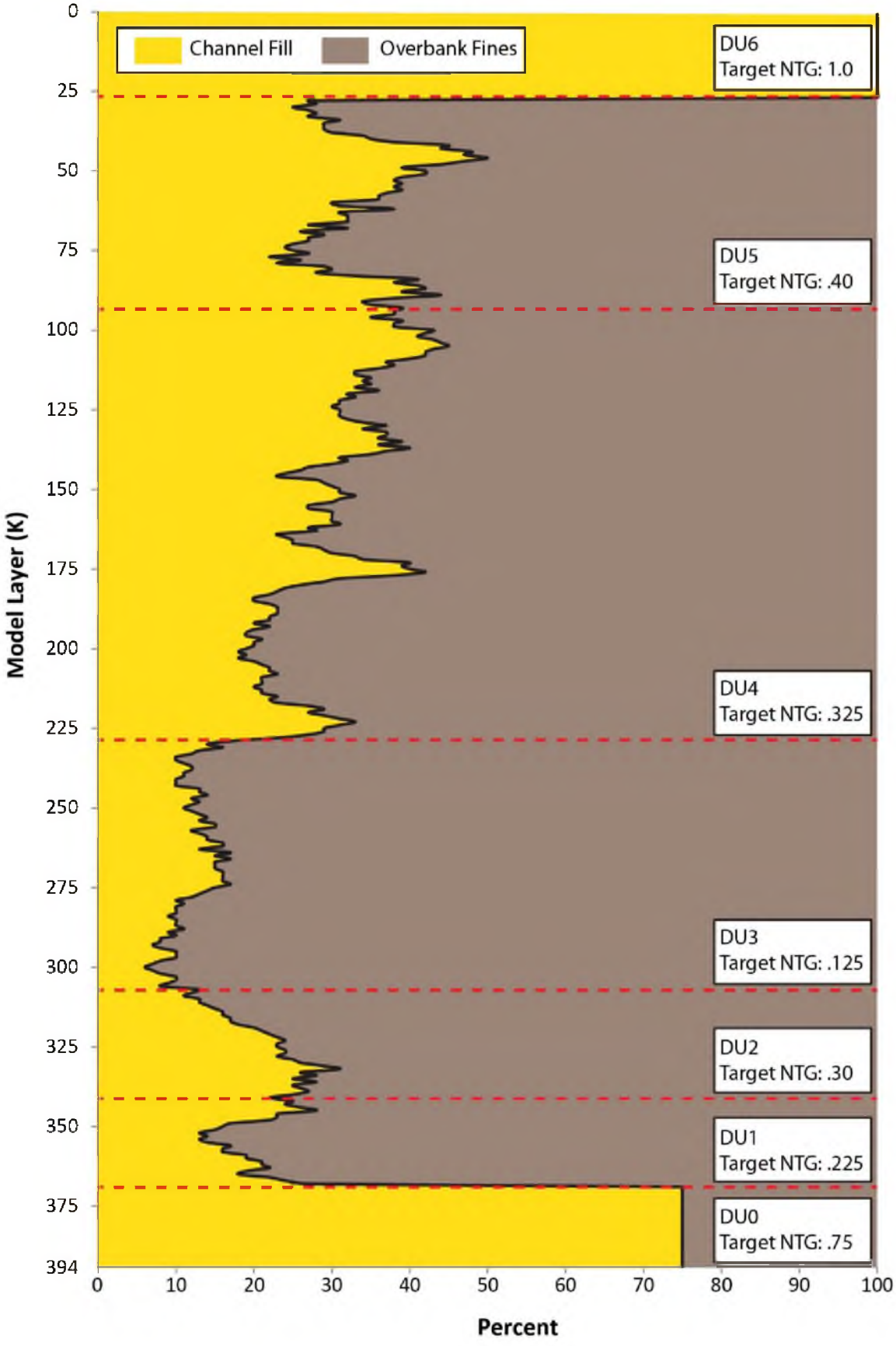
Channel Fill
Overbank Fines
DU6
Target NTG: 1.0
DU5
Target NTG: .40
DU4
Target NTG: .325
DU3
Target NTG: .125
DU2
Target NTG: .30
DU1
Target NTG: .225
DU0
Target NTG: .75
Model Layer (K)
0
25
50
75
100
125
150
175
200
225
250
275
300
325
350
375
394
0
10
20
30
40
50
60
70
80
90
100
Percent

Figure 7 – 40-, 160-, 640-, and 2560-acre well spacings and associated well patterns. Used for measuring static reservoir connectivity in each model realization. The model area of interest (red box) is 3.94 km^2 (1.52 mi^2). At 2560-acre spacing there can only be one well bore within the model area.

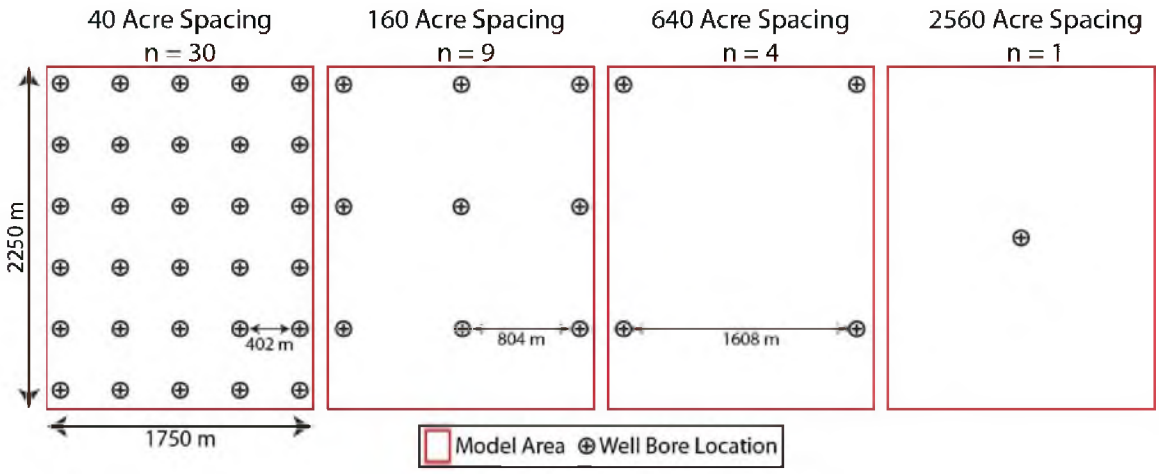
40 Acre Spacing
n = 30
160 Acre Spacing
n = 9
640 Acre Spacing
n = 4
2560 Acre Spacing
n = 1
2250 m
402 m
804 m
1608 m
1750 m
Model Area
Well Bore Location

RESULTS AND OBSERVATIONS

Alluvial Architecture Characterization

Lithofacies and Grain-Size Trends

The distribution of lithofacies in the John Henry Member at Bull Canyon was first described by Pettinga (2013) (Table 1). Lithofacies variability represents the foundation for a descriptive classification hierarchy that culminates in splitting the John Henry Member into seven depositional units (DUs). The seven depositional units are composed predominantly of trough cross-stratified sandstone, ripple cross-laminated sandstone, and laminated mudstone. The largest differentiating factors between depositional units include grain-size, proportion of sand versus nonsand lithofacies, abundance of coal, and abundance of gravel facies. Average grain-size decreases from DU-0 (coarse sand) to DU-3 (fine sand) and increases from DU-3 (fine sand) to DU-6 (coarse-to-very coarse sand). Coal is present in depositional units 1 and 3, and the thickest coal beds (1-m [3.28-ft] thick) occur in DU-3. Gravel facies, including massive and trough cross-stratified matrix supported conglomerate, are present in DU-6 and, to a lesser extent, in DU-0.

Paleocurrent, Accretion Set and Cross-set Height Measurements

Paleocurrent measurements (n = 1050; Figure 8) at Bull Canyon indicate east-northeasterly flow. Accretion set measurements (n = 1675; Figure 8) indicate oblique downstream accretion in the northeasterly direction. At the base of the John Henry Member (DU-0) paleoflow was directed towards the northeast. Paleoflow abruptly shifted to the east in DU-1 (90°) and afterwards slowly transitioned towards the east-northeast (78° in DU-6). Barform accretion was dominantly downstream in DUs 0, 1, and 3. Accretion set measurements show a mix of downstream and lateral accretion in DUs 2, 4, 5, and 6. Average cross-set height increases from DU-0 (26 cm [10.2 in]) to DU-2 (27 cm [10.6 in]), decreases from DU-2 (27 cm [10.6 in]) to DU-5 (17 cm [6.7 in]), and abruptly increases in DU-6 (30 cm [11.8 in]) (Figure 8).

Channel Belt Dimensions and Net-to-Gross

Width and thickness measurements for 196 channel belts as well as average width-to-thickness ratios for each depositional unit are presented in Table 2. Channel belts consists of laterally and, in some cases, vertically amalgamated channel stories that represent a river systems occupation and migration over a specific area of the floodplain. Two distinct populations are present in the data. The first population, composed of depositional units 1, 2, and 3, is characterized by channel belts that are 66–88 meters (217–289 ft) wide and 2–3 meters (7–10 ft) in thickness with an average width-to-thickness ratio of 30:1. Depositional units 1, 2, and 3 are also characterized by a low net-to-gross,

ranging from 12.5 to 30% (Table 1). The second population, composed of depositional units 0, 4, 5, and 6, is characterized by channel belts that are wider (162–273 meters [532–896 ft]) and thicker (3.5–6 meters [12–20 ft]) than the first population and have a range of width-to-thickness ratios from 43:1 to 58:1. Net-to-gross in this population is high, ranging from 32.5 to 100% (Table 1).

Paleochannel Reconstruction

The equations and results of the paleochannel reconstruction are presented for the fluvial strata at Bull Canyon. A summary of the raw data used to carry out this workflow (2,360 cross-set height measurements) is shown in Figure 8. Before calculating results, cross-set heights were first corrected for a 10% reduction in thickness from burial compaction estimated for well sorted sands (Ethridge and Schumm, 1978). The results of the workflow are summarized in Figure 9.

Mean Dune Height (h_m)

Mean dune height (h_m) was calculated directly from the distribution of cross-set thicknesses (S_m) (Leclair and Bridge, 2001). This equation, derived from experimental and empirical data from a range of flumes and rivers, relates cross-set thickness to the height of formative subaqueous dunes.

$$h_m = (2.9 \pm 0.7) \times S_m \quad (1)$$

Applying this relationship to the data from Bull Canyon results in three large-scale trends. Mean dune height increases from DU-0 (76 cm [29.9 in]) to DU-2 (80 cm [31.5 in]), decreases from DU-2 (80 cm [31.5 in]) to DU-5 (48 cm [18.9 in]), and increases in DU-6 (87 cm [34.3 in]). Calculations of bankfull channel depth, bankfull channel width, sinuosity, meander wavelength, and channel belt width are dependent upon mean dune height, so this general trend is carried through to subsequent results of the paleochannel reconstruction workflow.

Bankfull Depth (H)

Bankfull depth (*H*) is estimated via an empirical relationship proposed by Yalin (1964) and modified by Bridge and Tye (2000). This proportional relationship scales flow depth to approximately 6–10 times mean dune height (h_m). It is derived from laboratory flume studies as well as observations from various rivers throughout the northern hemisphere.

$$H = (8.0 \pm 2.0) \times h_m \quad (2)$$

Estimated bankfull channel depth across all seven depositional units ranges from 2.3 to 10.2 meters (7.5 to 33.25 ft). The calculation produced reasonable estimates of bankfull depth when compared to a limited number of nontruncated barforms within the study area (Pettinga, 2013). Bankfull channel depth increases from DU-0 (6.1 m [20 ft]) to DU-2 (6.7 m [22 ft]), decreases from

DU-2 (6.7 m [22 ft]) to DU-5 (3.9 m [12.8 ft]), and abruptly increases in DU-6 (7.0 m [23 ft]).

Bankfull Channel Width (B)

Bankfull channel width (*B*) is estimated using two separate equations, one for meandering channels and one for braided channels. For meandering channel systems, bankfull channel width is estimated from bankfull depth (*H*) using the relationship proposed by Williams (1986). The relationship is derived from modern meandering rivers found in a large variety of environments and countries including the USA, India, Pakistan, Canada, Sweden, and Australia:

$$B = 21.3 (H^{1.45}) \quad (3)$$

For braided channel systems bankfull channel width is estimated from bankfull depth (*H*) using an empirical relationship derived from modern braided rivers in the midcontinent USA (Leopold and Maddock, 1953):

$$B = 42 (H^{1.11}) \quad (4)$$

Equation (4) was applied to depositional units that show evidence of downstream accretion and are characterized by coarse grain sizes (DUs 0 and 6). Equation (3) was applied to the remainder of the depositional units. Across

the seven depositional units, estimated bankfull channel widths range from 71 to 553 meters (233 to 1,814 ft). The smallest mean values occur in depositional units 4 (142 m [466 ft]) and 5 (152 m [499 ft]), while the largest mean values occur in depositional units 0 (313 m [1,027 ft]) and 6 (361 m [1,184 ft]).

Sinuosity (P)

Sinuosity (P) is estimated using an empirical relationship derived by Schumm (1972) from meandering rivers in the midcontinent USA.

$$P = 3.5 \left(\frac{B}{H}\right)^{-0.27} \quad (5)$$

Estimates of channel sinuosity are low-to-moderate across all depositional units. In depositional units 0 and 6 sinuosity ranges from 1.19 to 1.22 with a mean value of 1.2. In depositional units 1 and 2, sinuosity ranges from 1.17 to 1.30 with a mean value of 1.22. The sinuosity index in depositional units 3, 4, and 5 ranges from 1.22 to 1.38 with mean values of 1.3. Statistical methods (e.g., Le Roux, 1992, 1994, 2001; Ghosh, 2000) are sometimes used to infer the relative sinuosity of ancient rivers; however, such a workflow is not applicable to this study because it requires hundreds of paleocurrent measurements at the individual channel scale.

Meander Wavelength (L)

Meander wavelength is estimated using an empirical relationship that relates wavelength to bankfull channel width (Leopold et al., 1964; Zeller, 1967; Yalin, 1971; Richards, 1982). Like many of the previous equations, it is derived from modern meandering river systems.

$$L \approx 10B \quad (6)$$

Estimated values of meander wavelength span a range 4.5 km (710–5,530 m [2,329–18,143 ft]) across the seven depositional units.

Channel Belt Width (B_{cb})

Channel belt width is estimated using an empirical relationship derived from modern meandering rivers in North America (Collinson, 1978). In this equation channel belt width is a function of bankfull depth. Due to the origin of this equation, it is best suited for channels that have been allowed to develop fully meandering profiles.

$$B_{cb} = 64.6 (H^{1.54}) \quad (7)$$

Estimated channel belt width is approximately 3–4 times bankfull channel width and values range from 231 to 2,308 meters (758 to 7,572 ft). In many

cases, most notably in the lower John Henry Member, estimated channel belt width greatly exceeds measurements from the outcrop (Table 2).

Paleohydraulic Analysis

The equations and results of the paleohydraulic analysis are presented for the fluvial strata at Bull Canyon. A summary of the raw data used to carry out this workflow (2360 cross-set height measurements and d50 grain size) is shown in Figure 8 and Table 1. The results of the workflow are summarized in Figure 10.

Paleoslope (S)

Channel slope is estimated via an empirical relationship proposed by Parker et al. (1998) and modified by Lynds (2005) for sand-bed rivers. It is a variation of Paola and Mohrig's (1996) relationship for gravel-bed rivers. In this equation, *T*, is the product of multiplying an empirically derived nondimensional bankfull shear stress (1.65) and the submerged specific gravity of sediment (1.65 for quartz). d50 is the median grain size of bedload, and it varies with each depositional unit. Slope is presented as a dimensionless gradient (rise/run).

$$S = (T \times d50)/H \quad (8)$$

Channel slope decreases from DU-0 to DU-2 from 0.00023 to 0.00011, rapidly increases from DU-2 to DU-5 from 0.00011 to 0.00036, and is marked by

a relatively steep gradient in DU-6 (mean – 0.00024). Overall these estimates are comparable to modern, low-gradient distributive fluvial systems that exist on or near coastal- and delta-plains such as the Nile river delta and the Danube delta plain (Jerolmack and Mohrig, 2007).

Backwater Length (L_w)

Backwater length is approximated using a simple equation which relates bankfull depth and slope (Hajek and Wolinsky, 2012). Backwater length is defined as the upstream extent of river flow that is affected by hydrodynamic processes in the receiving basin (Chatanantavet et al., 2012). This zone is of particular interest because it represents in area in which river morphology can vary significantly from upstream reaches.

$$L_w \approx \frac{H}{S} \tag{9}$$

Estimates of backwater length are highly variable in the John Henry Member. Within the seven depositional units, minimum, median, and maximum values span a range of 115 km (71.5 mi) (minimum of 4 km in DU-5 and maximum of 122 km in DU-2 [2.5 mi in DU-5 and 75.8 mi in DU-2]). Because backwater length is partly derived from channel slope, the trends present through the stratigraphic interval mimic those of channel slope. Mean backwater length increases from DU-0 to DU-2 from 26 to 56 km (16 to 35 mi), decreases from

DU-2 to DU-5 from 56 to 10 km (35 to 6 mi), and closes at a distance of 28 km (17 mi) in DU-6.

Flow Velocity (V)

Flow velocity is estimated qualitatively using the bedform-phase diagrams of Rubin and McCulloch (1980) (Appendix C). Empirical and flume studies have shown that flow velocity can be estimated from three parameters: bankfull depth, median bedload grain size, and dominant bedform type. In this case bankfull depth and median bedload grain size varies with each depositional unit; however, the dominant bedform type, 3-D dunes (as recorded by trough cross-bedding), remains the same. Estimated flow velocities range from 0.65 m/s to 1.65 m/s (2.13 ft/s to 5.41 ft/s).

Bankfull Discharge (Q)

Bankfull discharge is estimated using the method of Bhattacharya and Tye (2004) which multiplies the bankfull channel cross-sectional area (B*H) and flow velocity (V).

$$Q_w = 0.65(B \times H) \times V \qquad (10)$$

Estimated discharge is highly variable and ranges from 70 to 6,000 m^3s^{-1} (2,472 to 211,887 ft^3s^{-1}). Depositional units 0, 1, 2 and 6 are characterized by discharge ranging from 320 to 6,000 m^3s^{-1} (11,301 to 211,887 ft^3s^{-1}).

Depositional units 3, 4, and 5 are characterized by lower discharge ranging from 70 to 1,600 m^3s^{-1} (2,472 to 56,503 ft^3s^{-1}). The uncertainty associated with these numbers is high (e.g., wide bars showing bankfull discharge estimates; Figure 10) because these estimates are the result of combining a number of previously estimated parameters including bankfull depth, bankfull channel width, and flow velocity.

Drainage Area (A)

Discharge (Q) is strongly correlated with drainage area (Hajek and Wolinsky, 2012). The equation to estimate drainage area relates discharge with a constant precipitation rate (P [m/s]). This empirical relationship was derived from rivers around the world under mean bankfull flow conditions. The precipitation rate is held constant at 0.5 m/yr (1.6 ft/yr) (Hajek and Wolinsky, 2012).

$$A \approx Q_w/P \tag{11}$$

Estimates of drainage area are variable across depositional units, and mean values range from 23,000 km^2 to 122,000 km^2 (8,880 to 47,104 mi^2). Similar to bankfull discharge estimates, the depositional units can be broken out into two populations, one with higher values than the other. Depositional units 0, 1, 2, and 6 are characterized by mean values ranging from 80,000 km^2 to 122,000 km^2 (30,888 to 47,104 mi^2) while depositional units 3, 4, and 5 are

characterized by mean values ranging from 23,000 km^2 to 34,000 km^2 (8,880 to 13,127 mi^2).

Distance from Source (L)

Distance from source (*L*) is estimated using Hack's Law, an empirical equation relating the length of streams and the area (*A*) of their basins (Hack, 1957). Hack developed the power function by studying river basins in the eastern USA. Gary (1961) refined the analysis and found the exponent in the power law to be 0.568. L is explicitly defined as the length of the longest stream, in a straight line, from the outlet to the divide.

$$L = 1.4 (A^{0.568}) \quad (12)$$

Estimates of distance from source across the seven depositional units range from 150 to 1950 km (93 to 1212 mi). Mean values range from 800 to 1000 km (497 to 621 mi) in depositional units 0, 1, 2, and 6 and from 400 to 500 km (249 to 311 mi) in depositional units 3, 4, and 5.

Facies Modeling

The goal of the facies modeling was to recreate the alluvial architecture of the John Henry Member at Bull Canyon as closely as possible. Channel belt orientation, channel belt form, and target net-to-gross are derived from the conceptual model of river system morphology while statistical distributions of

channel belt orientation, channel belt width, channel belt thickness, meander wavelength, and meander amplitude reflect results and observations from the alluvial architecture characterization and paleomorphodynamic workflow. Data from each of the 30 realizations confirm that the object-based modeling algorithm was able to adequately match target model input parameters (Table 3) including facies proportions, paleochannel form, and paleochannel orientation. Additionally, the visual comparison in Figure 11 shows that runs 5, 10, 15, 20, and 25 exhibit a high level of similarity to the digital outcrop model above depositional unit 0. Channel belt boundaries are difficult to delineate in outcrop in depositional unit 0 and therefore, the digital outcrop model fails to capture the total net-to-gross in that unit. The results of the static connectivity analysis are reserved for the discussion portion of this study as it is beneficial to first present the conceptual model of river system morphology.

Figure 8 – Paleocurrent (PC), accretion set (AC), and cross-set height measurements from Bull Canyon. Dot-marks indicate average flow/accretion direction for each depositional unit. Rose diagrams are oriented so that north is up. Blue colored zones mark 45° on either side of the average flow direction. Accretion measurements within the blue zone are considered to be downstream accreting. The yellow zones each include 90° areas with their centers oriented perpendicular to the mean paleocurrent. Accretion measurements within the yellow zones are considered to be laterally accreting. Histograms and cumulative distribution functions summarize measured cross-set heights in Bull Canyon. The average cross-set height and the standard deviation are listed for each of the seven depositional units.

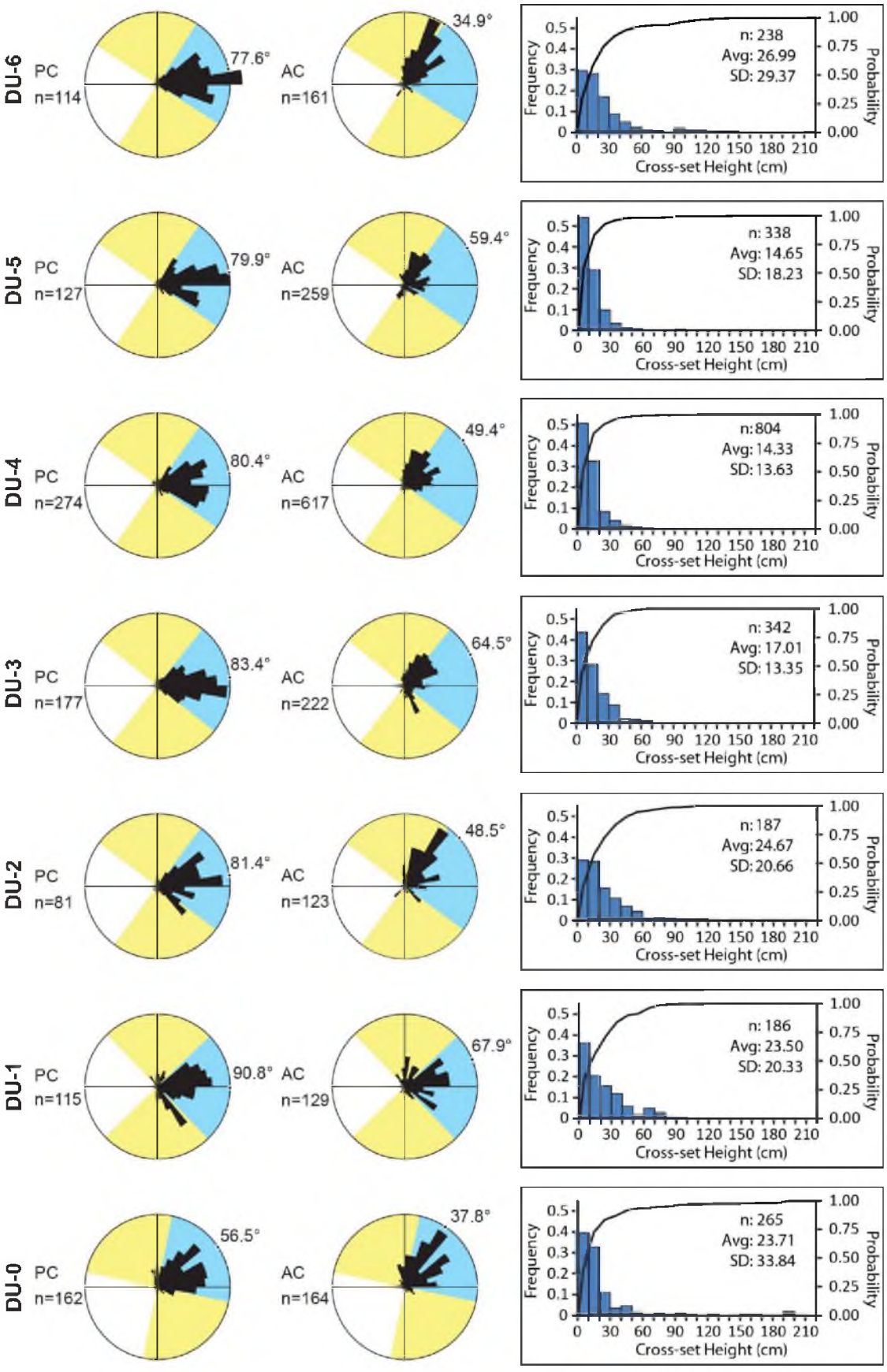
DU-6
PC
n=114
77.6°
AC
n=161
34.9°
n: 238
Avg: 26.99
SD: 29.37
DU-5
PC
n=127
79.9°
AC
n=259
59.4°
n: 338
Avg: 14.65
SD: 18.23
DU-4
PC
n=274
80.4°
AC
n=617
49.4°
n:804
Avg: 14.33
SD: 13.63
DU-3
PC
n=177
83.4°
AC
n=222
64.5°
n: 342
Avg: 17.01
SD: 13.35
DU-2
PC
n=81
81.4°
AC
n=123
48.5°
n: 187
Avg: 24.67
SD: 20.66
DU-1
PC
n=115
90.8°
AC
n=129
67.9°
n: 186
Avg: 23.50
SD: 20.33
DU-0
PC
n=162
56.5°
AC
n=164
37.8°
n: 265
Avg: 23.71
SD: 33.84
Frequency
Probability
Cross-set Height (cm)
0 30 60 90 120 150 180 210
0 0.1 0.2 0.3 0.4 0.5
0.00 0.25 0.50 0.75 1.00

Table 2

Channel Belt Dimensions Measured in Outcrop

	n	Average Width	Max Width	Min Width	Width Standard Deviation	Average Thickness	Max Thickness	Min Thickness	Thickness Standard Deviation	Average W/T Ratio
DU 6	16	181.16	360.90	77.64	83.05	3.45	5.85	1.67	1.56	52.51
DU 5	25	230.41	733.48	23.05	194.90	4.01	8.75	0.60	1.54	57.46
DU 4	66	161.91	637.31	12.45	143.08	3.78	6.93	1.17	1.25	42.83
DU 3	36	66.05	216.74	19.54	39.61	2.12	4.67	0.56	0.90	31.16
DU 2	41	88.28	273.27	14.50	65.14	2.86	5.93	0.76	1.32	30.87
DU 1	8	82.04	141.37	36.52	39.71	2.63	6.27	0.88	1.73	31.20

Table 2 Continued

	n	Average Width	Max Width	Min Width	Width Standard Deviation	Average Thickness	Max Thickness	Min Thickness	Thickness Standard Deviation	Average W/T Ratio
DU 0	4	273.06	455.90	142.35	132.94	6.00	6.82	4.84	0.83	45.55

*All units presented in meters (m)
W/T: Width-to-thickness

Figure 9 – Results of the paleochannel reconstruction workflow. Six distinct parameters are presented. The y-axis remains the same across all plots, while the units and the scale of the x-axis vary.

Paleochannel Reconstruction

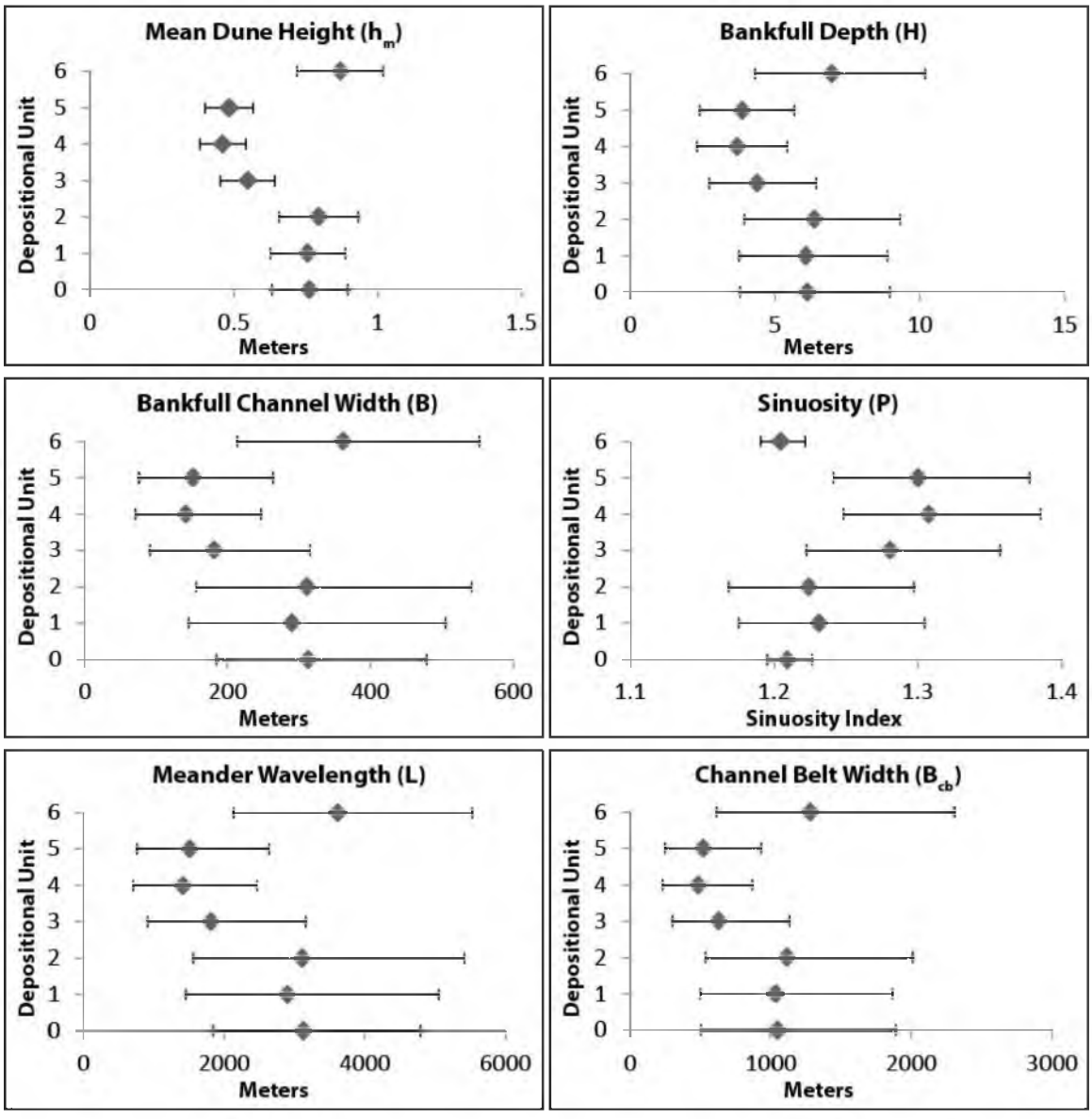

Figure 10 – Results of the paleohydraulic analysis workflow. Six distinct parameters are presented. The y-axis remains the same across all plots while the units, and the scale of the x-axis vary.

Paleohydraulic Analysis

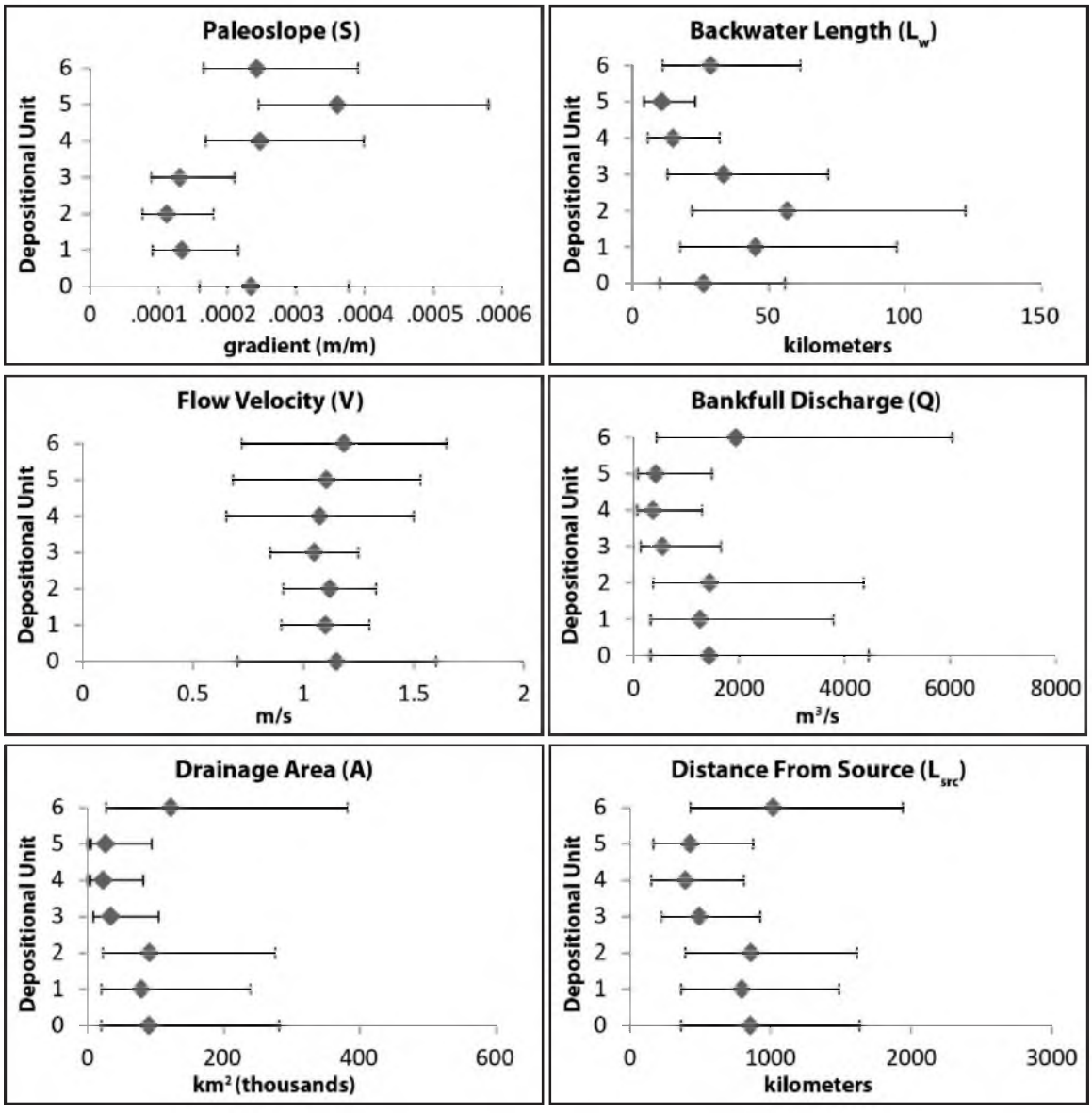

Table 3

Model Input Distributions

	Target Net-to-Gross	Channel Orientation (°)	Channel Width (m)	Channel Thickness (m)
		Min – Med – Max	Min – Med – Max	Min – Med – Max
DU6	99.00%	57.6 – 77.6 – 97.6	77.6 – 181.2 – 360.9	1.7 – 3.5 – 5.9
DU5	40.00%	59.9 – 79.9 – 99.9	23.1 – 230.4 – 733.5	0.6 – 4.0 – 8.8
DU4	32.00%	60.4 – 80.4 – 100.4	12.5 – 161.9 – 637.3	1.2 – 3.8 – 4.7
DU3	12.00%	63.4 – 83.4 – 103.4	19.5 – 66.1 – 216.7	0.6 – 2.1 – 4.7
DU2	30.00%	61.4 – 81.4 – 101.4	14.5 – 88.3 – 273.3	0.8 – 2.9 – 5.9
DU1	22.00%	70.8 – 90.8 – 110.8	36.5 – 82.0 – 141.4	0.9 – 2.6 – 6.3
DU0	75.00%	36.5 – 56.5 – 76.5	142.4 – 273.1 – 455.9	4.8 – 6.0 – 6.8

Table 3 Continued

	Meander Wavelength (m) Min – Med – Max	Meander Amplitude (m) Min – Med – Max	Vertical Trend Conditioning	Measured Section Conditioning # of Cells
DU6	2130 – 3620 – 5530	213 – 362 – 553	Yes	134
DU5	760 – 1515 – 2640	228 – 455 – 791	Yes	155
DU4	710 – 1420 – 2465	213 – 425 – 740	Yes	585
DU3	200 – 660 – 2170	20 – 66 – 217	Yes	88
DU2	150 – 880 – 2730	15 – 80 – 273	Yes	65
DU1	370 – 820 – 1410	37 – 82 – 141	Yes	25
DU0	1845 – 3130 – 4790	184 – 313 – 479	Yes	13

Figure 11 – Visual comparison of five model realizations (5, 10, 15, 20, and 25) and the digital outcrop model (top left). Cells that intersect the east canyon wall of Bull Canyon were isolated from each run in order to achieve a simple comparison. Overall there is a high level of similarity between outcrop 'truth' and each facies model realization above depositional unit 0. Channel belt boundaries are difficult in delineate in outcrop in depositional unit 0 and therefore, the digital outcrop model fails to capture the total net-to-gross in that unit.

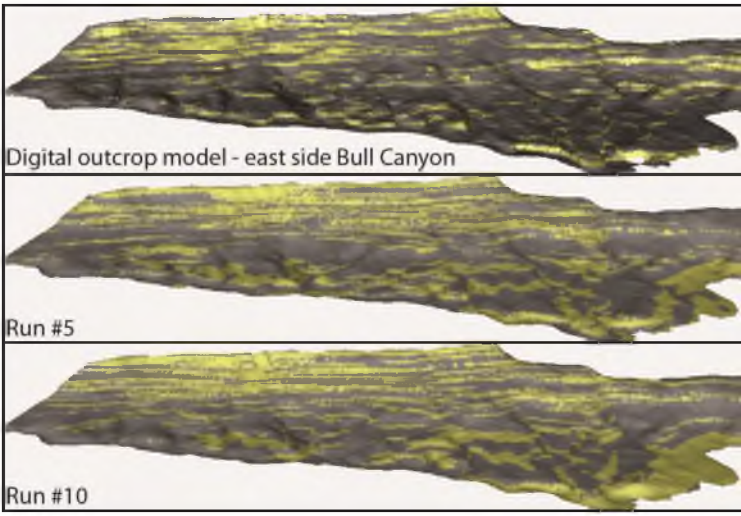
Digital outcrop model - east side Bull Canyon
Run #5
Run #10

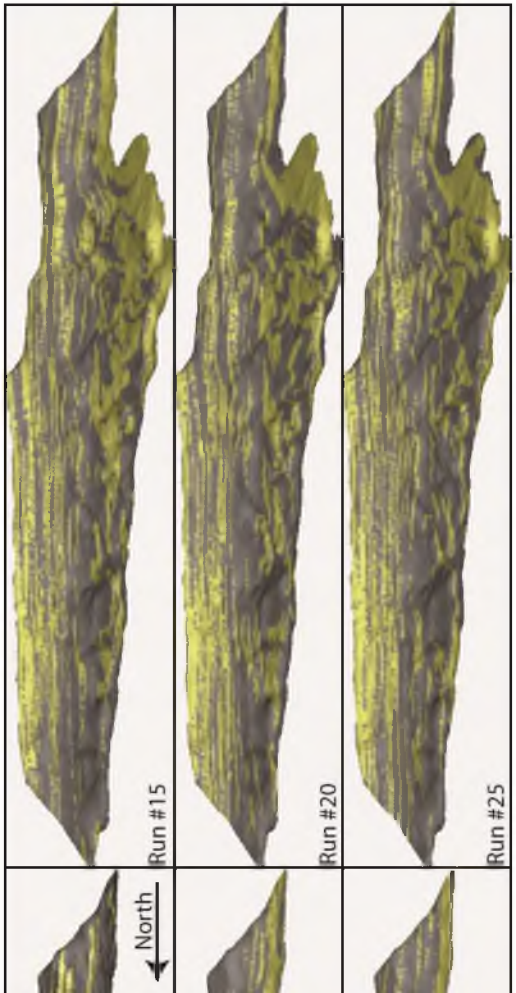
Run #15
Run #20
Run #25
North

DISCUSSION

Observations from the alluvial architecture characterization along with results of the paleochannel reconstruction and paleohydraulic analysis are used to define a 3-D conceptual model of river system morphology that shows temporal variability in fluvial style in the John Henry Member at Bull Canyon. The results of a static connectivity analysis provide evidence that suggest variability in fluvial style has implications for subsurface reservoir connectivity. Furthermore, the variability in fluvial style is discussed in the context of formative hydraulic conditions and autogenic sedimentary processes. Finally, the role and limitations of using scaling relationships to reconstruct channel dimensions is discussed as is the role of paleohydraulic estimates in supporting paleogeographic reconstructions.

Conceptual Model of River System Morphology

Observations from the alluvial architecture characterization are combined with results of the paleochannel reconstruction and paleohydraulic analysis in order to define a 3-D conceptual model of river system morphology in the John Henry Member (Figures 12, 13). Formative hydraulic conditions (i.e., flow depth, discharge, and slope), grain-size trends, dominant lithofacies, and dominant barform accretion direction were analyzed for each depositional unit. The

conceptual model reveals that fluvial style is highly variable in the John Henry Member. Specifically, results indicate depositional units 0 through 6 record a spectrum of fluvial styles that are transitional between braided, meandering, and straight planforms.

Depositional units 0 and 6 are interpreted as braided/meandering systems. These are high net-to-gross (>75%) units characterized by large channel belt complexes (181–273 m [594–896 ft] wide), coarse grain sizes (0.53–0.625 mm [0.020–0.024 in] sand), high bankfull discharges (1,431–1,939 m^3/s [50,535–68,475 ft^3/s]), steep paleoslopes (0.00024), and short backwater lengths (26–29 km [16–18 mi). Laterally extensive channel belt complexes indicate fluvial processes dominated by channel-belt migration rather than avulsion. Undulating scour surfaces are common and, in a few cases, marked by several meters of relief. Sand bodies in these two units are characterized by uniformly thick cross-sets (>26 cm [>10 in]) and the presence of gravel lithofacies including massive and trough cross-stratified matrix supported conglomerate.

Depositional units 4 and 5 are interpreted as meandering systems. Depositional units 4 and 5 are moderate net-to-gross (32.5–40%) units characterized by channel stories that coalesce to form extensive channel belts and, in some cases, channel belt complexes. Because channel stories show strong evidence of lateral accretion it is likely that fluvial processes were dominated by channel-belt migration rather than avulsion. Sand bodies in these two units are composed of fine-to-coarse grained sand (0.3385–0.516 mm [0.013–0.020 in]) and thin cross-sets (17 cm [7 in]). Paleomorphodynamic

calculations result in low bankfull discharges (366–421 m^3/s [12,925–14,867 ft^3/s]), steep paleoslopes (0.00030), short backwater zones (<15 km [<9 mi]), and moderate levels of sinuosity (sinuosity index 1.3).

Depositional units 1, 2, and 3 are interpreted as straight systems. These are low net-to-gross (12.5–30%) units characterized by narrow (82–88 m [269–289 ft]), laterally isolated channel belts encased in thick overbank successions. Sand bodies in depositional units 1 and 2 are predominantly composed of fine and/or lower-medium grained sand (0.2635–0.301 mm [0.010–0.012 in]) and are characterized by thick cross-sets (>26 cm [>10 in]). The grain size and scale of these sand bodies results in calculations of deep channels (6.5 m [21 ft] flow depth), high discharges (1,350 m^3/s [47,675 ft^3/s]), gentle paleoslopes (0.00012), and lengthy backwater zones (>45 km [>28 mi]). Furthermore, the paleochannel reconstruction in these two units results in low sinuosities (1.25 sinuosity index) and long meander wavelengths (3 km [1.9 mi]). Sand bodies in depositional unit 3 consist of fine-to-very fine grained sand (0.2125 mm [0.008 in]) and thin cross-sets (19 cm [7.5 in]), resulting in a calculation of low bankfull discharge (544 m^3/s [19,211 ft^3/s]). Additionally, depositional unit 3 is notable for the presence of laterally discontinuous coals, which, in some areas of Bull Canyon, can be up to 1 meter (3.3 ft) thick. In the absence of a significant change in basin configuration resulting in a reduced catchment size, low bankfull discharges along with the prevalence of coal suggest multiple channels simultaneously active and healthy interfluvial wetlands. In the case of all three units, sand body

stacking is aggradational, and the observed random dispersion of narrow, laterally isolated channel belts indicates avulsive depositional processes.

Static Reservoir Connectivity Analysis

Results of the static reservoir connectivity analysis are discussed in relation to the conceptual model of river system morphology. By coupling the measured stratigraphic data and conceptual models to analyze connectivity for different well spacings, conclusions are drawn regarding how temporal variability in alluvial architecture can impact subsurface reservoir connectivity. An important caveat is that static reservoir connectivity differs from dynamic connectivity in that it does not take into account porosity/permeability heterogeneity and therefore does not directly evaluate subsurface fluid flow (Larue and Hovadik, 2006).

Results of the static reservoir connectivity analysis in each depositional unit show that average connectivity is greater than 95% when net-to-gross is greater than 30% (Figure 14). This holds true no matter what the well spacing pattern, as is evident by the fact that depositional units 0, 4, 5, and 6 show nearly 100% connectivity at all four well spacing patterns. This result supports a prior observation that 3-D stratigraphic connectivity in channelized reservoirs is greater than 90% if net-to-gross is greater than 30% (Larue and Hovadik, 2006).

Cumulative gross connected sandstone volume (Figure 15) shows that the highest net-to-gross units, depositional units 0, 4, 5, and 6, contribute 80% of the total sand to the system. Furthermore these four units are associated with little

uncertainty in the amount of connected sand volume. This is in stark contrast to depositional units 1, 2, and 3, which contribute 20% of the total sand to the system and show significant uncertainty in the amount of connected sand volume at 640 and 2560 acre spacing.

When examining total connected sandstone volume per depositional unit (Figure 16), three distinct groups are apparent. Depositional units 0 and 6, the braided/meandering systems, show no uncertainty associated with total connected sand volumes. Depositional units 4 and 5, the meandering systems, also show no uncertainty associated with total connected sand volumes The wide bars associated with DUs 4 and 5 are attributed to the variability in the total amount of sand (connected or unconnected) across stochastic simulations. On the other hand, depositional units 1, 2, and 3, the straight systems, are associated with a significant level of uncertainty in total connected sand volume. Together, depositional units 1, 2, and 3 contribute 20% of the sand to the John Henry Member at Bull Canyon. However, at sparse well spacing patterns, such as 2560 acres, average reservoir connectivity across 30 stochastic model simulations for depositional units 1, 2, and 3 is only 63%. Forty percent of model runs show zero reservoir connectivity in at least one depositional unit of the lower John Henry Member at 2560 acre spacing. This means that although depositional units 1, 2, and 3 contribute one-fifth of the total sand volume to the system they have the potential to be completely missed during field development.

Depositional units 1, 2, and 3 are notable for channel belts that are straight, narrow, and highly dispersive. This sort of reservoir geometry, or

dimensionality, leads to the compartmentalization of parallel and continuous channel belts. Consequently, static reservoir connectivity diminishes in the lower John Henry Member. Unlike the laterally continuous meander-belts of depositional units 4 and 5 or the multistoried channel belt complexes of depositional units 0 and 6, units 1, 2, and 3 lack sand body connectedness.

Depositional Controls on Reservoir Dimensionality

A number of authors have proposed explanations for the variability in alluvial architecture evident in the John Henry. Shanley and McCabe (1991, 1993) interpret eustatic sea level as the primary allogenic control on architectural trends, while Little (1995, 1997) and Pettinga (2013) interpret hinterland tectonics as the primary allogenic control. Alluvial architectural trends are likely the product of complex interaction between allogenic controls and autogenic sedimentary processes. Recent studies (Jerolmack and Paola, 2007; Sheets et al., 2007; Wang et al., 2011; Hajek and Wolinsky, 2012; Hajek et al., 2012; Hampson et al., 2013) emphasize the importance of autogenic, or 'internal', processes (i.e., avulsion) in sedimentary systems and stress a need for further understanding of autogenic stratigraphy in order to provide the most plausible interpretations of alluvial basin fill. Previous studies in the John Henry Member have not addressed how changing basin boundary conditions influence autogenic sedimentary processes such as avulsion.

Backwater hydraulic conditions are known to cause changes in autogenic sedimentary processes including heightened avulsion frequency (Chatanantavet

et al., 2012; Milliken et al., 2012). The backwater zone is an area proximal to the shoreline in which rivers behave fundamentally different because they are affected by static water in the receiving basin (Chow, 1959). Chatanantavet et al. (2012) show that flow deceleration near the upstream extent of the backwater zone causes enhanced deposition and reduced channel-fill timescales, both mechanisms that favor preferential avulsion. Flow deceleration also diminishes stream power and bank erodibility which leads to straight channel planforms towards the river mouth (Gouw and Berendsen, 2007). Observations from modern depositional environments show that many deltaic rivers tend to avulse at a nodal avulsion point that sits at a distance upstream from the shoreline equal to the backwater length (Jerolmack and Swenson, 2007) (Figure 17). Recent studies have also shown that during high discharge events the backwater zone can transform into an area of riverbed erosion (Nittrouer et al., 2011; Lamb et al., 2012; Shaw et al., 2013). This is the case when normal flow depth is larger than the water depth at the river mouth, causing drawdown of the water surface and consequently flow acceleration (Figure 18).

Calculations of backwater length are correlated with temporal trends in fluvial style in the John Henry Member. Depositional units 1, 2, and 3 exhibit characteristics that suggest these units were subject to backwater hydraulic effects. The characteristics include channel deepening, reduced sinuosity, and avulsive character. The laterally restricted channel belts reflect a short period of activity of the formative channel due to frequent avulsions over an unconstrained coastal plain. Lengthening the backwater zone during deposition of units 1, 2,

and 3 could have been caused by a relative rise in base level driven by a change in basin boundary conditions. Barth et al. (2004) estimate a significant reduction in Maria thrust belt activity at approximately 86 Ma and DeCelles, and Coogan (2006) propose a contemporaneous activation of the Paxton thrust sheet in the Servier thrust belt. These two events may have led to an increases in basin subsidence and a corresponding rise in base level during deposition of the lower John Henry Member. Even if the magnitude of these tectonic events were small and their effect on basin subsidence minor, it only requires a slight rise in base level over a low-sloping coastal plain to significantly lengthen the zone of backwater influence. For example, a 2 meter rise in base level over a low-sloping coastal plain (gradient - 0.00013) could extend the zone of backwater influence by 15 kilometers (9.3 miles) (equation 9).

Results of the static connectivity analysis show that backwater affected zones have lower total sand body connectivity than zones that are not influenced by backwater hydraulics. Channel belts in the lower John Henry Member are straight, narrow, and highly dispersive, creating a reservoir dimensionality characterized by the compartmentalization of parallel channel belts. Furthermore, backwater hydraulic affects may have implications for sediment volume partitioning and source to sink relationships. As discussed earlier, recent studies, including that of Lamb et al. (2012), have shown that during high discharge events the backwater zone transforms into an area of riverbed erosion due to drawdown of the water surface and acceleration of flow towards the river mouth (Figure 18). Fluvial erosion during high discharge events decreases the

likelihood of sand preservation in the backwater zone and consequently enhances sediment delivery basinward. In the lower John Henry Member it is possible that sand may be preferentially preserved downdip of the shoreline due to sediment bypass of the backwater zone during high discharge events. This relationship is important when delineating the spatial distribution of key reservoir facies and may explain why there is a significant decrease in sand volume (net-to-gross) in the lower John Henry Member.

Limitations of Using Scaling Relationships

Scaling relationships in fluvial systems have been used to reconstruct paleochannel dimensions such as width and thickness. Knowing the approximate size of a fluvial sand body can help guide subsurface interpretations and correlations as well as help predict the spatial extent of fundamental reservoir flow units such as channel belts (Milliken et al., 2012). Scaling relationships, examples of which are found in the paleochannel reconstruction workflow, are often derived from modern systems or Quaternary deposits (Gibling, 2006b; Miall, 2006; Gouw and Berendsen, 2007; Milliken et al., 2012). Miall (2006) cautions that applying scaling relationships to ancient fluvial systems is problematic because studies of modern systems cannot address the question of long-term preservation, and fluvial successions are often characterized by significant variability in fluvial style over short distances and vertical intervals. Although using scaling relationships provides a good starting point for conducting

subsurface interpretations and correlations, the limitations of such a workflow are reverberated here.

Two key conclusions arise from reconstructing fluvial form in the John Henry Member: (1) fluvial style can change rapidly over short vertical intervals and (2) channel belt development is dependent on the period of activity of the formative channel. Variability in fluvial style highlights the necessity of using a suite of scaling relationships in order to adequately capture vertical heterogeneity in alluvial architecture. As an example, if flow depth is held equal, braided and meandering systems will develop channel stories of different widths because braided systems are characterized by downstream accretion while meandering systems are characterized by lateral accretion. Therefore two separate scaling relationships, such as equations 3 and 4, are necessary in order to accurately capture the variability in channel width. Additionally, using scaling relationships to estimate channel belt widths (see equation 7) in highly avulsive systems is problematic. Because of the highly avulsive nature of river systems influenced by backwater hydraulics, formative channels avulse frequently and therefore, channel belts may never fully develop. In depositional units 1 and 2, results of the paleochannel reconstruction indicate average channel belt widths of 1 kilometer (0.62 mi). Measurements at the outcrop differ from this prediction; however, actual average channel belt widths are only 80 meters (262 ft) (Table 2). This highlights the importance of considering possible backwater effects when using scaling relationships to reconstruct channel belt dimensions.

Paleohydraulic Analysis in Support of Paleogeographic Reconstructions

Recent studies have proposed using workflows, similar to the paleohydraulic analysis presented here, to place quantitative constraints on paleogeographic reconstructions. Davidson and North (2009) and Davidson and Hartley (2010) conclude that by utilizing established relationships between bankfull discharge and drainage area derived from modern systems it is possible to determine first-order estimates of catchment size in ancient fluvial successions and use those estimates to quantitatively constrain paleogeographic reconstructions. Results of the paleohydraulic analysis for the fluvial sand bodies at Bull Canyon were compared to the areal dimensions of a reconstruction of the Cordilleran foreland basin during deposition of the John Henry Member from Szwarc (2014). A paleodrainage area of approximately 115,000 km^2 (44,402 mi^2) and a maximum straight line distance from outlet to divide of approximately 525 km (326 mi) can be calculated from Szwarc's map. These numbers are consistent with the paleohydraulic analysis carried out in Bull Canyon. Estimates of drainage area are in the range of 23,000–122,000 km^2 (8,880–47,104 mi^2), and estimates of distance from source range from 39–1,000 km (24–621 mi). It is important to note that the results of the paleohydraulic analysis represent estimates and are associated with considerable error (e.g., wide bars indicating values that range from -80% to +200%; Figure 10). Nevertheless the consistency of these calculations with Szwarc's reconstruction lends confidence to using a paleohydraulic workflow to place quantitative constraints on paleogeographic reconstructions.

A number of different approaches could be used to strengthen the drainage area estimates with the most notable being a more complete understating of precipitation rates during Santonian–Campanian time. Additionally the use of regional hydraulic geometry curves, as has been proposed by Davidson and North (2009) and Davidson and Hartley (2010), could potentially lead to a better assessment of the uncertainty associated with catchment size estimations. Regional hydraulic geometry curves relate drainage area size to bankfull discharge in small geographic regions and account for the catchment response to specific climates, lithologies, and hydrologic processes.

Figure 12 – Conceptual model of river system morphology in the John Henry Member at Bull Canyon. Observations from the alluvial architecture characterization along with results of the paleochannel reconstruction and paleohydraulic analysis are used to define a 3-D conceptual model. The figure illustrates how depositional units 0 through 6 record a spectrum of fluvial styles that are transitional between braided, meandering, and straight planforms. Plan- and cross-sectional views are presented as well as a summary list of distinguishing characteristics.

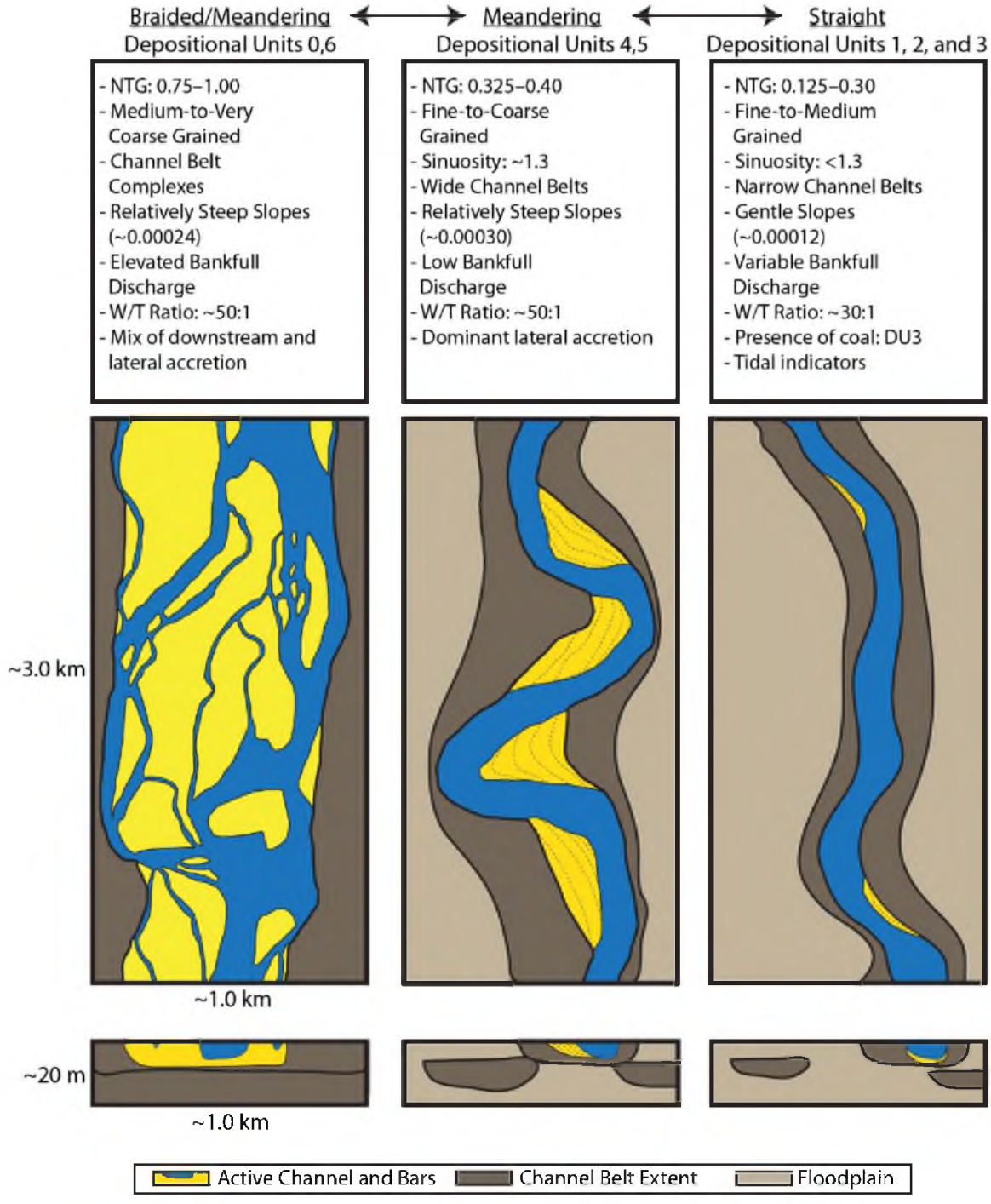
Braided/Meandering
Depositional Units 0,6
- NTG: 0.75–1.00
- Medium-to-Very Coarse Grained
- Channel Belt Complexes
- Relatively Steep Slopes (~0.00024)
- Elevated Bankfull Discharge
- W/T Ratio: ~50:1
- Mix of downstream and lateral accretion
Meandering
Depositional Units 4,5
- NTG: 0.325–0.40
- Fine-to-Coarse Grained
- Sinuosity: ~1.3
- Wide Channel Belts
- Relatively Steep Slopes (~0.00030)
- Low Bankfull Discharge
- W/T Ratio: ~50:1
- Dominant lateral accretion
Straight
Depositional Units 1, 2, and 3
- NTG: 0.125–0.30
- Fine-to-Medium Grained
- Sinuosity: <1.3
- Narrow Channel Belts
- Gentle Slopes (~0.00012)
- Variable Bankfull Discharge
- W/T Ratio: ~30:1
- Presence of coal: DU3
- Tidal indicators
~3.0 km
~1.0 km
~20 m
~1.0 km
Active Channel and Bars
Channel Belt Extent
Floodplain

Figure 13 – Crossplot showing how the paleorivers of each depositional unit plot in relation to bankfull discharge and slope. The relationship, summarized by Bridge (2003), states that channel pattern primarily depends on formative hydraulic conditions such as discharge, sediment load, and slope. Figure modified from Bridge (2003).

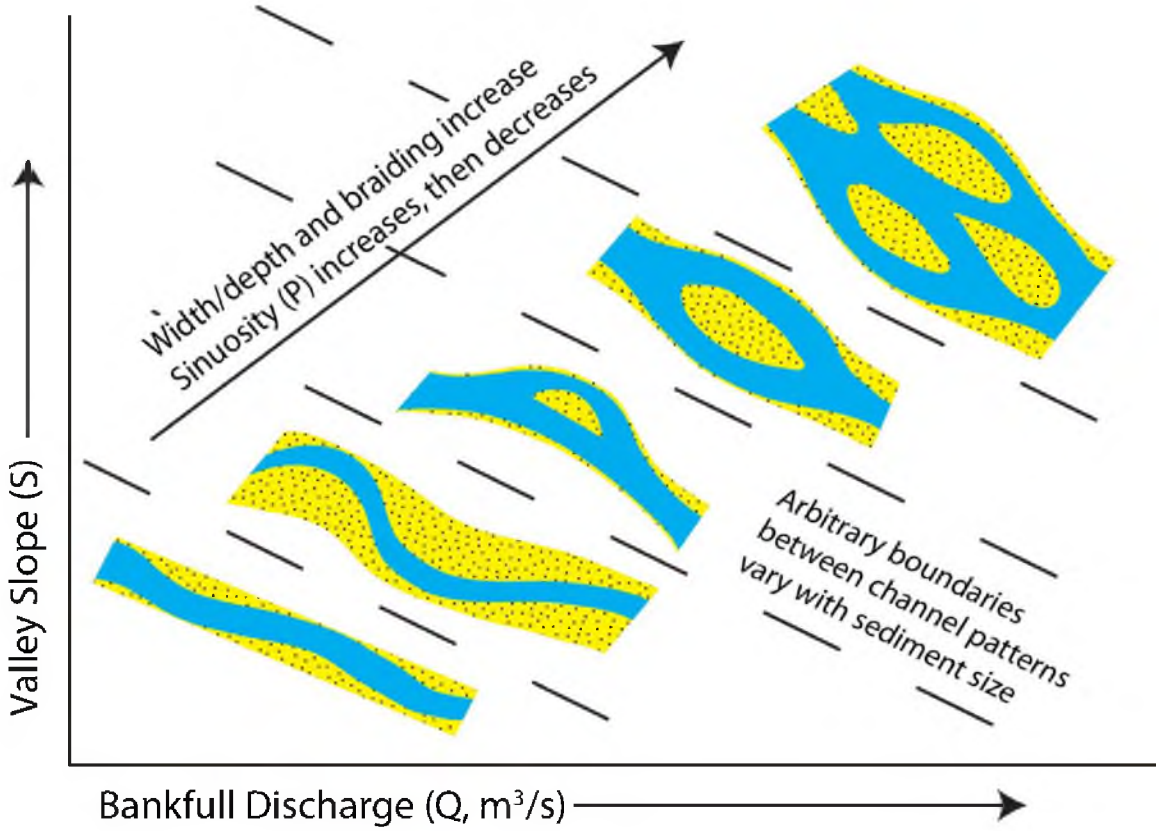
Width/depth and braiding increase
Sinuosity (P) increases, then decreases
Arbitrary boundaries between channel patterns vary with sediment size
Valley Slope (S)
Bankfull Discharge (Q, m³/s)

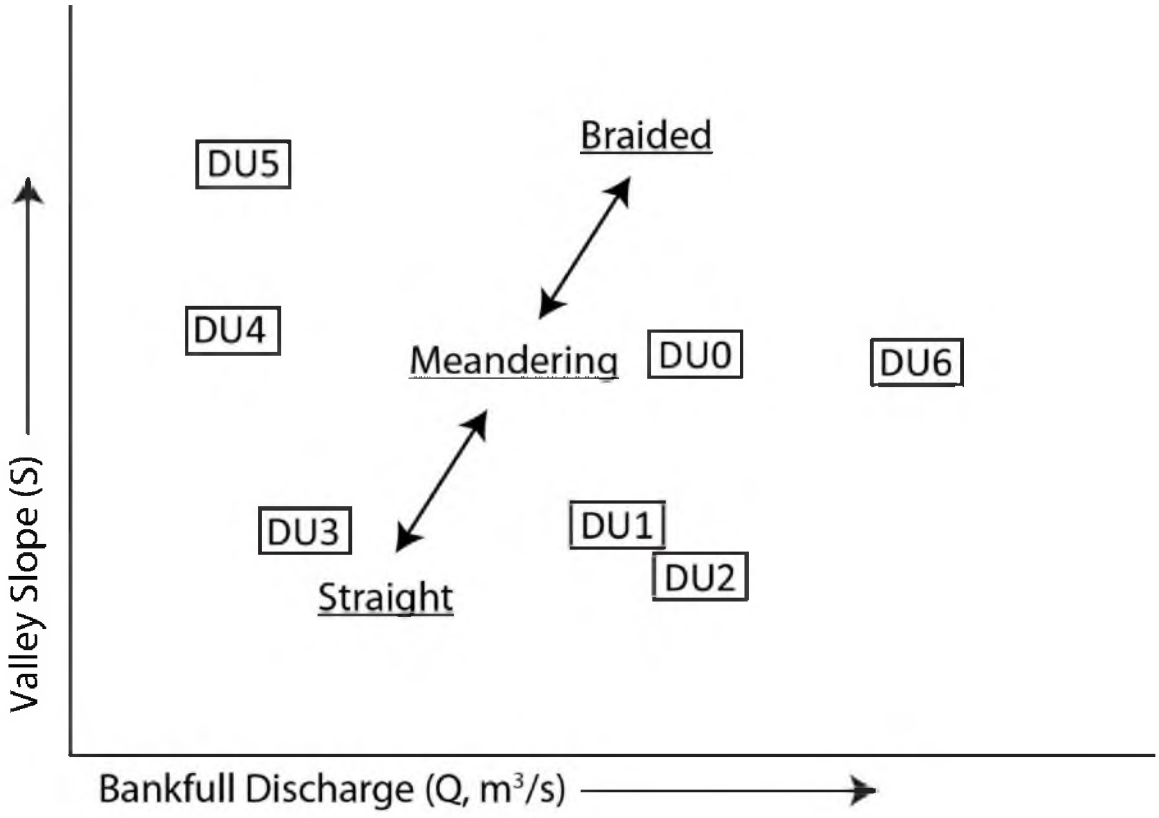
DU5
Braided
DU4
Meandering
DU0
DU6
DU3
DU1
DU2
Straight
Valley Slope (S)
Bankfull Discharge (Q, m³/s)

Figure 14 – Average reservoir connectivity (%) in each depositional unit at four unique well spacing patterns. In depositional units characterized by a net-to-gross less than or equal to 30% (DUs 1, 2, and 3) average reservoir connectivity decreases for sparse well spacing patterns.

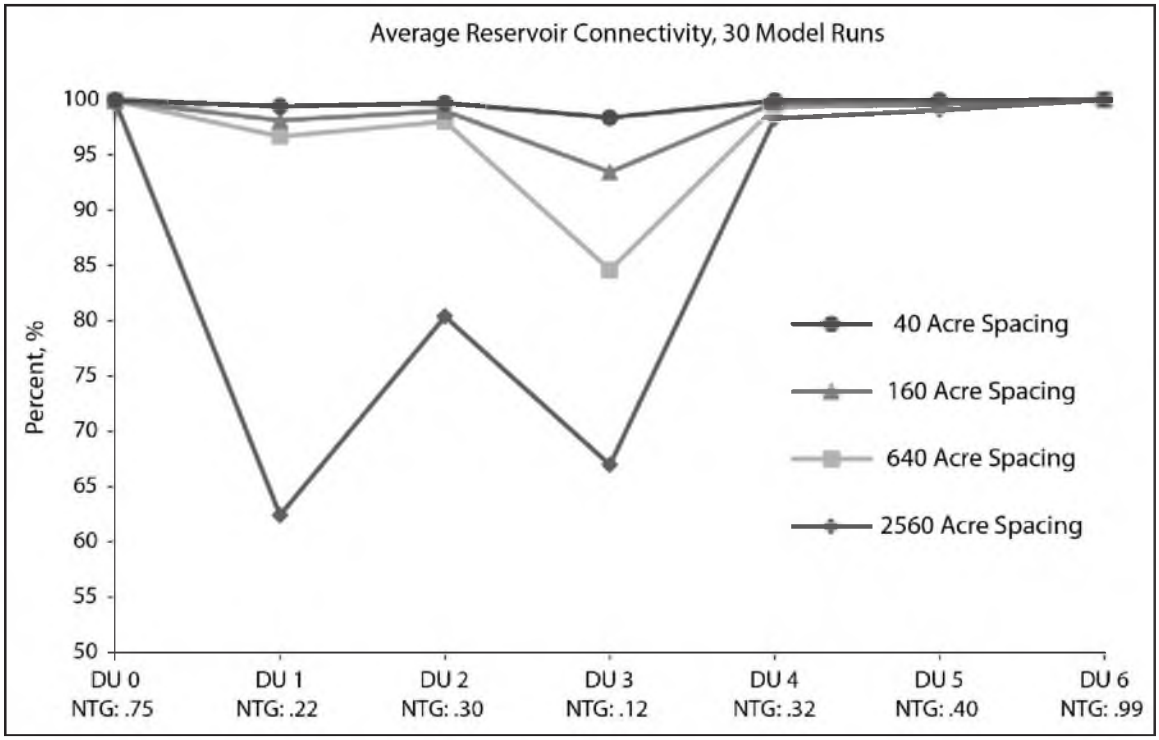
Average Reservoir Connectivity, 30 Model Runs
Percent, %
100
95
90
85
80
75
70
65
60
55
50
DU 0
NTG: .75
DU 1
NTG: .22
DU 2
NTG: .30
DU 3
NTG: .12
DU 4
NTG: .32
DU 5
NTG: .40
DU 6
NTG: .99
40 Acre Spacing
160 Acre Spacing
640 Acre Spacing
2560 Acre Spacing

Figure 15 – Cumulative gross connected sandstone volume (km^3) at four well spacing patterns. Depositional units 0, 4, 5, and 6 contribute the most sand volume to the system and are highly connected at all times. Depositional units 1, 2, and 3 contribute the least amount of sand to the system and are associated with the highest levels of connectivity uncertainty at sparse well spacing patterns.

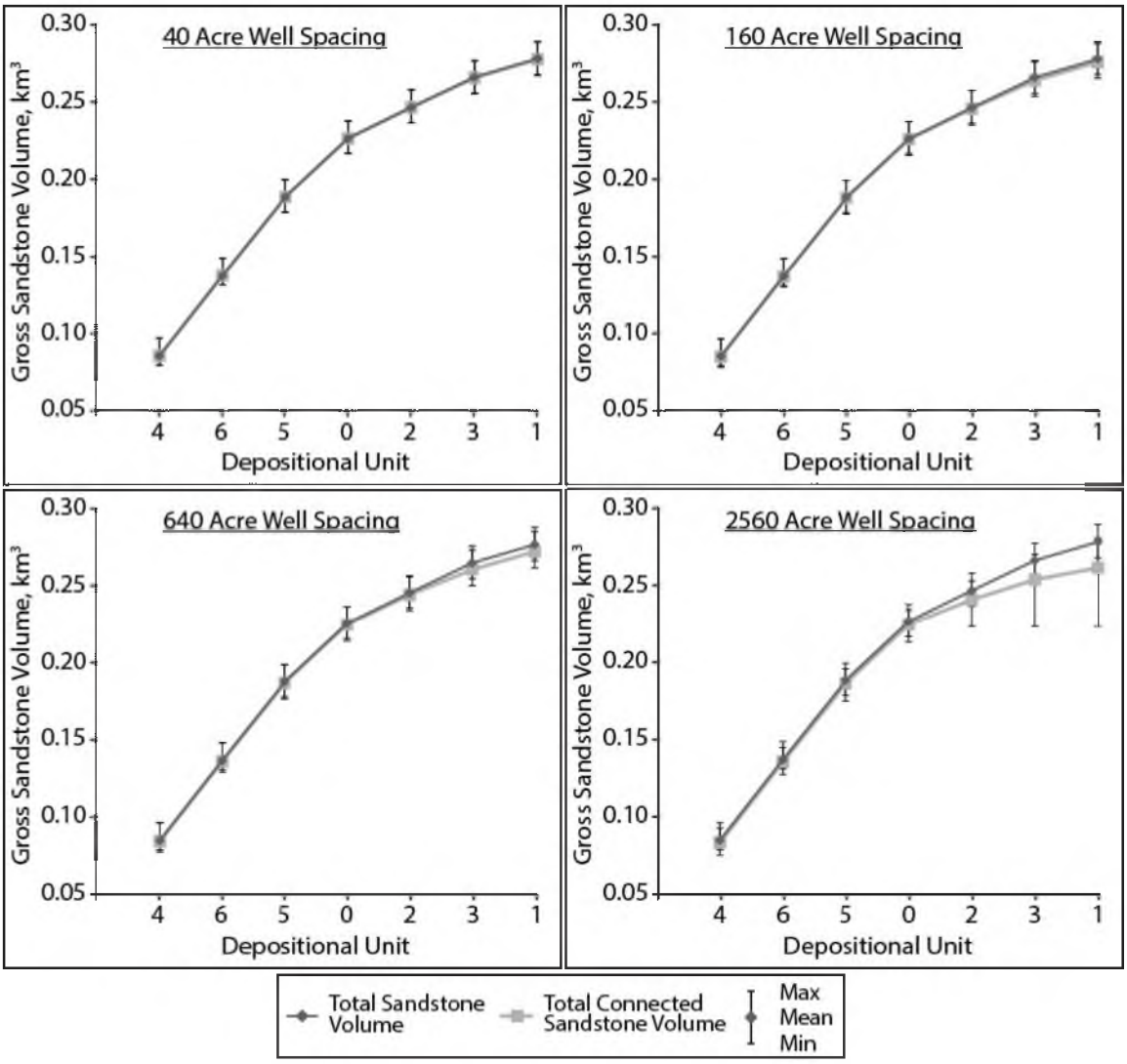
40 Acre Well Spacing
160 Acre Well Spacing
640 Acre Well Spacing
2560 Acre Well Spacing
Gross Sandstone Volume, km³
0.30
0.25
0.20
0.15
0.10
0.05
4 6 5 0 2 3 1
Depositional Unit
Total Sandstone Volume
Total Connected Sandstone Volume
Max
Mean
Min

Figure 16 – Total sandstone volume per depositional unit and total connected sandstone volume per depositional unit. (A) Total sandstone volume per depositional unit. (B, C, D, E) Total connected sandstone volume per depositional unit at each of the four well spacing patterns. Depositional units 0, 4, 5, and 6, the braided/meandering systems, show no uncertainty associated with total connected sand volumes, even though the total amount of sand (connected or unconnected) in the meandering systems varies across stochastic simulations. The large range of uncertainty in depositional units 1, 2, and 3 is associated with increasingly irregular connectivity values at sparse well spacing patterns. Depositional units 1, 2, and 3 represent the straight/anastomosing systems, and channel belts in these three units tend to be straight, narrow, and highly dispersive.

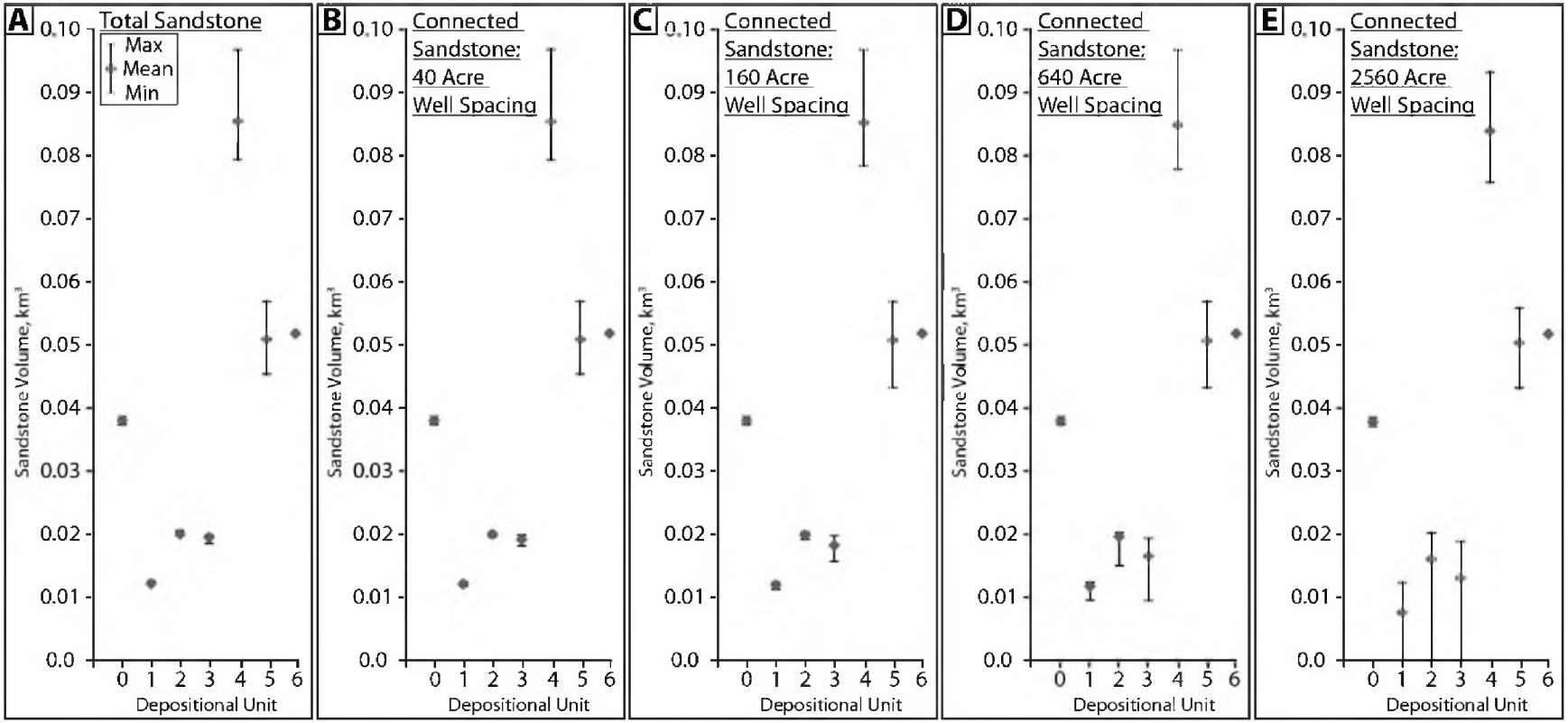
A
Total Sandstone
Max
Mean
Min
B
Connected Sandstone: 40 Acre Well Spacing
C
Connected Sandstone: 160 Acre Well Spacing
D
Connected Sandstone: 640 Acre Well Spacing
E
Connected Sandstone: 2560 Acre Well Spacing
Sandstone Volume, km³
0.0
0.01
0.02
0.03
0.04
0.05
0.06
0.07
0.08
0.09
0.10
0 1 2 3 4 5 6
Depositional Unit

Figure 17 – Satellite images of fluvial distributary networks. Each fluvio-deltaic setting shows a high degree of wave influence. Known backwater lengths, L_w, are taken from published data (Abdel-Fattah et al., 2004; Jerolmack and Mohrig, 2007). Unknown backwater lengths are postulated. Slope is calculated by the author. Satellite images courtesy of Google Earth.

	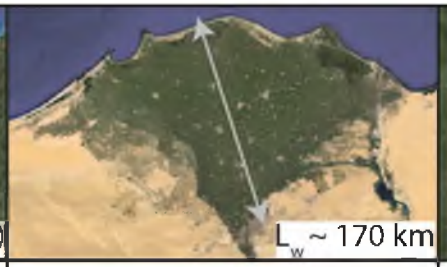		
Grijalva River Gradient of distributary network: 0.000037	Nile River 0.00023	Zambezi River 0.00018	Danube River 0.000012

Figure 18 – Schematic cross section of a river as it approaches and enters the receiving basin. L_w represents the length of the backwater zone. At low discharge (blue line) the water depth at the shoreline (h_s) is greater than the normal flow depth (h_n). This results in deceleration of flow in the backwater zone. At high discharge (red line) the water depth at the shoreline (h_s) is less than the high discharge flow depth (h_d). This results in drawdown of the water surface and acceleration of flow in the backwater zone. Figure modified from Lamb et al. (2012).

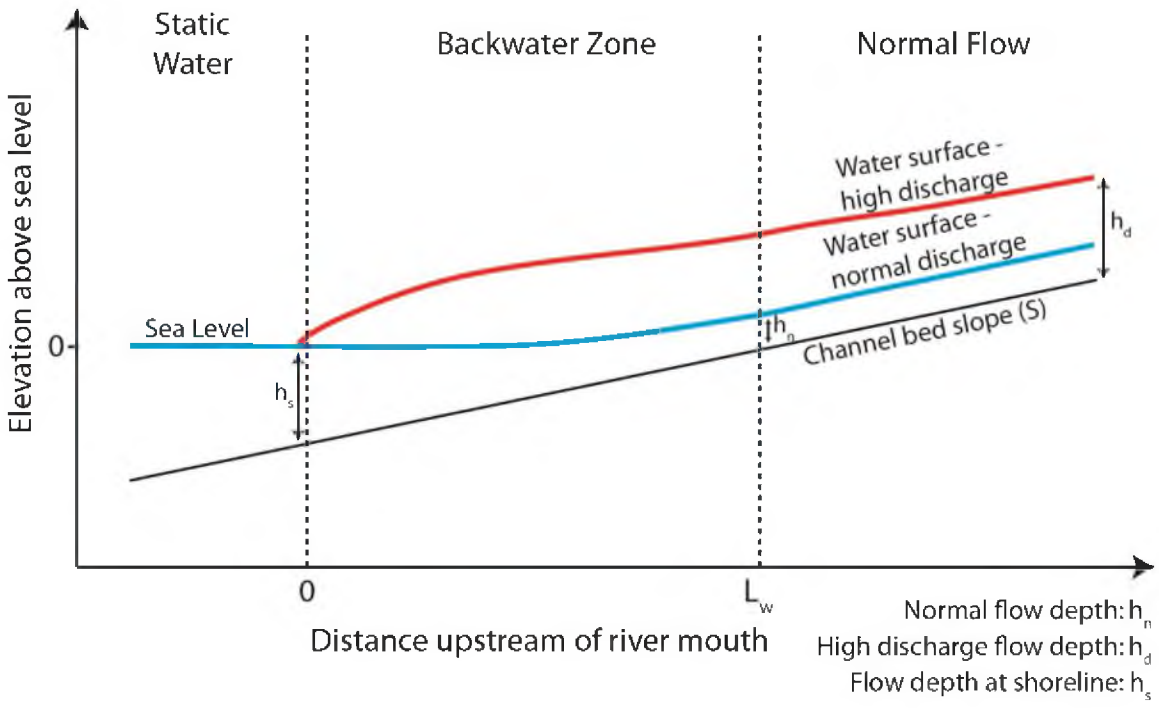
Static
Water
Backwater Zone
Normal Flow
Water surface -
high discharge
Water surface -
normal discharge
Channel bed slope (S)
Sea Level
0
Elevation above sea level
h_s
h_n
h_d
0
L_w
Distance upstream of river mouth
Normal flow depth: h_n
High discharge flow depth: h_d
Flow depth at shoreline: h_s

CONCLUSIONS AND FUTURE WORK

Outcrops of the John Henry Member at Bull Canyon show evidence of significant variability in fluvial form over a 180-meter (591-ft) thick interval. Depositional units 0 through 6 record a spectrum of fluvial styles that are transitional between braided, meandering, and straight planforms. The temporal variability in alluvial architecture significantly impacts static reservoir connectivity. The fundamental difference in channel belt scales and fluvial style between depositional units 1, 2, and 3, and the rest of the John Henry Member can be explained by changes in hydraulic conditions that influence autogenic sedimentary processes. It is proposed that fluctuations in paleohydraulic conditions, specifically backwater length, may be the result of a subtle change in basin boundary conditions.

Depositional units 1, 2, and 3, which make up the lower John Henry Member, are characterized by very fine-to-medium grained and laterally and vertically isolated channel belts. These three units display aggradational stacking as well as channel deepening. The evidence indicates that the lower John Henry Member was deposited in an area subject to backwater hydraulics. Within this 'backwater zone', changes in hydraulic conditions, such as decelerating water, created nonuniform flow towards the river mouth. The result is a period of deposition in which fluvial style is different from what is

stratigraphically above and below. Depositional units 1, 2, and 3 represent the remnants of a distributive system in which formative channels avulsed at very short time intervals and sand bypasses during high discharge events in favor of preservation along the shoreline.

The results of the static reservoir connectivity analysis show that connectivity is significantly diminished in the lower John Henry Member. This is substantiated by a lower overall net-to-gross and a change in fluvial style. Individual channel belts, deposited in straight planform style, are dispersed and narrow, resulting in a compartmentalization of parallel sand bodies. This type of reservoir dimensionality negatively impacts sand body connectivity. The results suggest that backwater hydraulics can have a significant effect on alluvial architecture and therefore reservoir connectivity. The broader implications of these results may be twofold. If compartmentalization of the reservoir is desirable because it reduces the risk of early water breakthrough, then diminished reservoir connectivity is appropriate. On the other hand, if the goal is to identify zones with a high proportion of key reservoir facies, then it may be necessary to shift focus updip of the nodal avulsion point or downdip towards the shoreline.

Additional results of this study give perspective on using scaling relationships to reconstruct channel dimensions as well as using paleohydraulic estimations to constrain paleogeographic reconstructions. In highly avulsive systems characterized by enhanced deposition and reduced channel-fill timescales, the predicted dimensions of channel belts using scaling relationships

drastically overestimates what is present in the outcrop. This highlights the importance of considering the paleohydraulic conditions and the sedimentary processes at work when applying scaling relationships to guide interpretations and correlations. Additionally it was found that applying a rigorous paleohydraulic workflow, similar to the one presented here, may assist in placing quantitative constraints on paleogeographic reconstructions. Results of the paleohydraulic workflow carried out at Bull Canyon produce estimates of catchment size and distance from source that match and give credence to a recently proposed paleogeographic reconstruction.

Future Work

The results presented in this text represent the first application of a 3-D facies modeling workflow to fluvial dominated outcrops in the Straight Cliffs Formation. Because of questions unearthed during this study as well as technological advancements in digital outcrop geology, many opportunities are available for ongoing and future work. First, Light Detection and Ranging (LiDAR) datasets can and should be used to build complete digital outcrop models. LiDAR presents a significant step forward in virtual outcrop geology, and it enables geoscientists to build photorealistic outcrop models with relative ease compared to traditional field techniques that might include 2-D photo panels (Buckley et al., 2008, 2010; Fabuel-Perez et al., 2009; Rittersbacher et al., 2013). Fortunately, some of the old challenges associated with LiDAR, including the large size of datasets, are quickly being overcome by advances in computation

efficiency. Secondly, event-based (EB) forward models derived from outcrop datasets in the Straight Cliffs Formation can be applied to subsurface reservoir modeling workflows in order to predict depositional facies consistent with observations from well, core, and seismic data. Event-based models, sometimes referred to as 'pseudo process-based models', incorporate process-based rules but do not require the tremendous amount of CPU power and computational time characteristic of fully process-based models. Utilizing an event-based modeling approach has been shown to improve the integration of geological information into geostatistics because the approach involves building models as a sequence of depositional events (see Pyrcz et al., 2009, 2011; McHargue et al., 2011; Stright et al., 2013). Finally, conducting a comprehensive study on climate conditions during deposition of the Straight Cliffs Formation could provide further insights into important basin boundary conditions. Little recent work has been conducted regarding Santonian–Campanian climate in North America (see Kauffman, 1984; Wolfe and Upchurch, J., 1987; Huber et al., 1995; Roberts and Kirschbaum, 1995). A climate study incorporating advanced methodologies such as isotopic analysis would be beneficial in building basin-scale depositional models and resolving important source to sink relationships.

APPENDIX A

MEASURED STRATIGRAPHIC SECTIONS

The stratigraphic sections measured in Bull Canyon of the Kaiparowits Plateau are included in Appendix A. A symbols legend precedes the measured sections, which include: Westside #1 and Westside #2. The locations of the measured stratigraphic sections are shown on the map in Figure 3 and are marked in the interpreted photomosaics in Figure 4 and Appendix B.

Figure A.1 – Stratigraphic sections symbols legend.

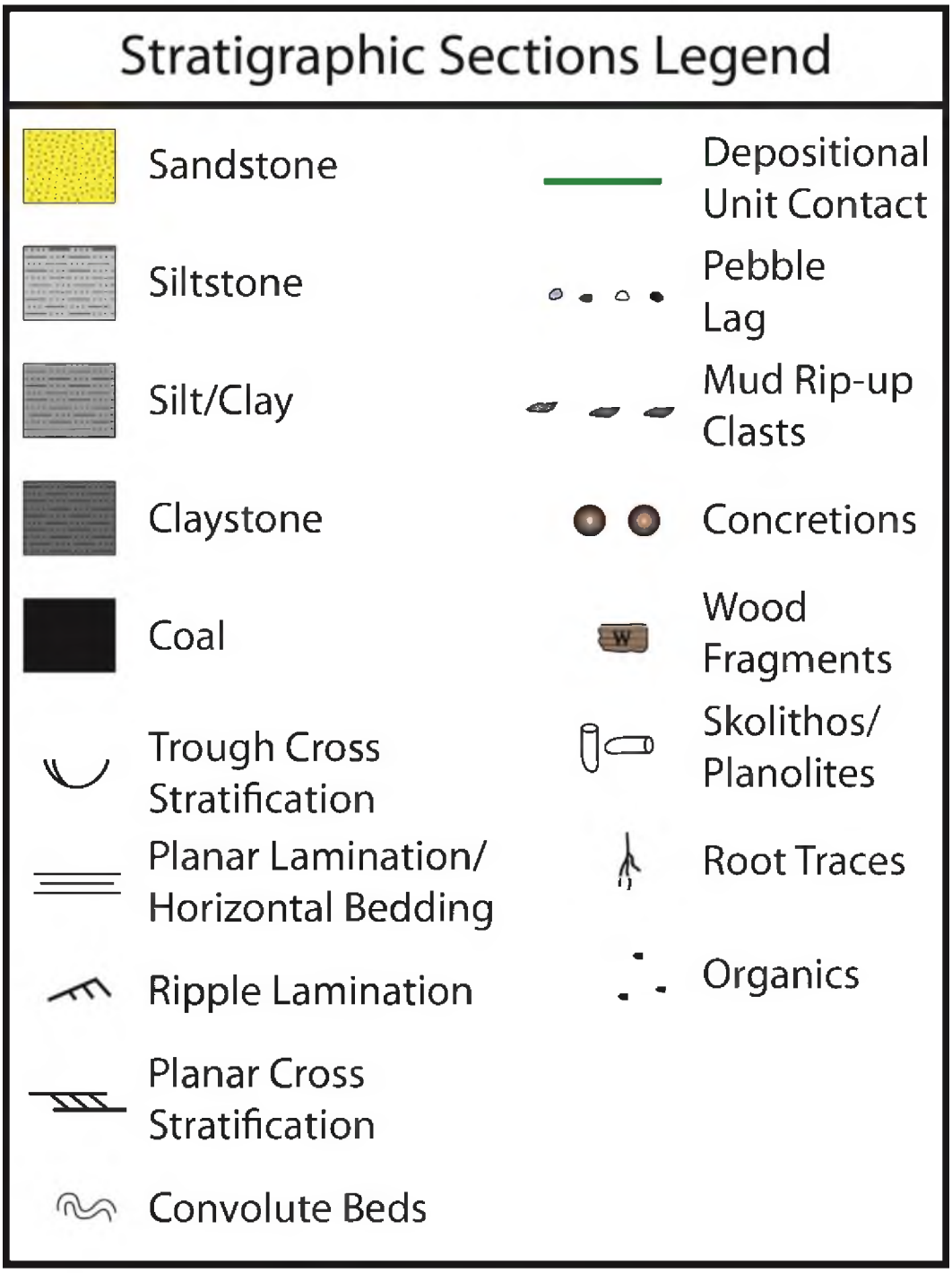
Stratigraphic Sections Legend
Sandstone
Siltstone
Silt/Clay
Claystone
Coal
Trough Cross Stratification
Planar Lamination/ Horizontal Bedding
Ripple Lamination
Planar Cross Stratification
Convolute Beds
Depositional Unit Contact
Pebble Lag
Mud Rip-up Clasts
Concretions
Wood Fragments
Skolithos/ Planolites
Root Traces
Organics

Figure A.2 – Measured stratigraphic section from Bull Canyon: Westside #1. (A) 0–20 m, (B) 20–40 m, (C) 40–60 m, (D) 60–80 m, (E) 80–100 m, (F) 100–120 m, (G) 120–140 m, (H) 140–160 m, (I) 160–180 m, (J) 180–200 m, and (K) 200–212 m.

A. Bull Canyon Westside #1 Section (0–20 m [0–66 ft])

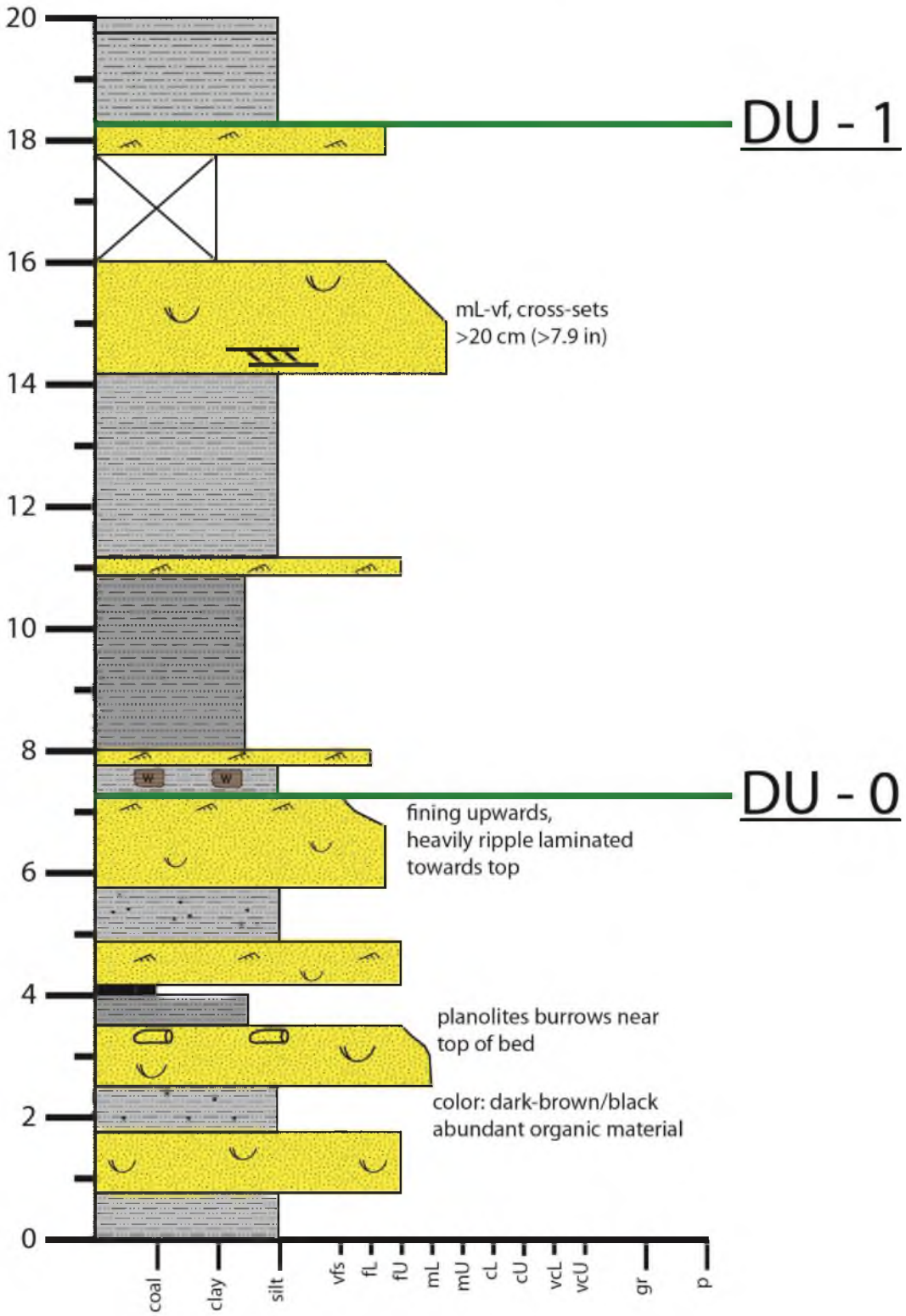

Figure A.2

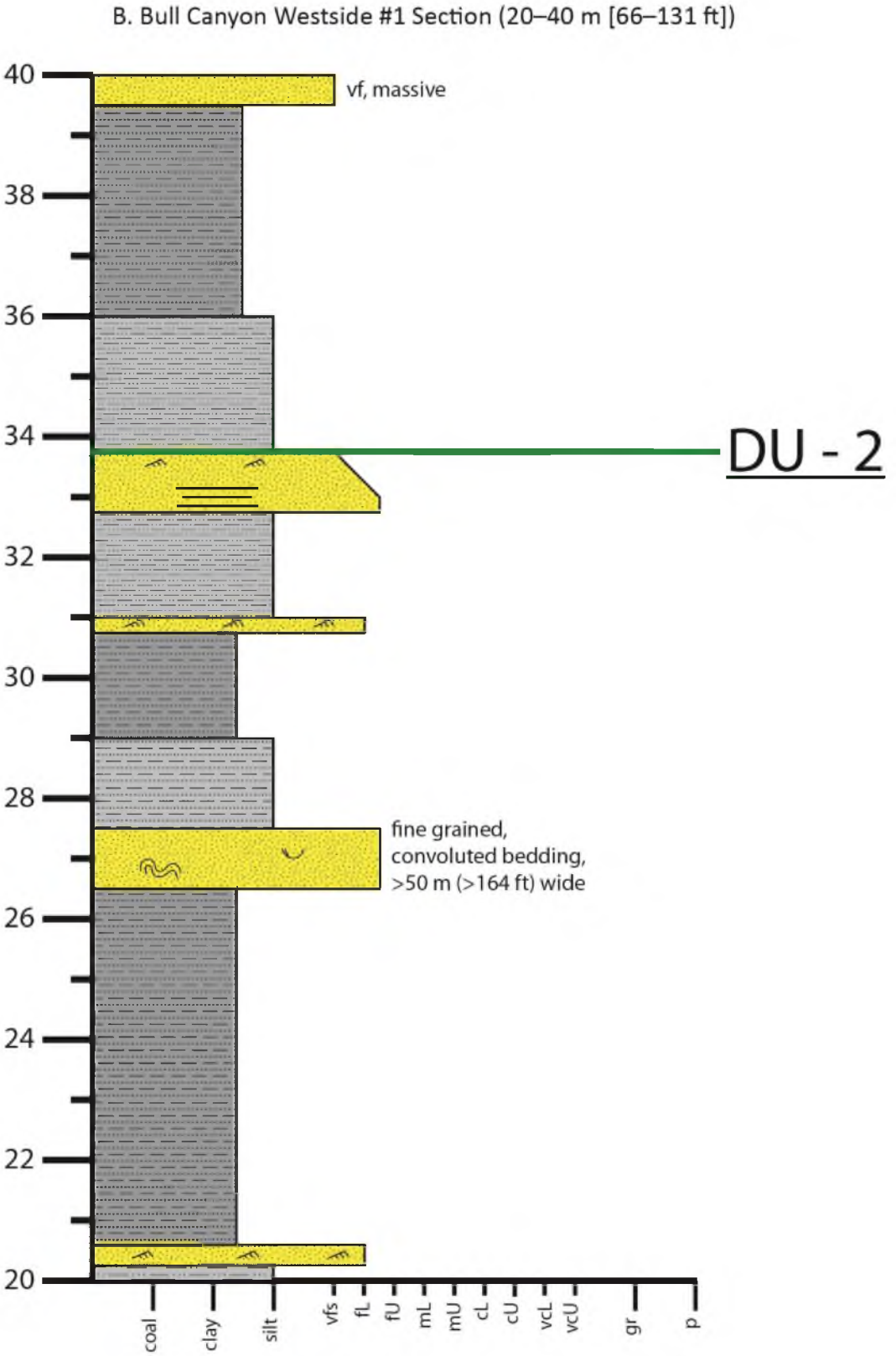

Figure A.2 continued

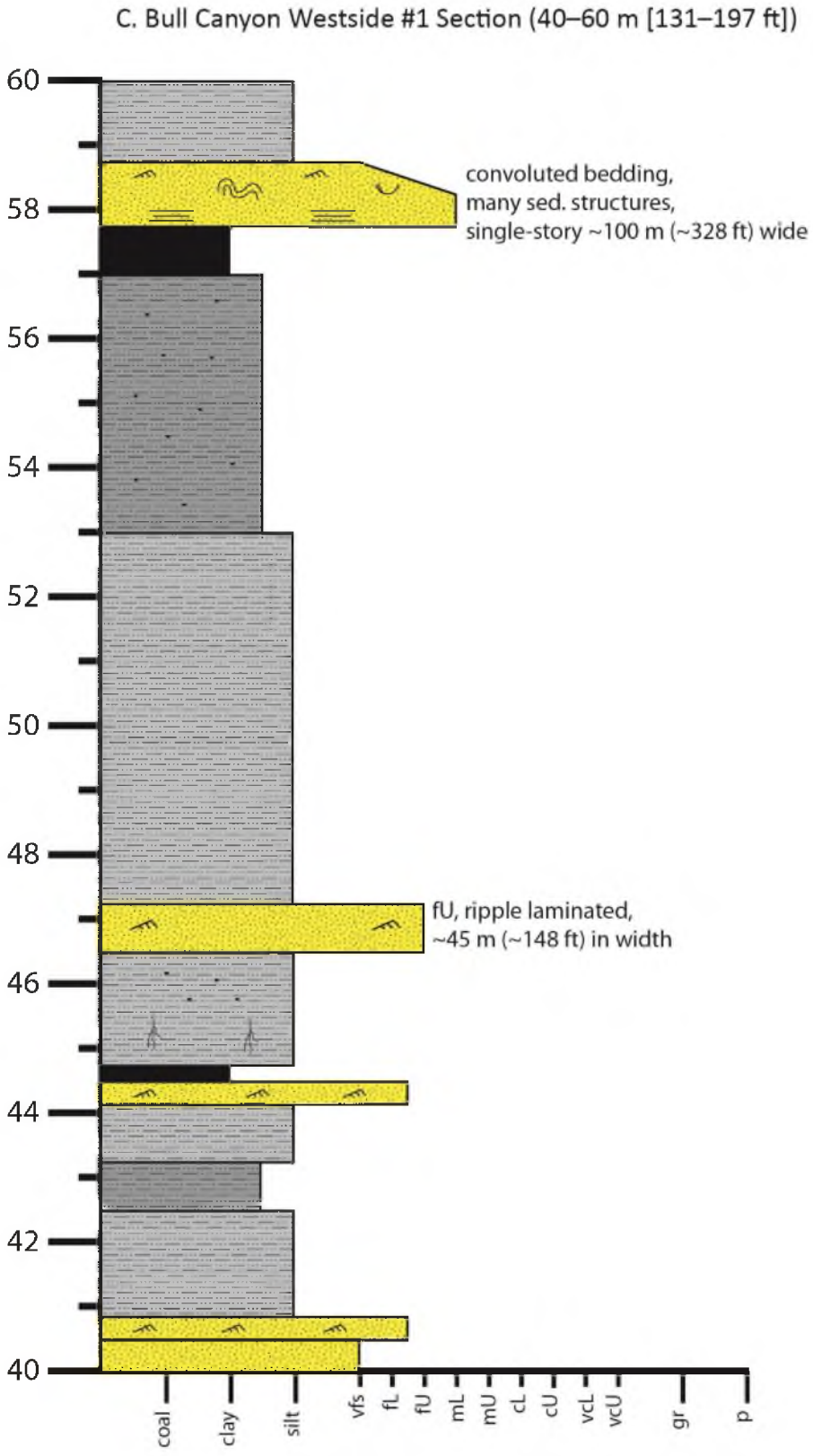

Figure A.2 continued

D. Bull Canyon Westside #1 Section (60–80 m [197–262 ft])

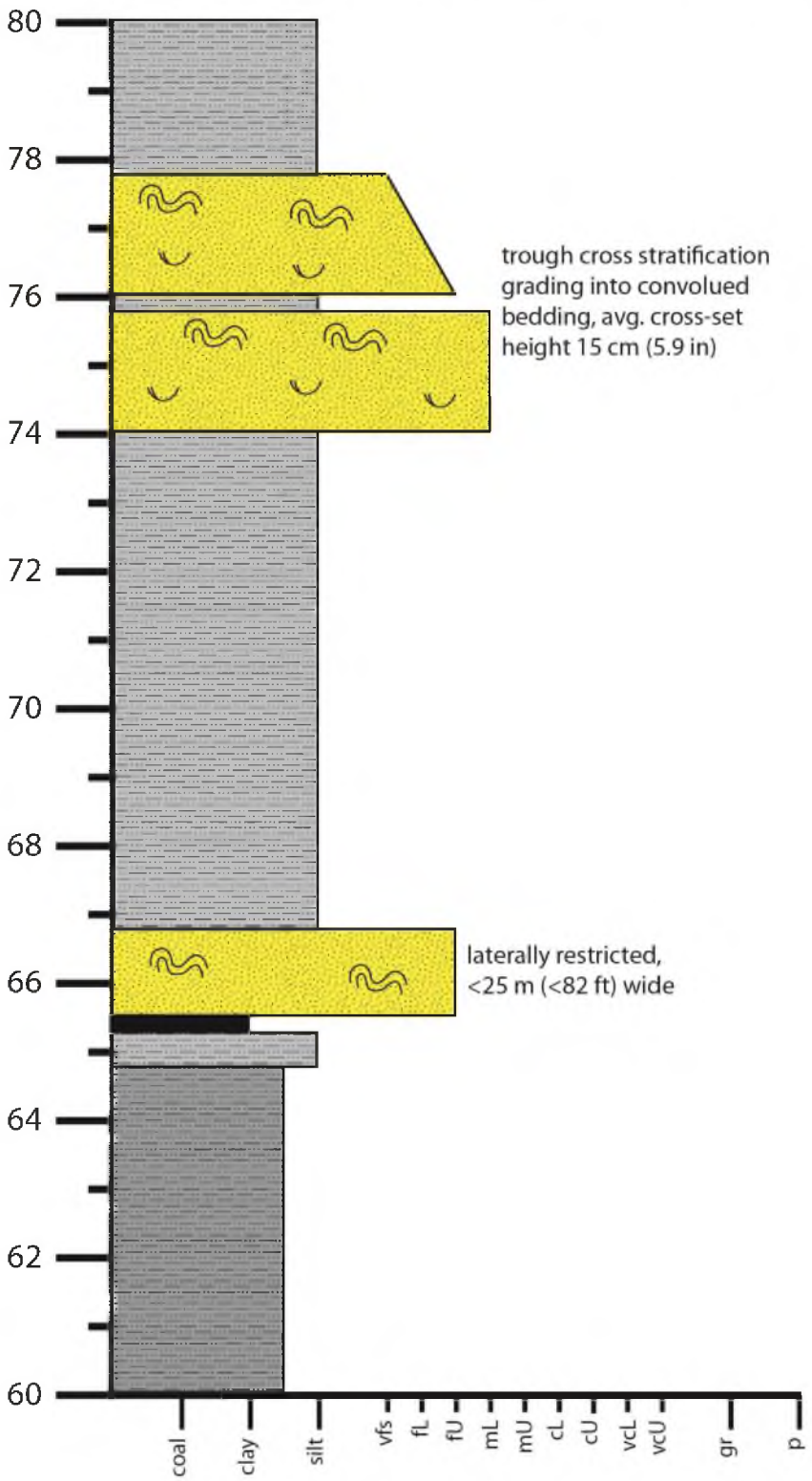

Figure A.2 continued

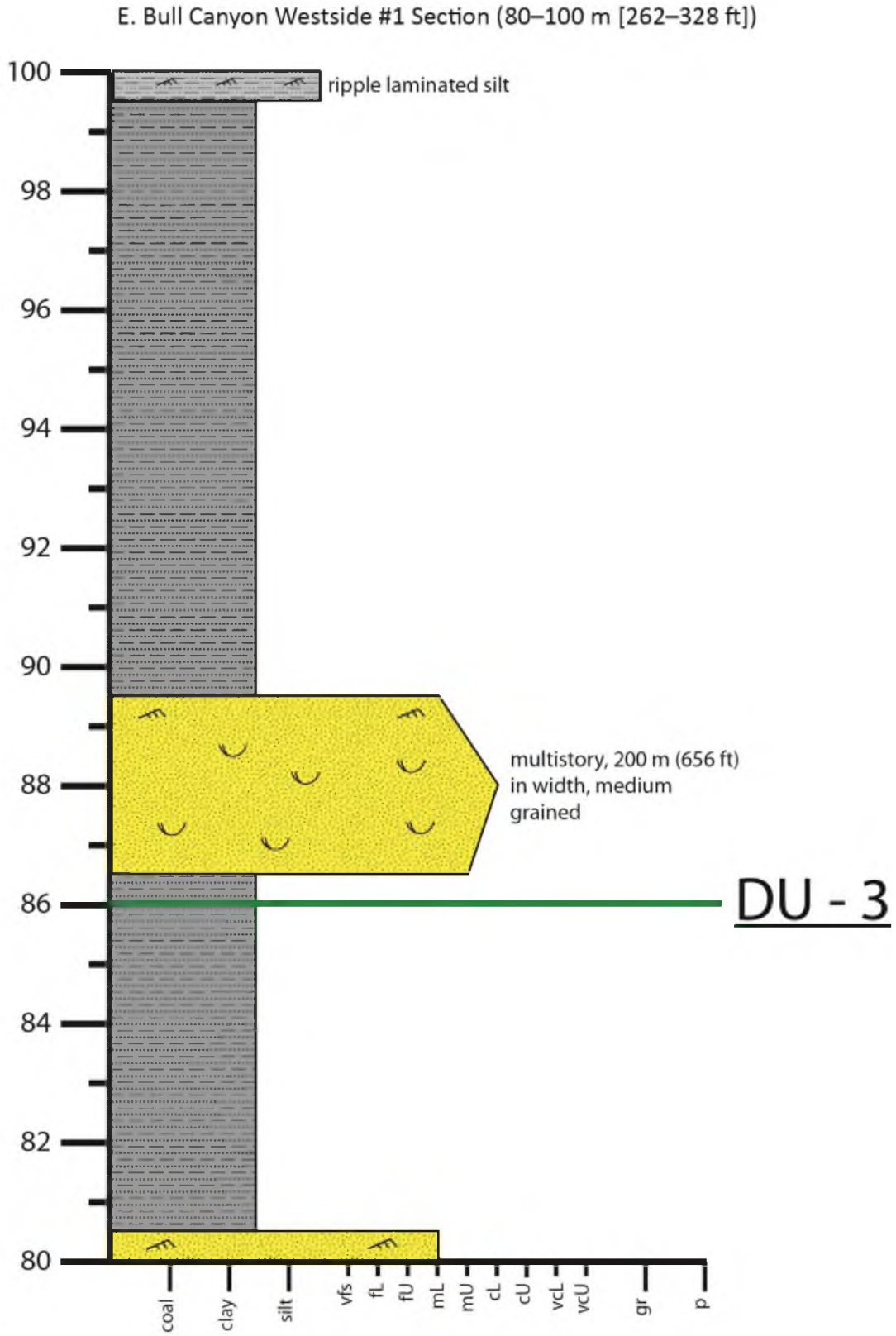

Figure A.2 continued

F. Bull Canyon Westside #1 Section (100–120 m [328–394 ft])

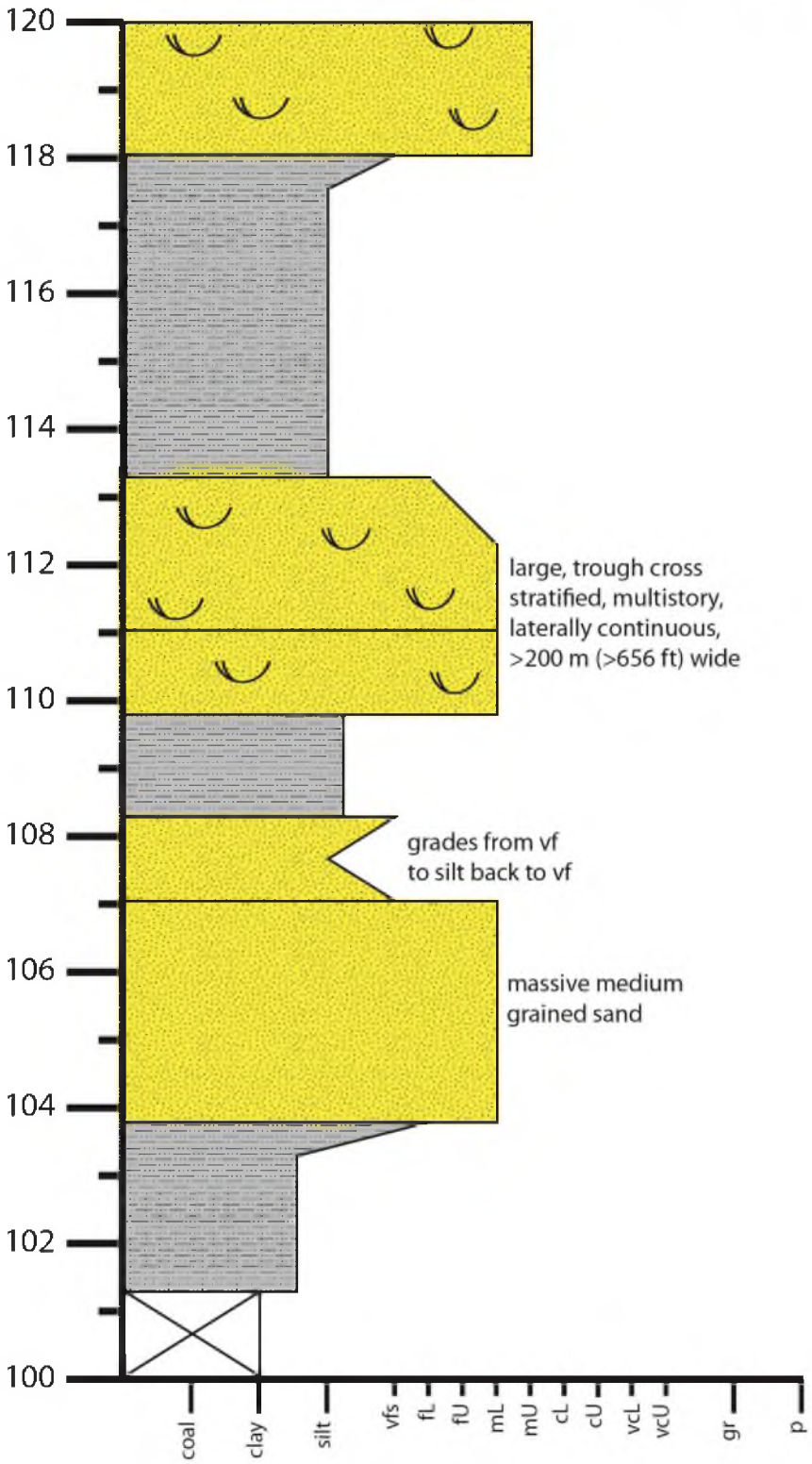

Figure A.2 continued

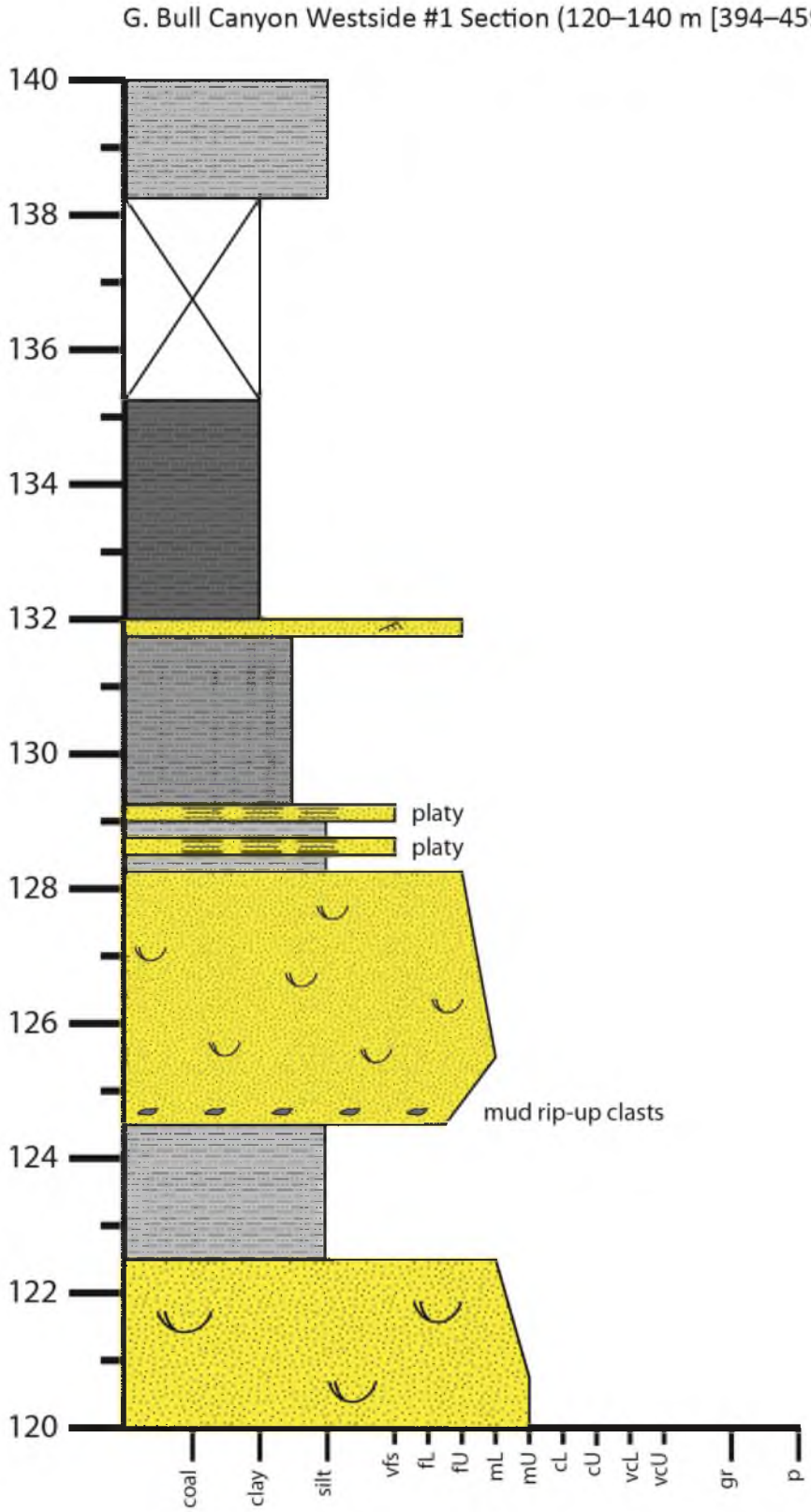

Figure A.2 continued

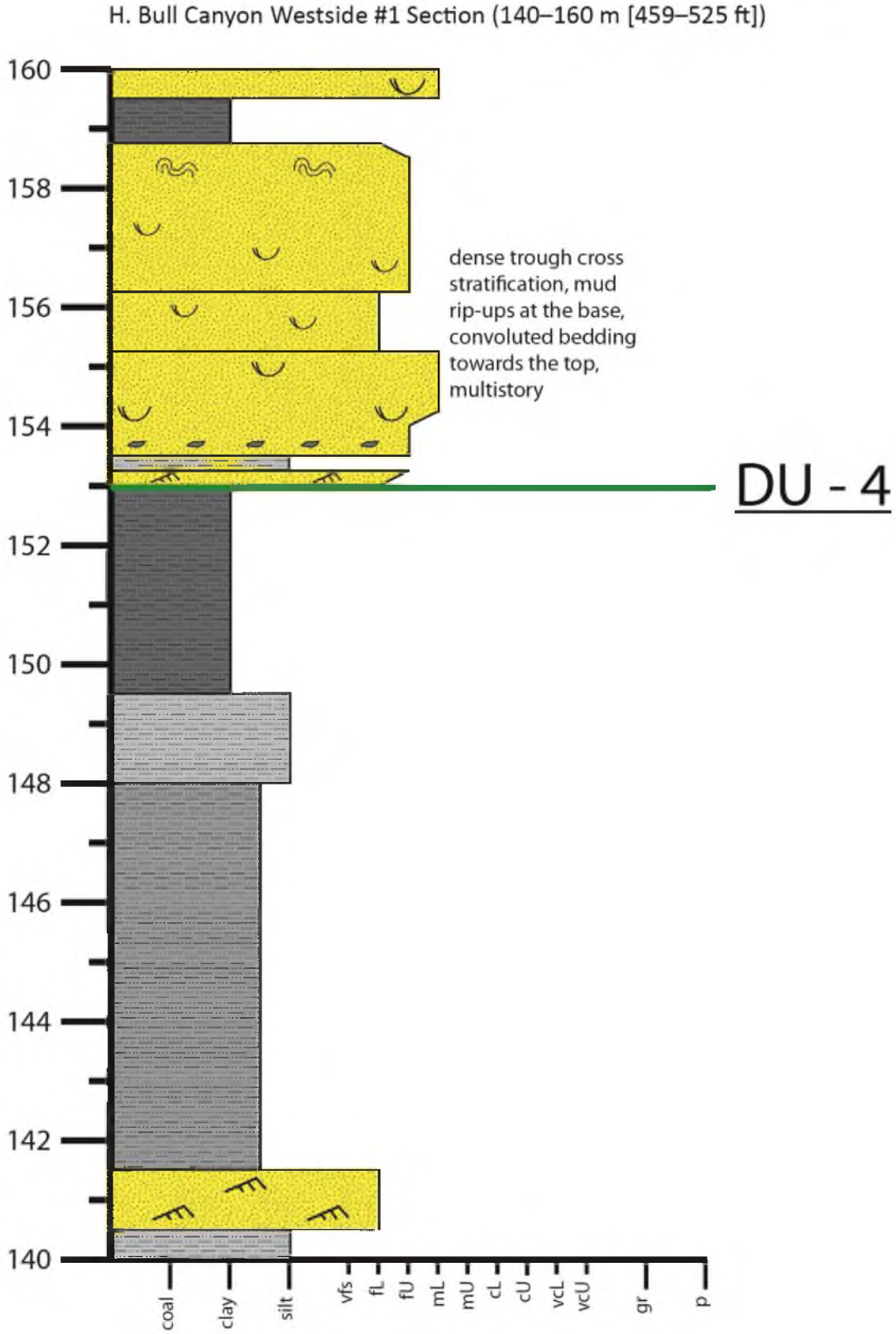

Figure A.2 continued

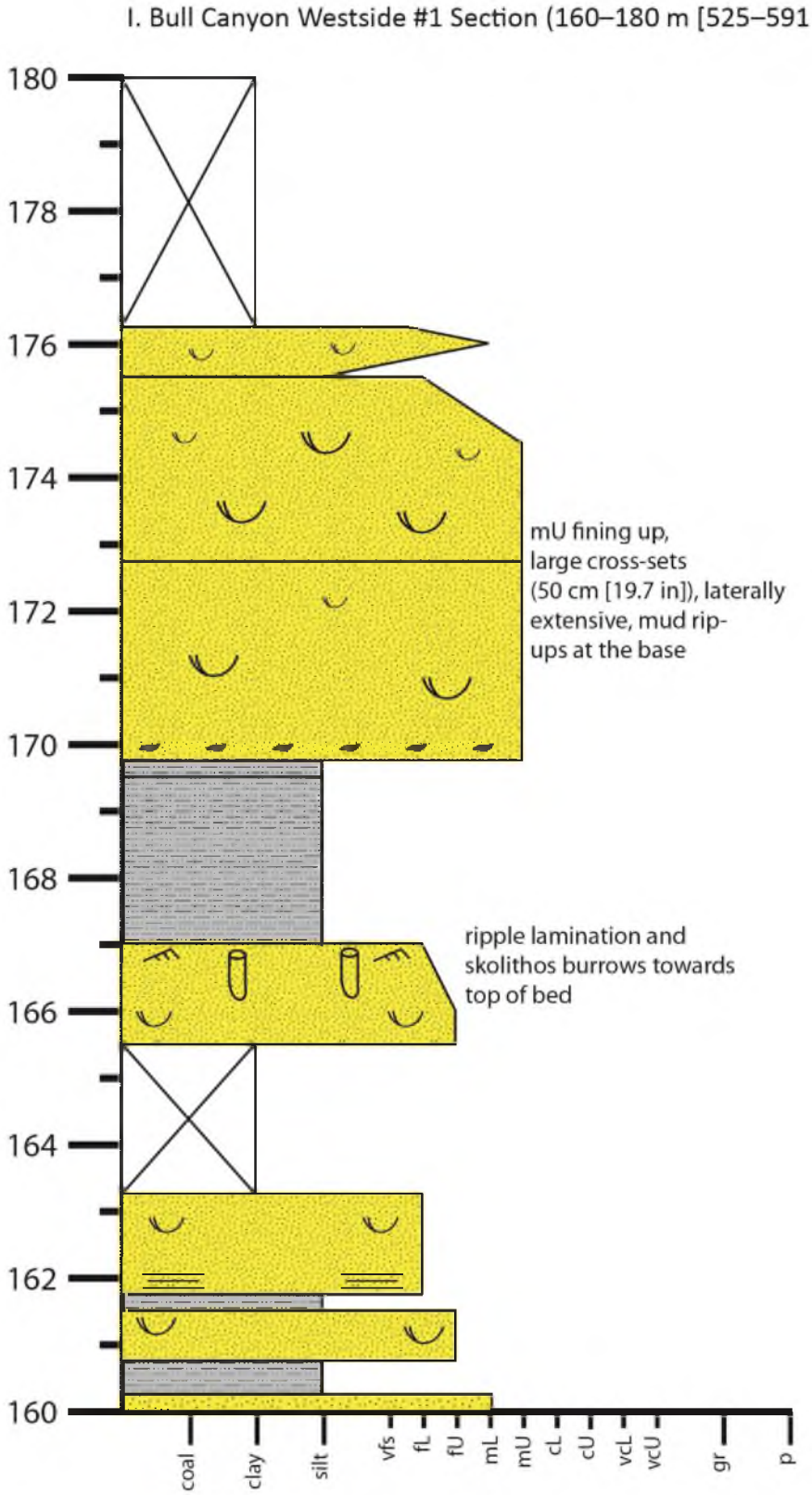

Figure A.2 continued

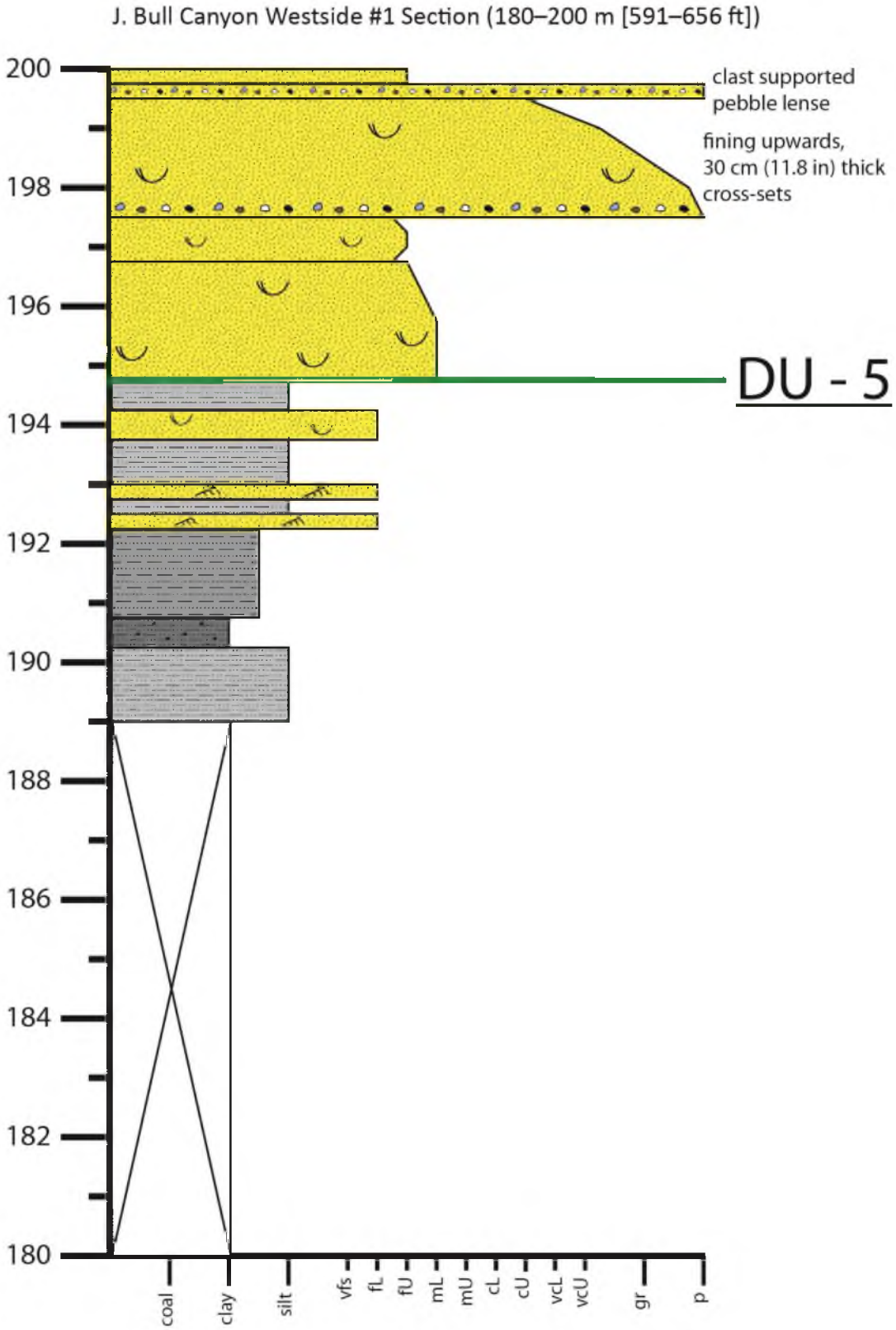

Figure A.2 continued

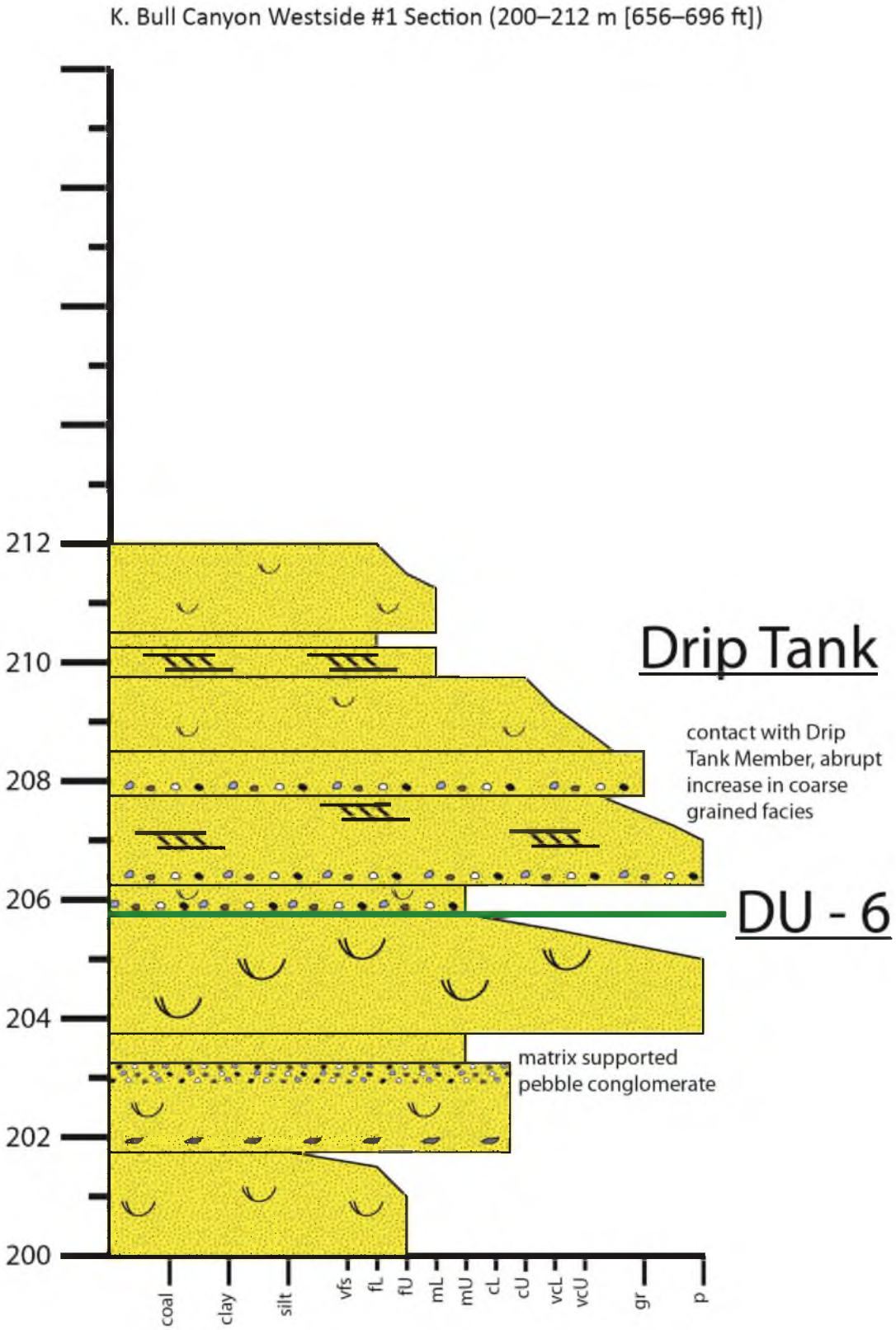

Figure A.2 continued

Figure A.3 – Measured stratigraphic section from Bull Canyon: Westside #2. (A) 0–20 m, (B) 20–40 m, (C) 40–60 m, (D) 60–80 m, (E) 80–100 m, (F) 100–120 m, (G) 120–140 m, (H) 140–160 m, and (I) 160–168 m.

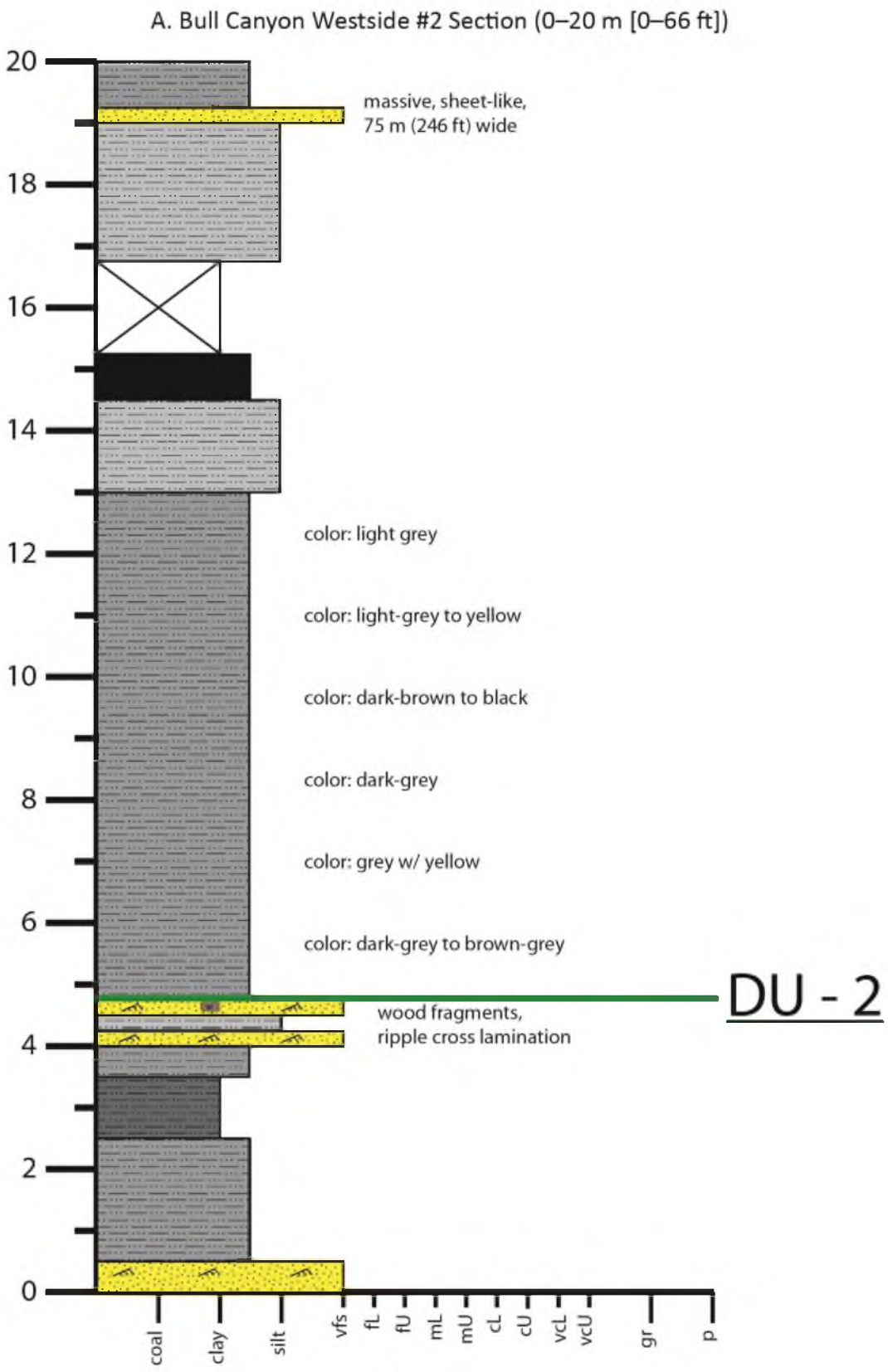
A. Bull Canyon Westside #2 Section (0–20 m [0–66 ft])
20
18
16
14
12
10
8
6
4
2
0
massive, sheet-like,
75 m (246 ft) wide
color: light grey
color: light-grey to yellow
color: dark-brown to black
color: dark-grey
color: grey w/ yellow
color: dark-grey to brown-grey
DU - 2
wood fragments,
ripple cross lamination
coal
clay
silt
vfs
fL
fU
mL
mU
cL
cU
vcL
vcU
gr
p

Figure A.3

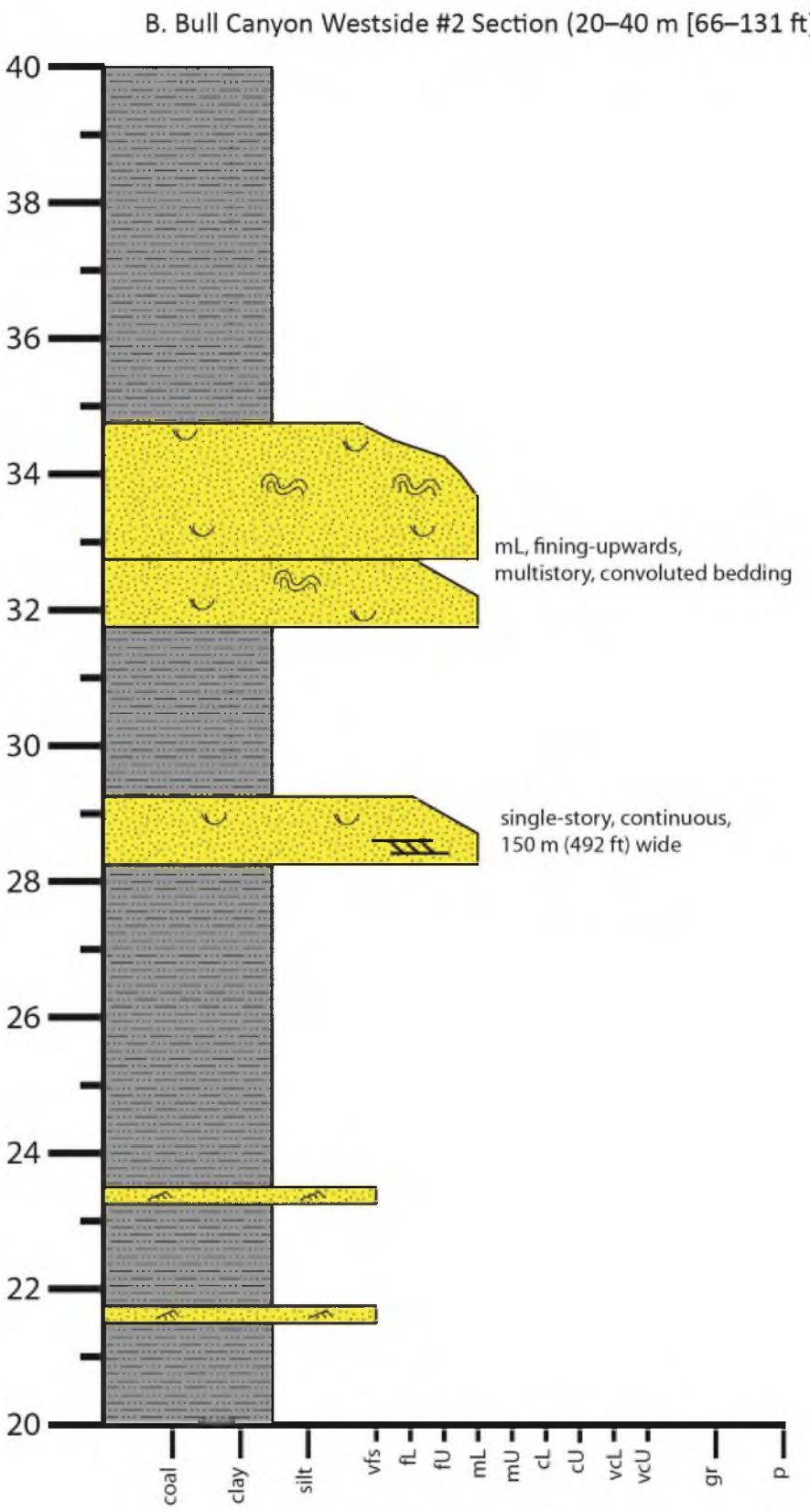

Figure A.3 continued

C. Bull Canyon Westside #2 Section (40–60 m [131–197 ft])

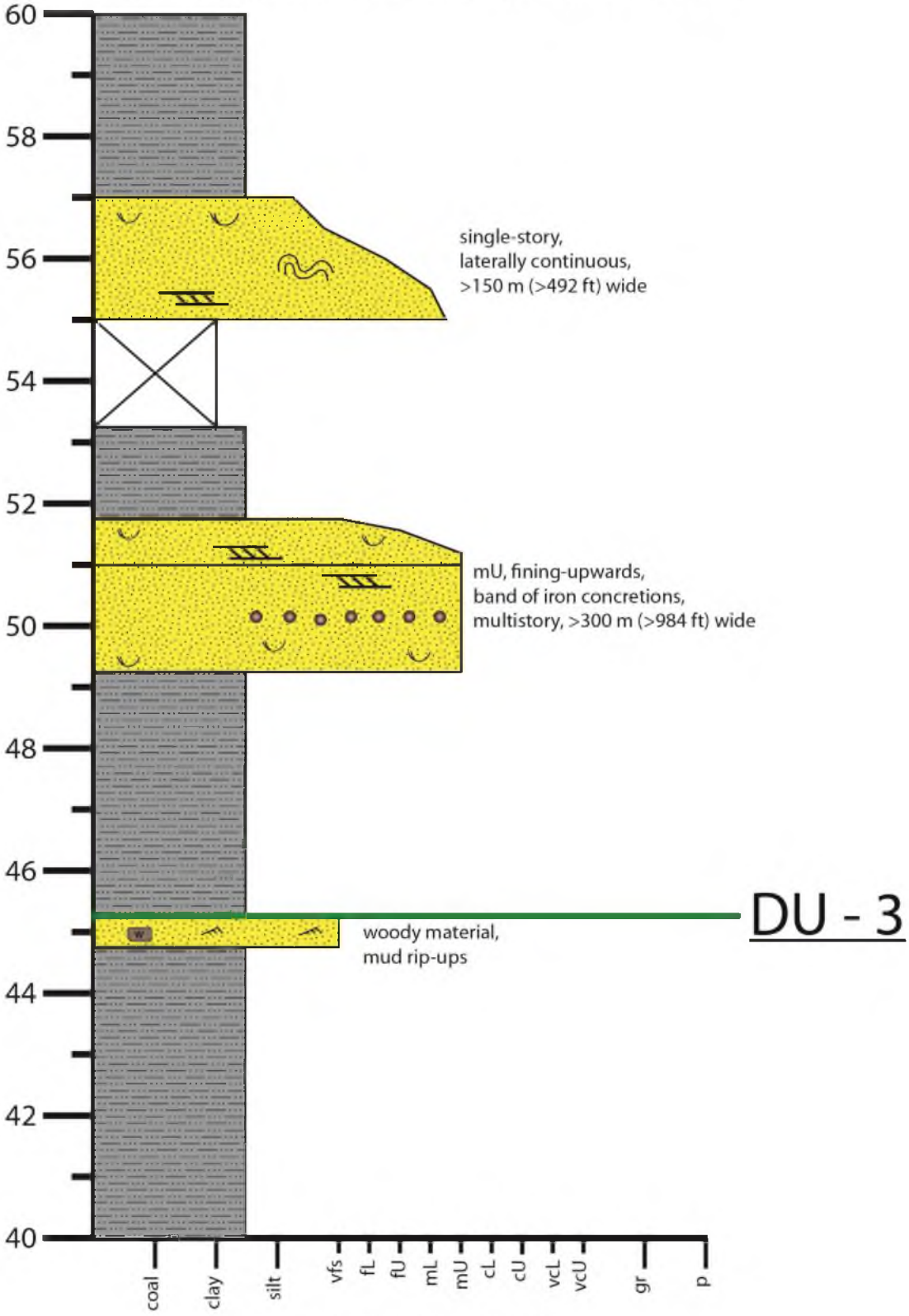

Figure A.3 continued

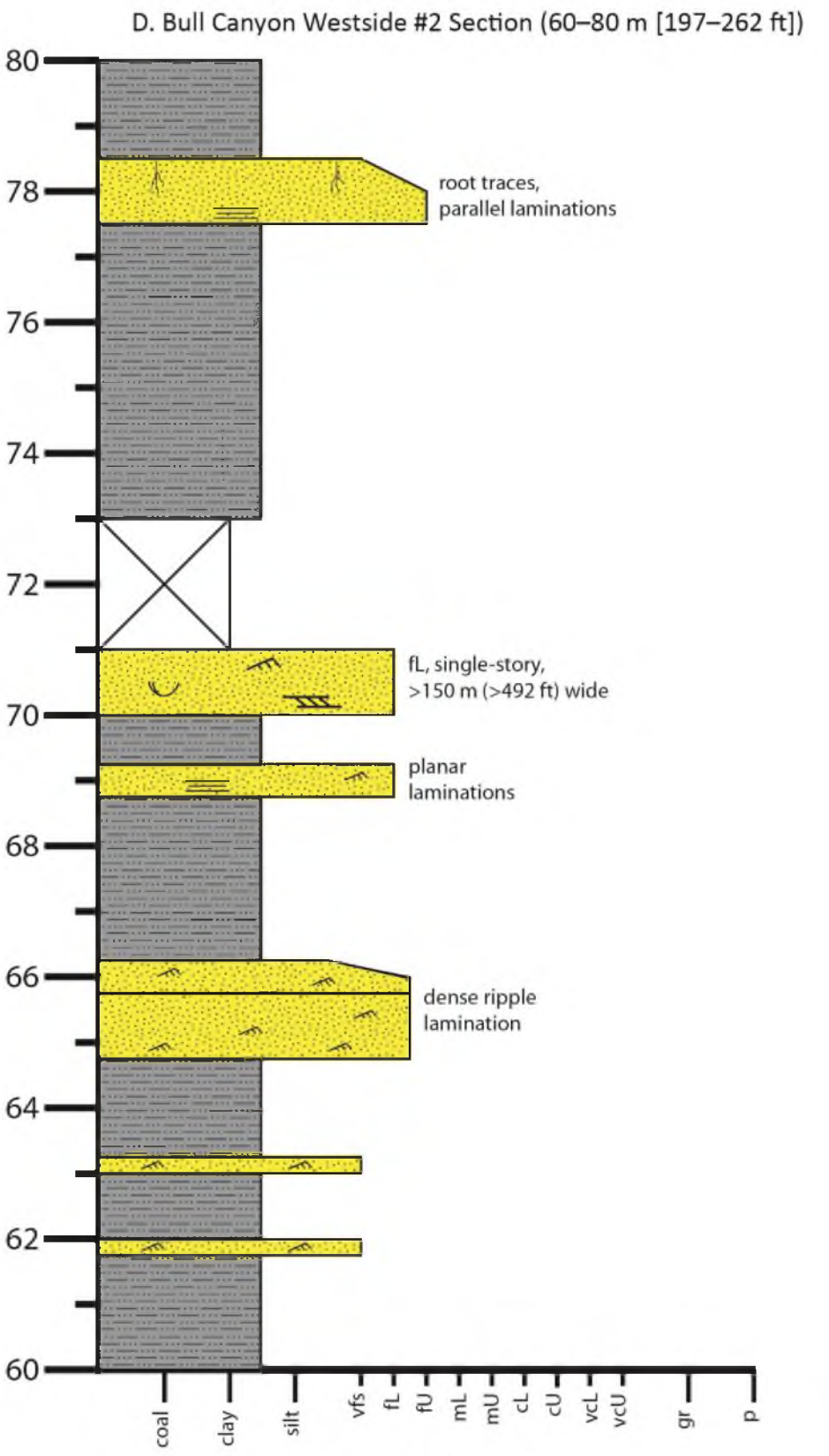

Figure A.3 continued

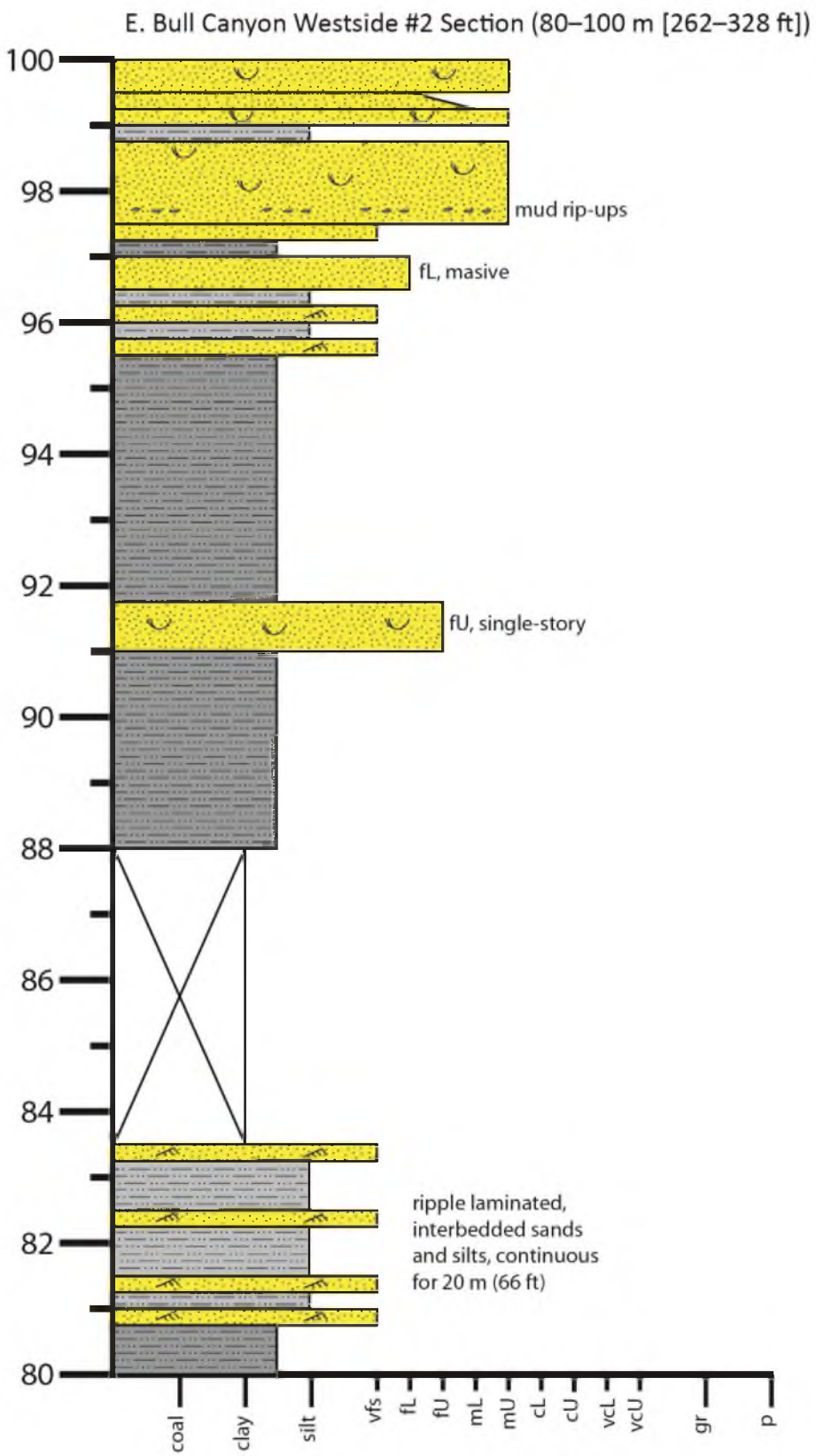

Figure A.3 continued

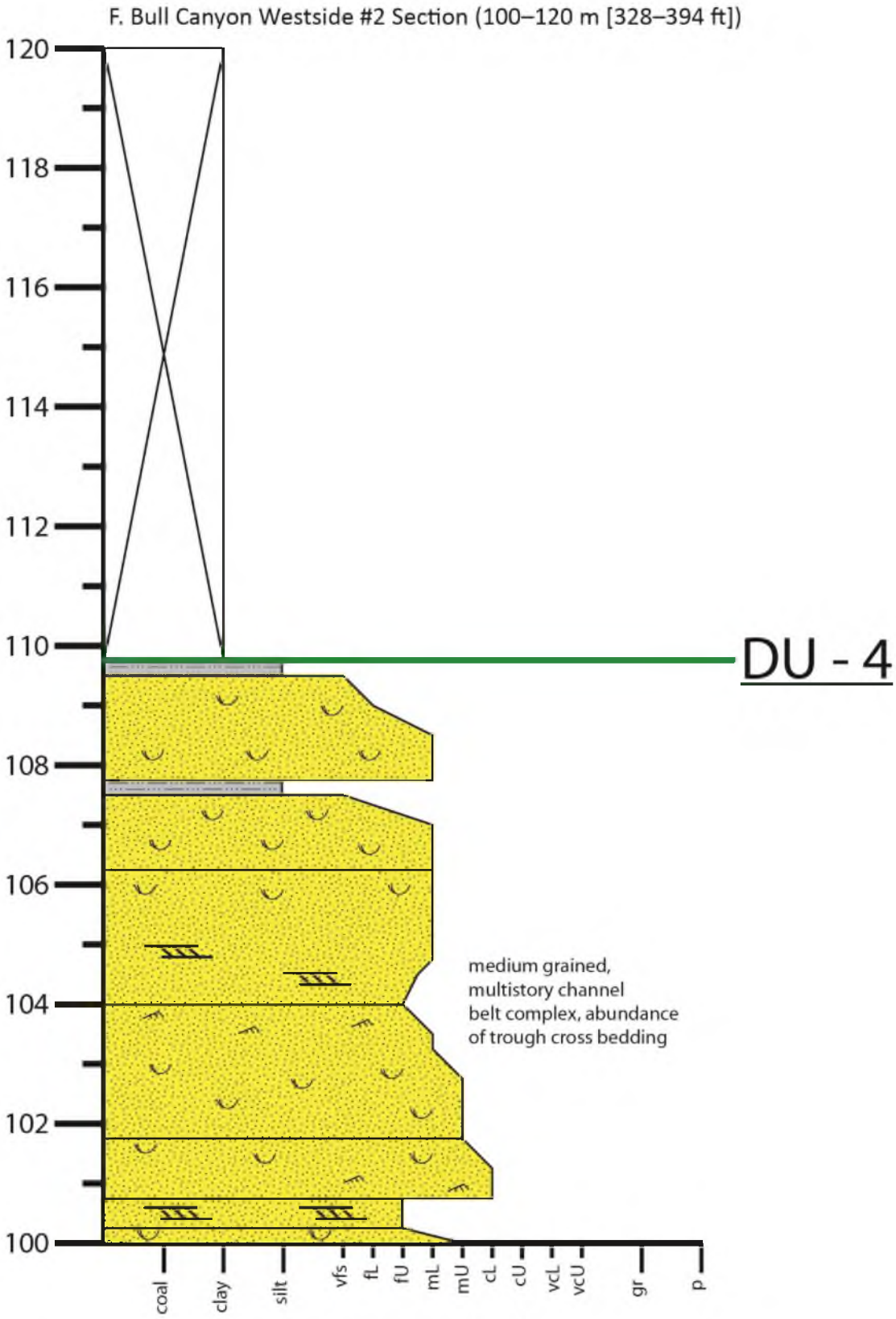

Figure A.3 continued

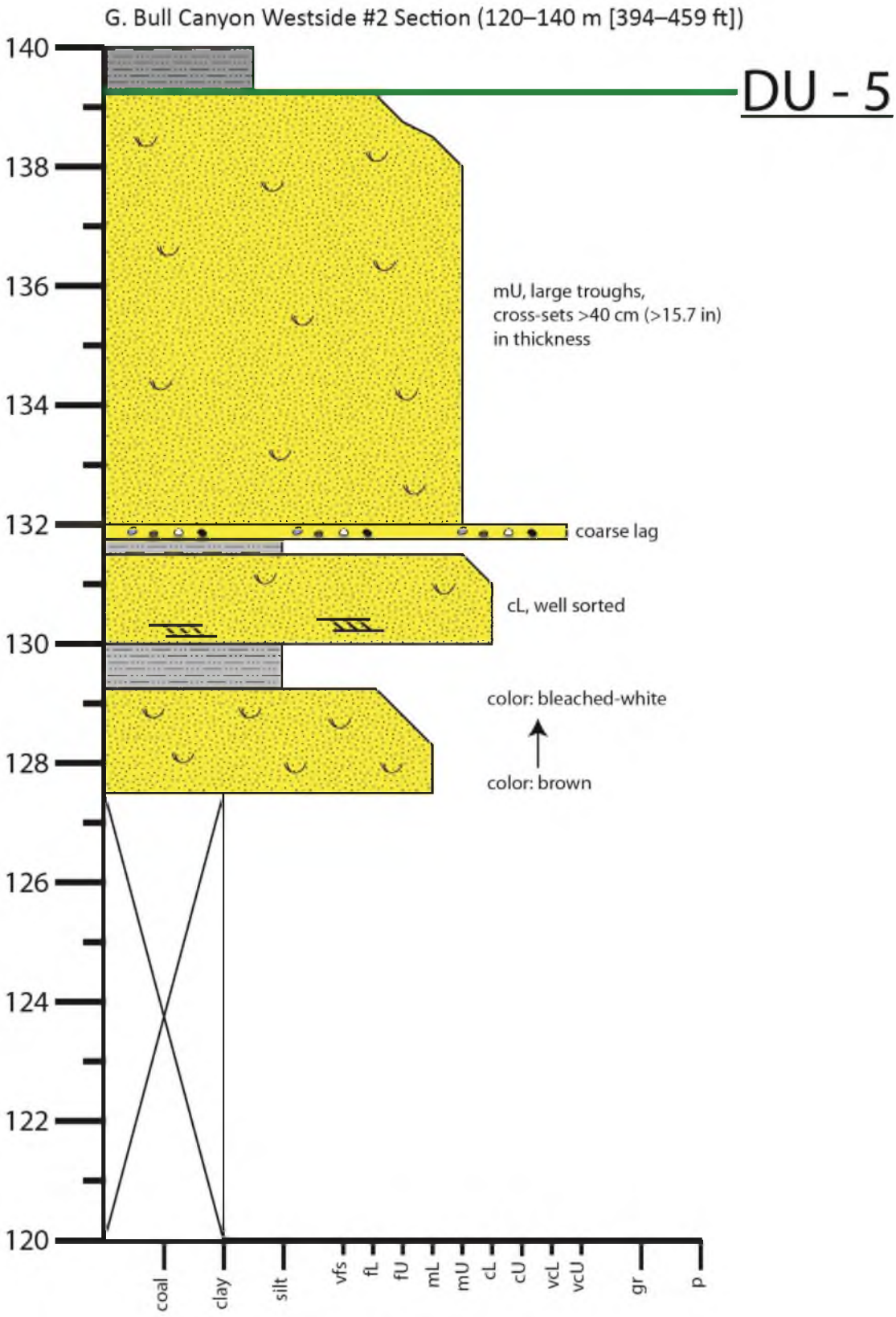

Figure A.3 continued

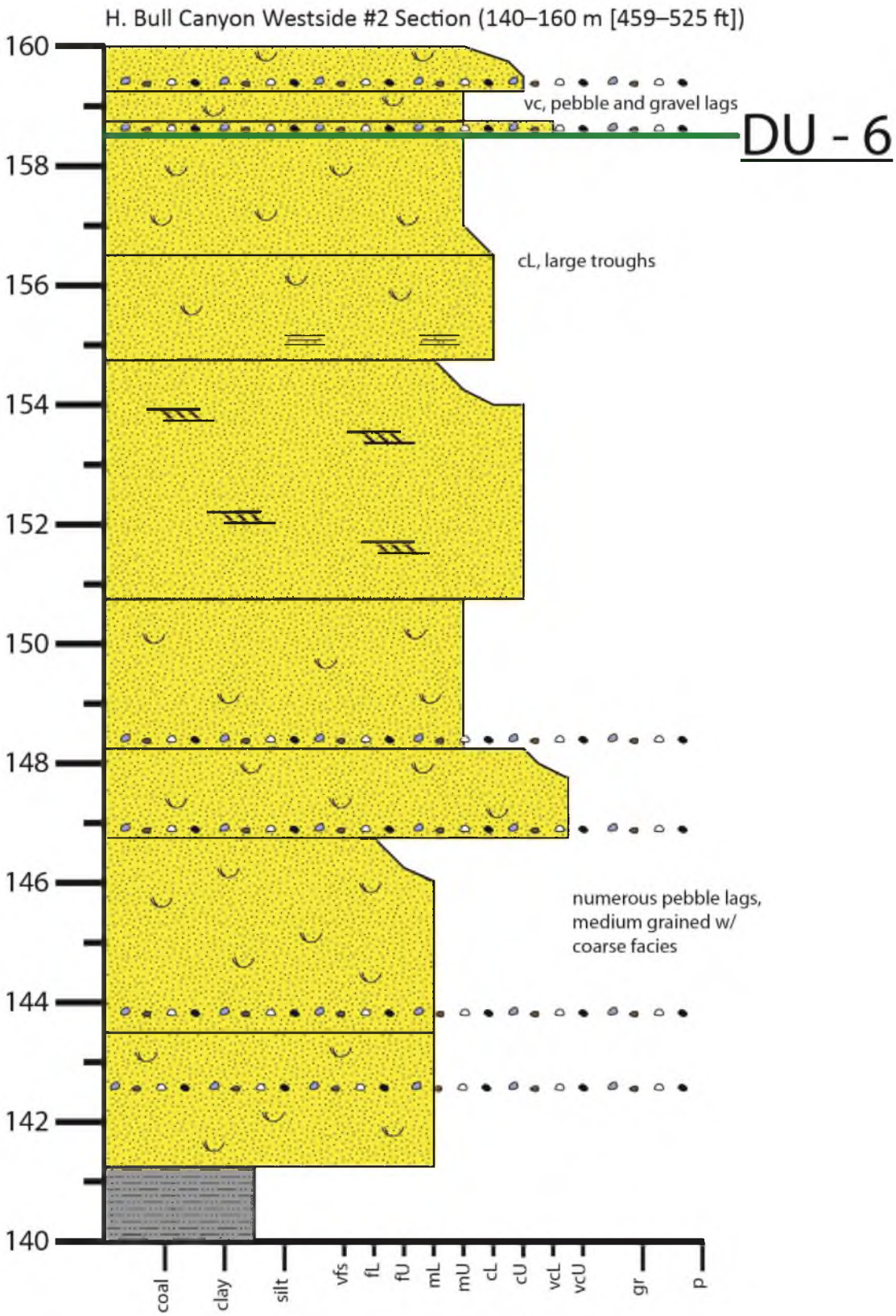

Figure A.3 continued

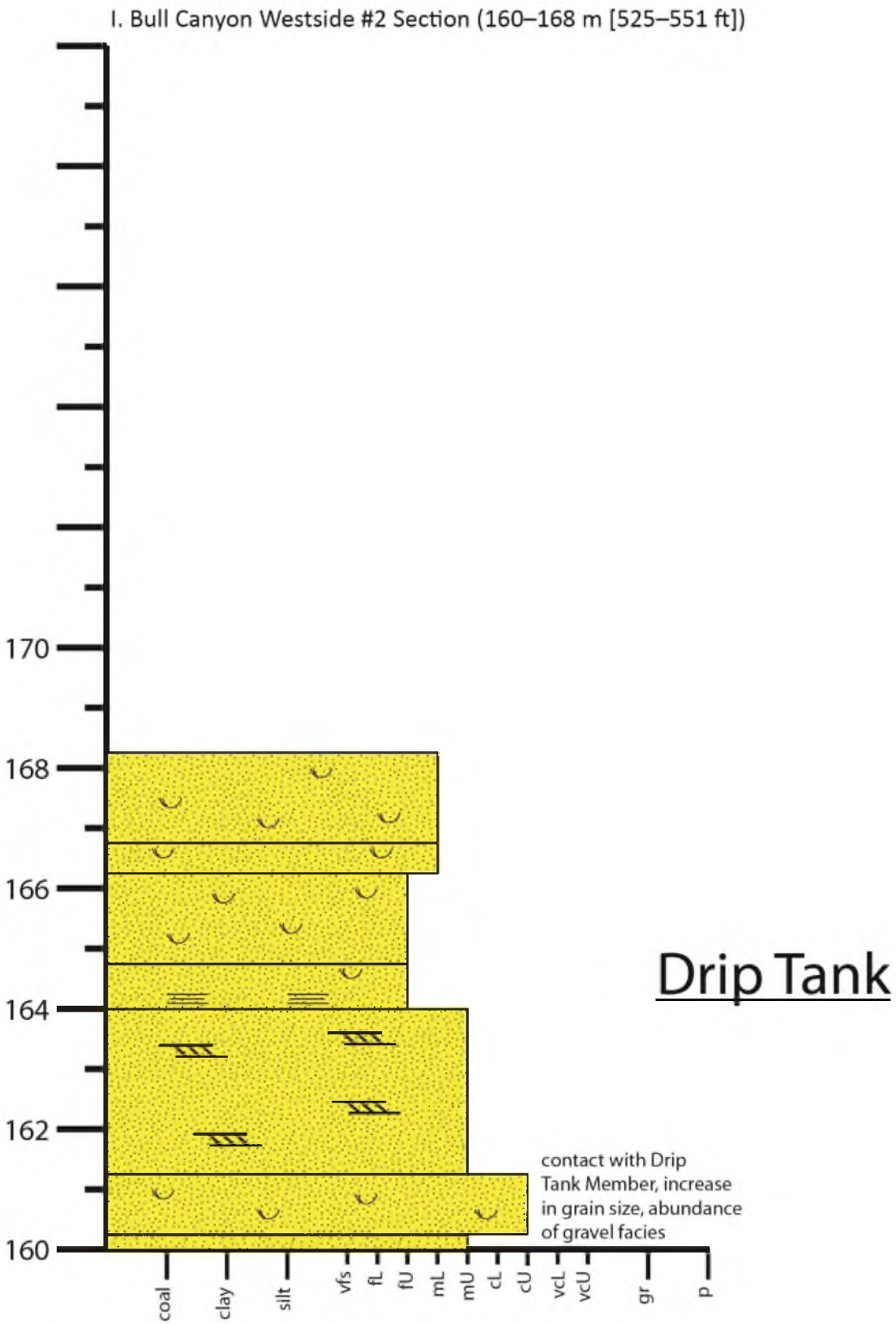

Figure A.3 continued

APPENDIX B

INTERPRETED PHOTOMOSAICS

A symbols legend (Figure B.1) is included for the interpreted photomosaics from Bull Canyon: northwestern Bull Canyon, southeastern Bull Canyon, and northeastern Bull Canyon (Figures. B.2, B.3, and B.4). The locations of these photographs are shown in Figure 3.

Figure B.1 – Legend for the symbols and labels used in interpreted photomosaics (Figs. B.2, B.3, and B.4).

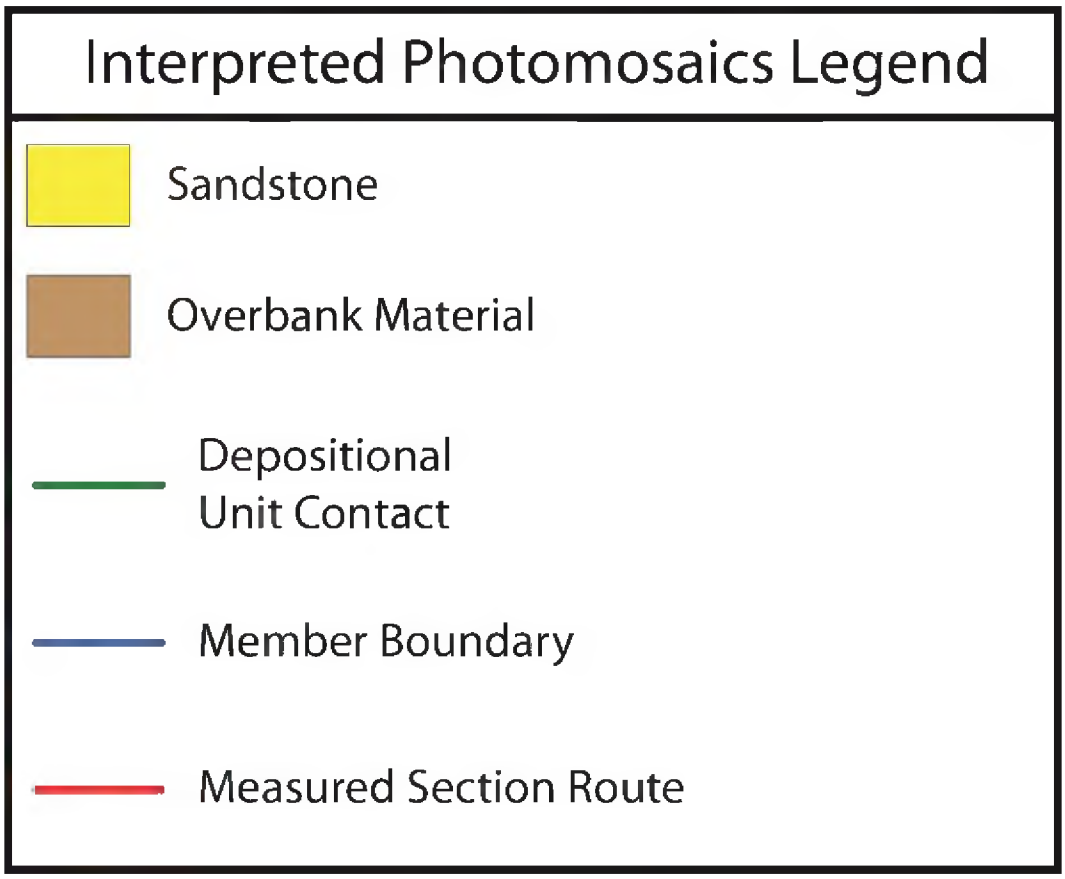
Interpreted Photomosaics Legend
Sandstone
Overbank Material
Depositional
Unit Contact
Member Boundary
Measured Section Route

Figure B.2 – Composite photograph and interpretation of the John Henry and Drip Tank Members at the northwestern portion of Bull Canyon. The interpretation shows sandstone bodies (yellow) distributed throughout floodplain silts and muds (light brown). Depositional unit boundaries three through six are interpreted from changes in fluvial architecture. These boundaries are denoted by green lines. The red line shows the approximate location of measured section 'Westside #2'. The red fill that caps the canyon wall is the Drip Tank Member.

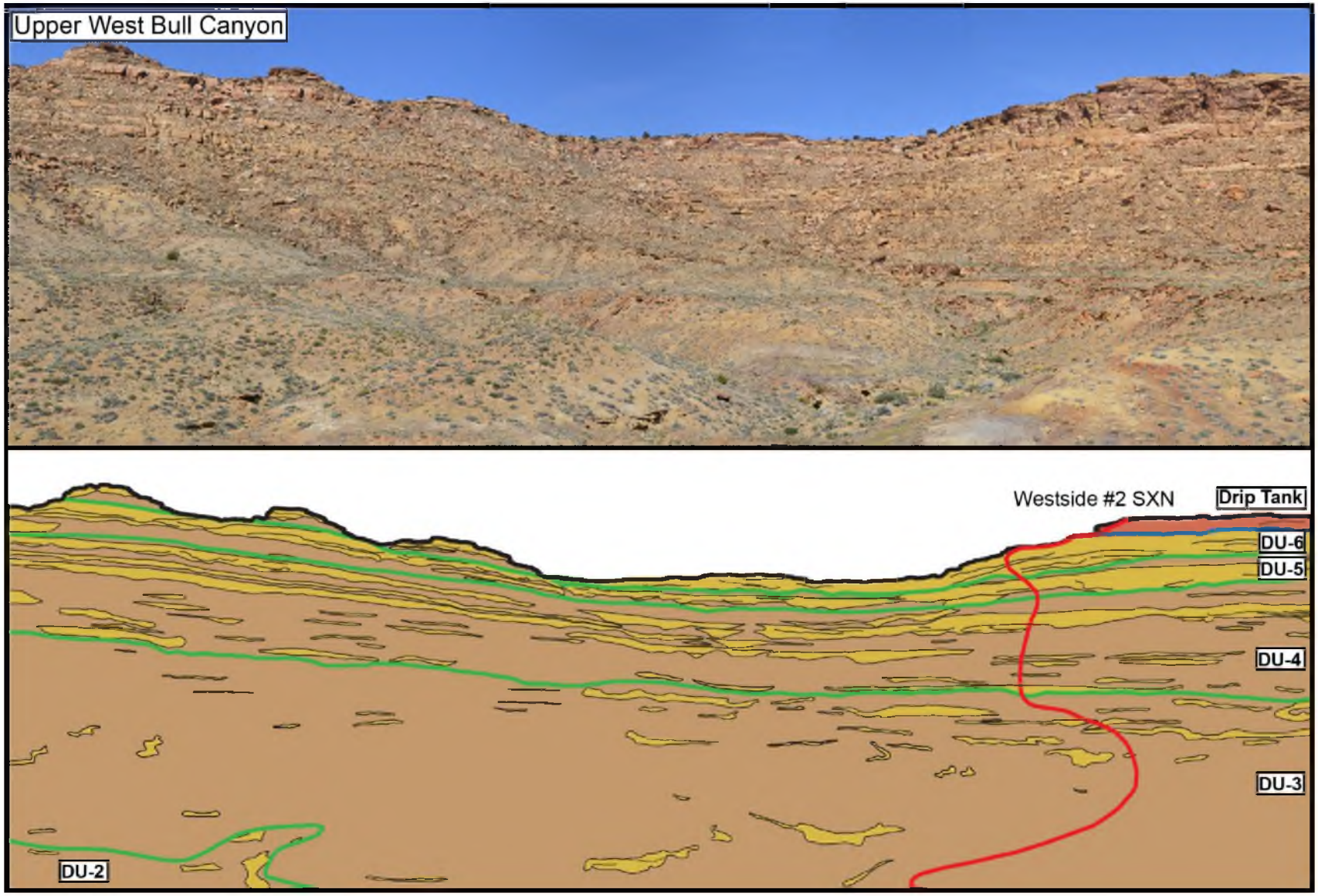
Upper West Bull Canyon
Westside #2 SXN
Drip Tank
DU-6
DU-5
DU-4
DU-3
DU-2

Figure B.3 – Composite photograph and interpretation of the John Henry and Drip Tank Members at the southeastern portion of Bull Canyon. The interpretation shows sandstone bodies (light yellow) distributed throughout floodplain silts and muds (light brown). Depositional units are interpreted from changes in fluvial architecture. Depositional unit boundaries are denoted by green lines. The approximate location of measured sections is denoted by the purple and blue lines. The red fill that caps the canyon wall is the Drip Tank Member. Modified from Pettinga (2013).

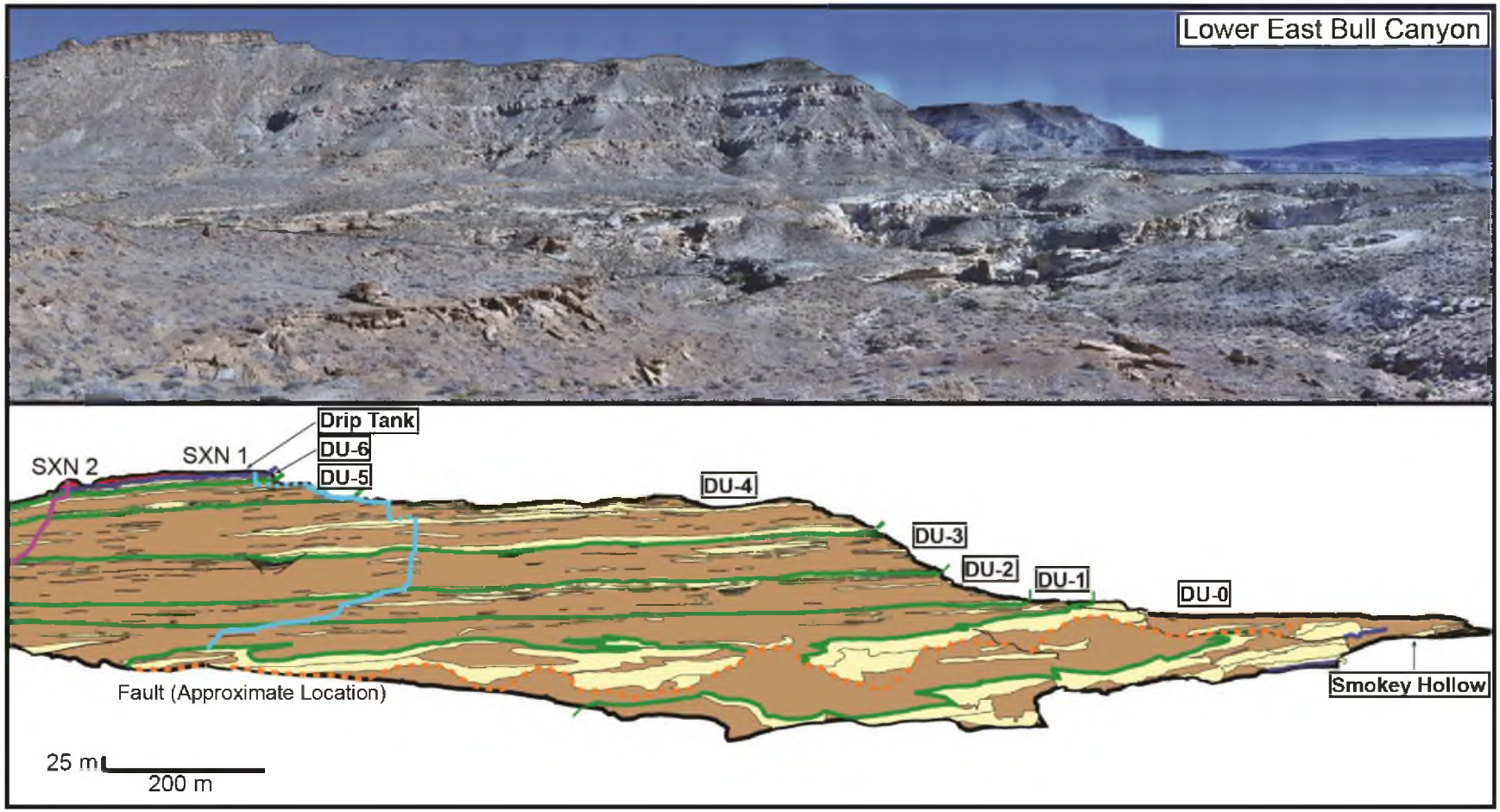
Lower East Bull Canyon
Drip Tank
DU-6
DU-5
SXN 2
SXN 1
DU-4
DU-3
DU-2
DU-1
DU-0
Fault (Approximate Location)
Smokey Hollow
25 m
200 m

Figure B.4 – Composite photograph and interpretation of the John Henry and Drip Tank Members at the northeastern portion of Bull Canyon. The interpretation shows sandstone bodies (light yellow) distributed throughout floodplain silts and muds (light brown). Depositional units are interpreted from changes in fluvial architecture. Depositional unit boundaries are denoted by green lines. The approximate location of measured sections is denoted by the purple, blue, and orange lines. The red fill that caps the canyon wall is the Drip Tank Member. Modified from Pettinga (2013).

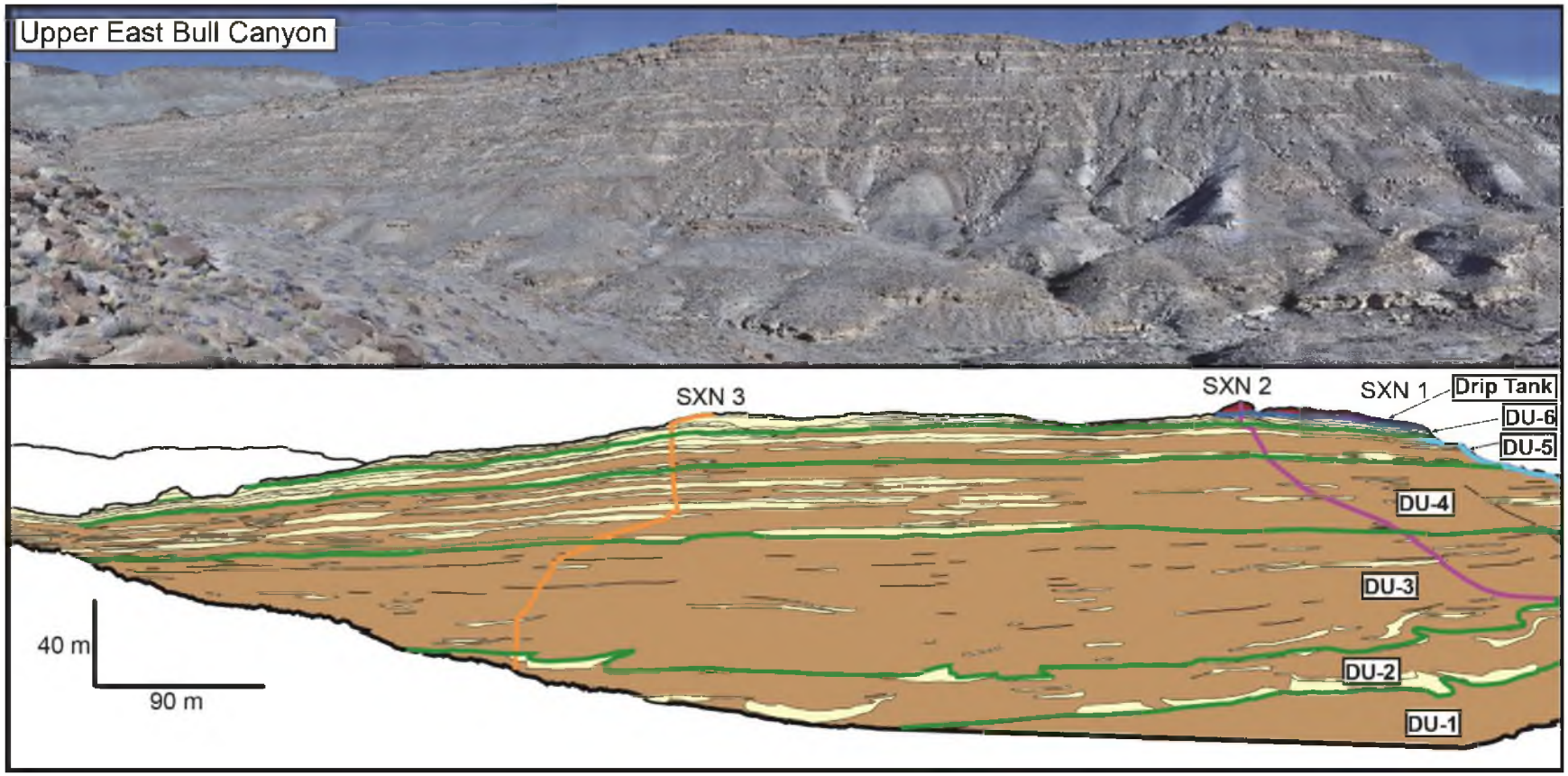
Upper East Bull Canyon
SXN 3
SXN 2
SXN 1
Drip Tank
DU-6
DU-5
DU-4
DU-3
DU-2
DU-1
40 m
90 m

APPENDIX C

BEDFORM PHASE DIAGRAMS

The bedform phase diagrams used to determine flow velocity are included in Figure C.1.

Figure C.1 – Bedform-phase diagrams that show the relationship between flow velocity, bankfull depth, median bedload grain size, and dominant bedform type. These diagrams were used to estimate flow velocity in each depositional unit. Modified from Rubin and McCulloch (1980).

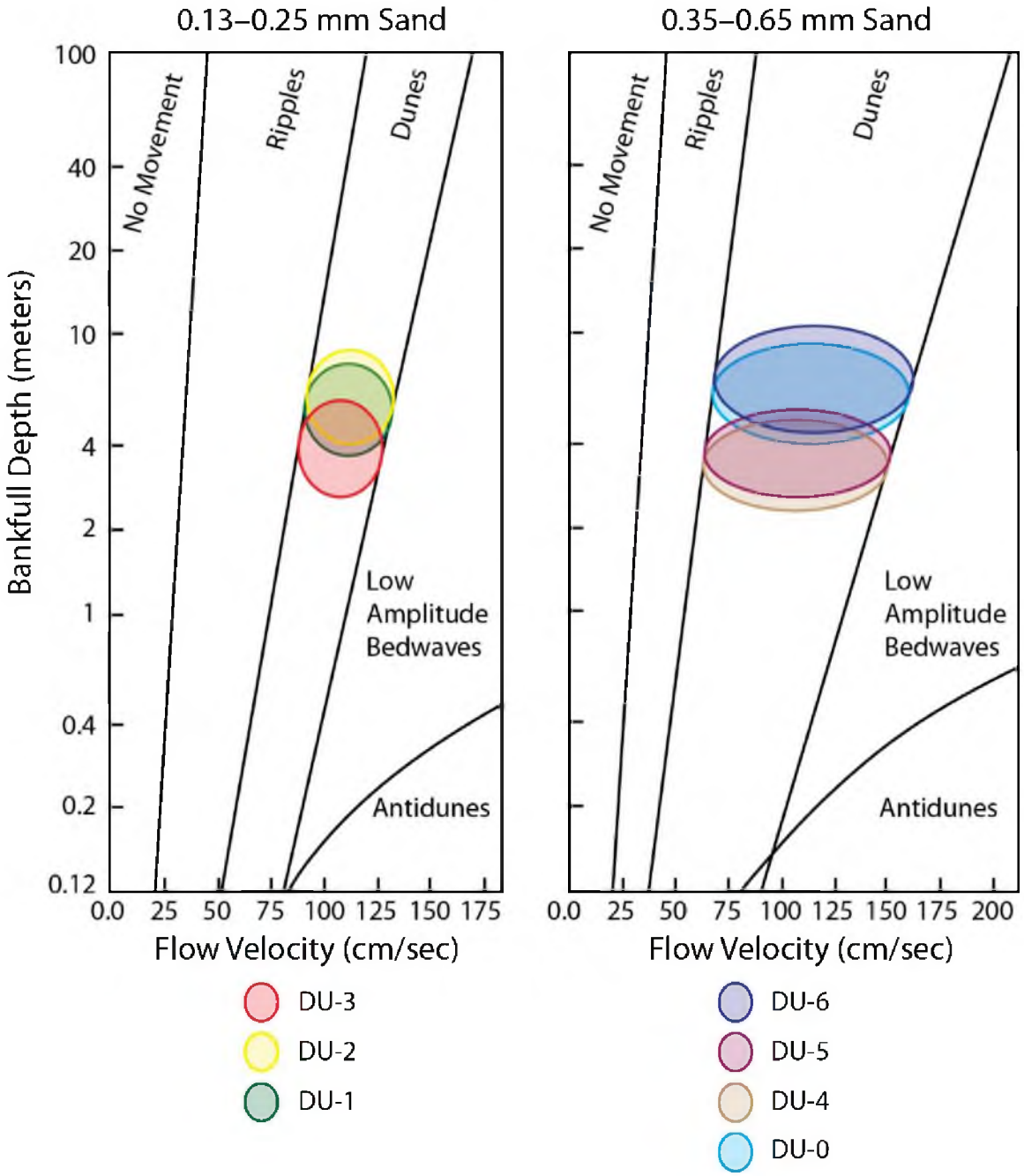
0.13–0.25 mm Sand
0.35–0.65 mm Sand
Bankfull Depth (meters)
100
40
20
10
4
2
1
0.4
0.2
0.12
No Movement
Ripples
Dunes
Low Amplitude Bedwaves
Antidunes
0.0 25 50 75 100 125 150 175
0.0 25 50 75 100 125 150 175 200
Flow Velocity (cm/sec)
DU-3
DU-2
DU-1
DU-6
DU-5
DU-4
DU-0

REFERENCES

Abdel-Fattah, S., A. Amin, and L. C. Van Rijn, 2004, Sand transport in the Nile River, Egypt: Journal of Hydraulic Engineering, v. 130, p. 488–500.

Allen, J. L., 2009, Transgressive-regressive cycles in the John Henry Member, Straight Cliffs Formation, Southern Utah, USA, PhD disseration, University of Utah, Salt Lake City, 188 p.

Allen, J. L., and C. L. Johnson, 2010, Facies control on sandstone composition (and influence of statistical methods on interpretations) in the John Henry Member, Straight Cliffs Formation, Southern Utah, USA: Sedimentary Geology, v. 230, no. 1-2, p. 60–76, doi:10.1016/j.sedgeo.2010.06.023.

Barth, A. P., J. K. Wooden, C. E. Jacobson, and K. Probst, 2004, U-Pb geochronology and geochemistry of the McCoy Mountains Formation, southeastern California: a Cretaceous retroarc foreland basin: Geological Society of America Bulletin, v. 116, p. 142–153.

Benhallam, W., 2014, Point pattern analysis of channel organization from the Cretaceous John Henry Member of the Straight Cliffs Formation, Kaiparowits Plateau, Southern Utah, in AAPG Annual Convention and Exhibition, Houston, Texas, April 6–9, 2014.

Bhattacharya, J. P., and R. S. Tye, 2004, Searching for modern Ferron analogs and application to subsurface interpretation, in T. C. Chidsey, R. D. Adams, and T. H. Morris, eds., Regional to wellbore analog for fluvial–deltaic reservoir modeling: the Ferron Sandstone of Utah: American Association of Petroleum Geologists, Studies in Geology 50: p. 39–57.

Blum, M. D., and T. E. Törnqvist, 2000, Fluvial responses to climate and sea level change: a review and look forward: Sedimentology, v. 47, p. 2–48, doi:10.1046/j.1365-3091.2000.00008.x.

Bridge, J. S., 2004, Fluvial facies models for petroleum geologists: AAPG Annual Meeting, Abstracts with Programs.

Bridge, J. S., 2003, Rivers and floodplains: forms, processes, and sedimentary record: Oxford, United Kingdom, Blackwell, 491 p.

Bridge, J., and R. Tye, 2000, Interpreting the dimensions of ancient fluvial channel bars, channels, and channel belts from wireline-logs and cores: AAPG Bulletin, v. 8, no. 8, p. 1205–1228.

Bryant, I. D., and S. S. Flint, 1993, Quantitative clastic reservoir geological modeling: problems and perspectives, in S. S. Flint, and I. D. Bryant, eds., The geologic modeling of hydrocarbon reservoirs and outcrop analogs: International Association of Sedimentologists Special Publication 15, p. 3–20.

Buckley, S. J., H. D. Enge, and C. Carlsson, 2010, Terrestrial laser scanning for use in virtual outcrop geology: The Photogrammetric, v. 25, September, p. 225–239.

Buckley, S. J., J. A. Howell, and H. D. Enge, 2008, Terrestrial laser scanning in geology: data acquisition, processing and accuracy considerations: Journal of the Geological Society, v. 165, no. 2002, p. 625–638.

Chatanantavet, P., M. P. Lamb, and J. A. Nittrouer, 2012, Backwater controls of avulsion location on deltas: Geophysical Research Letters, v. 39, no. 1, doi:10.1029/2011GL050197.

Chow, V. T., 1959, Open-channel hydraulics: New York, McGraw-Hill, 680 p.

Collinson, J. D., 1978, Vertical sequence and sand body shape in alluvial sequences, in A. D. Miall, ed., Fluvial sedimentology, Canadian Society of Petroleum Geologists Memoir 5, p. 577–586.

Cuevas Gozalo, M. C., and A. W. Martinius, 1993, Outcrop database for the geological characterization of fluvial reservoirs: an example from distal fluvial-fan deposits in the Loranca Basin, Spain, in C. P. North, and D. J. Prosser, eds., Characterization of fluvial and eolian reservoirs: Geological Society Special Publication 73, p. 79–94.

Davidson, S. K., and A. J. Hartley, 2010, Towards a quantitative method for estimating paleohydrology from clast size and comparison with modern rivers: Journal of Sedimentary Research, v. 80, no. 7, p. 688–702, doi:10.2110/jsr.2010.062.

Davidson, S. K., and C. P. North, 2009, Geomorphological regional curves for prediction of drainage area and screening modern analogues for rivers in the rock record: Journal of Sedimentary Research, v. 79, no. 10, p. 773–792, doi:10.2110/jsr.2009.080.

DeCelles, P. G., and J. C. Coogan, 2006, Regional structure and kinematic history of the Sevier fold-and-thrust belt, central Utah: Geological Society of America Bulletin, v. 118, no. 7-8, p. 841–864, doi:10.1130/B25759.1.

Doelling, H., and R. Blackett, 2000, Geology of Grand Staircase-Escalante National Monument, Utah, in D. A. Sprinkel, T. C. Chidsey, and P. B. Anderson, eds., Geology of Utah's parks and monuments, Utah Geological Association Publication 28.

Doelling, H. H., and R. L. Graham, 1972, Kaiparowits Plateau coal field, in H. H. Doelling, and R. L. Graham, eds., Southwestern Utah coal fields: Alton, Kaiparowits Plateau, and Kolob-Harmony: Utah Geological and Mineralogical Survey Monograph Series No. 1, p. 67–249.

Doelling, H. H., and G. C. Willis, 2006, Geologic map of the Smoky Mountain 30' x 60' quadrangle, Kane and San Juan Counties, Utah and Coconino County, Arizona: Utah Geological Survey, map 213, scale 1:100,000.

Dooling, P. R., 2013, Tidal facies, stratigraphic architecture, and along-strike variability of a high energy, transgressive shoreline, Late Cretaceous, Kaiparowits Plateau, Southern Utah, Master's thesis, University of Utah, Salt Lake City, 135 p.

Dreyer, T., M. Falt, T. Hoy, R. Knarud, R. Steel, and J. L. Cuevas, 1993, Sedimentary architecture of field analogs for reservoir information (SAFARI): a case study of the fluvial Escanilla Formation, Spanish Pyrenees, in S. S. Flint, and I. D. Bryant, eds., The geologic modeling of hydrocarbon reservoirs and outcrop analogs: International Association of Sedimentologists Special Publication 15, p. 57–80.

Eaton, J. G., 1991, Biostratigraphic framework for the Upper Cretaceous rocks of the Kaiparowits Plateau, Southern Utah: Geological Society of America Special Paper 260.

Eaton, J. G., 1987, The Campanian-Maastrichtian boundary in the Western Interior of North America: Newsletters on Stratigraphy.

Ethridge, F. G., and S. A. Schumm, 1978, Reconstructing paleochannel morphologic and flow characteristics: methodology, limitations, and assessment, in A. D. Miall, ed., Fluvial sedimentology: Canadian Society of Petroleum Geologists, Memoir 5, p. 703–722.

Fabuel-Perez, I., D. Hodgetts, and J. Redfern, 2009, A new approach for outcrop characterization and geostatistical analysis of a low-sinuosity fluvial-dominated succession using digital outcrop models: Upper Triassic

Oukaimeden Sandstone Formation, central High Atlas, Morocco: AAPG Bulletin, v. 93, no. 6, p. 795–827, doi:10.1306/02230908102.

Gallin, W., C. Johnson, and J. Allen, 2010, Fluvial and marginal marine architecture of the John Henry Member, Straight Cliffs Formation, Kelly Grade of the Kaiparowits Plateau, South-Central Utah: Geology of South-Central Utah, v. 39.

Ghosh, P., 2000, Estimation of channel sinuosity from paleocurrent data: a method using fractal geometry: Journal of Sedimentary Research, v. 70, no. 3, p. 449–455.

Gibling, M. R., 2006, Width and thickness of fluvial channel bodies and valley fills in the geological record: a literature compilation and classification: Journal of Sedimentary Research, v. 76, p. 731–770.

Gooley, J. T., 2010, Alluvial architecture and predictive modeling of the Late Cretaceous John Henry Member, Straight Cliffs Formation, Southern Utah, Master's thesis, University of Utah, Salt Lake City, 376 p.

Gouw, M. J. P., and H. J. a. Berendsen, 2007, Variability of channel-belt dimensions and the consequences for alluvial architecture: observations from the Holocene Rhine-Meuse Delta (The Netherlands) and Lower Mississippi Valley (U.S.A.): Journal of Sedimentary Research, v. 77, no. 2, p. 124–138, doi:10.2110/jsr.2007.013.

Grammer, G. M., P. M. Harris, and G. P. Elberli, 2004, Integration of outcrop and modern analogs in reservoir modeling: overview with examples from the Bahamas, in Integration of outcrop and modern analogs in reservoir modeling: AAPG Memoir, v. 80, p. 1–22.

Gray, D. M., 1961, Interrelationships of watershed characteristics: Journal of Geophysical Research, v. 66, no. 4, p. 1215–1223.

Gregory, H. E., and R. C. Moore, 1931, The Kaiparowits region, a geographic and geologic reconnaissance of parts of Utah and Arizona: U.S. Geological Survey Professional Paper, v. 164, p. 161.

Hack, J. T., 1957, Studies of longitudinal stream profiles in Virginia and Maryland: Geological Survey Professional Paper, v. 294 - B.

Hajek, E. A., P. L. Heller, and E. L. Schur, 2012, Field test of autogenic control on alluvial stratigraphy (Ferris Formation, Upper Cretaceous-Paleogene, Wyoming): Geological Society of America Bulletin, v. 124, no. 11-12, p. 1898–1912, doi:10.1130/B30526.1.

Hajek, E. A., and M. A. Wolinsky, 2012, Simplified process modeling of river avulsion and alluvial architecture: connecting models and field data: Sedimentary Geology, v. 257-260, p. 1–30, doi:10.1016/j.sedgeo.2011.09.005.

Hampson, G. J., T. O. Jewell, N. Irfan, M. R. Gani, and B. Bracken, 2013, Modest change In fluvial style with varying accommodation in regressive alluvial-to-coastal-plain wedge: Upper Cretaceous Blackhawk Formation, Wasatch Plateau, Central Utah, USA: Journal of Sedimentary Research, v. 83, no. 2, p. 145–169, doi:10.2110/jsr.2013.8.

Hettinger, R. D., P. J. McCabe, and K. W. Shanley, 1993, Detailed facies anatomy of transgressive and highstand systems tracts from the Upper Cretaceous of southern Utah, USA: AAPG Memoir, v. 58, p. 235–257.

Huber, B. T., D. A. Hodell, and C. P. Hamilton, 1995, Middle–Late Cretaceous climate of the southern high latitudes: stable isotopic evidence for minimal equator-to-pole thermal gradients: Geological Society of America Bulletin, v. 107, no. 10, p. 1164–1191.

Jerolmack, D. J., and D. Mohrig, 2007, Conditions for branching in depositional rivers: Geology, v. 35, no. 5, p. 463, doi:10.1130/G23308A.1.

Jerolmack, D. J., and C. Paola, 2007, Complexity in a cellular model of river avulsion: Geomorphology, v. 91, no. 3-4, p. 259–270, doi:10.1016/j.geomorph.2007.04.022.

Jerolmack, D. J., and J. B. Swenson, 2007, Scaling relationships and evolution of distributary networks on wave-influenced deltas: Geophysical Research Letters, v. 34, no. 23, doi:10.1029/2007GL031823.

Kauffman, E. G., 1977, Geological and biological overview: Western Interior Cretaceous Basin: The Mountain Geologist, v. 14, no. 3–4, p. 75–99.

Kauffman, E. G., 1984, Paleobiogeographic and evolutionary response dynamic in the Cretaceous Western Interior Seaway of North America, in G. E. G. Westermann, ed., Jurassic-Cretaceous Biochronology and paleogeography of North America: Geological Association of Canada Special Paper, v. 27, p. 273–306.

Kauffman, E. G., and W. G. E. Caldwell, 1993, The Western Interior Basin in space and time, in W. G. E. Caldwell, and E. G. Kauffman, eds., Evolution of the Western Interior Basin: Geological Association of Canada Special Paper 39, p. 1–30.

Keogh, K. J., A. W. Martinius, and R. Osland, 2007, The development of fluvial stochastic modelling in the Norwegian oil industry: a historical review, subsurface implementation and future directions: Sedimentary Geology, v. 202, no. 1-2, p. 249–268, doi:10.1016/j.sedgeo.2007.05.009.

Labourdette, R., and R. R. Jones, 2007, Characterization of fluvial architectural elements using a three-dimensional outcrop data set: Escanilla braided system, South-Central Pyrenees, Spain: Geosphere, v. 3, no. 6, p. 422, doi:10.1130/GES00087.1.

Lamb, M. P., J. a. Nittrouer, D. Mohrig, and J. Shaw, 2012, Backwater and river plume controls on scour upstream of river mouths: implications for fluvio-deltaic morphodynamics: Journal of Geophysical Research, v. 117, doi:10.1029/2011JF002079.

Larue, D. K., and F. Friedmann, 2005, The controversy concerning stratigraphic architecture of channelized reservoirs and recovery by waterflooding: Petroleum Geoscience, v. 11, no. 2, p. 131–146, doi:10.1144/1354-079304-626.

Larue, D. K., and J. Hovadik, 2006, Connectivity of channelized reservoirs: a modelling approach: Petroleum Geoscience, v. 12, no. 4, p. 291–308, doi:10.1144/1354-079306-699.

Larue, D. K., and Y. Yue, 2003, How stratigraphy influences oil recovery: a comparative reservoir database study concentrating on deepwater reservoirs: The Leading Edge, v. 22, no. 4, p. 332–339.

Lawton, T. F., S. L. Pollock, and R. a. J. Robinson, 2003, Integrating sandstone petrology and nonmarine sequence stratigraphy: application to the Late Cretaceous fluvial systems of Southwestern Utah, USA: Journal of Sedimentary Research, v. 73, no. 3, p. 389–406, doi:10.1306/100702730389.

Leclair, S., and J. Bridge, 2001, Quantitative interpretation of sedimentary structures formed by river dunes: Journal of Sedimentary Research, v. 71, no. 5, p. 713–716.

Leopold, L. B., and T. Maddock, 1953, The hydraulic geometry of stream channels and some physiographic implications: U.S. Geological Survey Professional Paper 252, p. 57.

Leopold, L. B., M. G. Wolman, and J. P. Miller, 1964, Fluvial processes in geomorphology: San Francisco, Freeman, 522 p.

Le Roux, J. P., 1992, Determining the channel sinuosity of ancient fluvial systems from paleocurrent data: Journal of Sedimentary Research, v. 62, no. 2, p. 283–291, doi:10.1306/D42678E3-2B26-11D7-8648000102C1865D.

Le Roux, J. P., 2001, Estimation of channel sinuosity from paleocurrent data: a method using fractal geometry: discussion: Journal of Sedimentary Research, v. 71, no. 6, p. 1029–1030, doi:10.1306/042301711029.

Le Roux, J. P., 1994, The angular deviation of paleocurrent directions as applied to the calculation of channel sinuosities: Journal of Sedimentary Research, v. 64, no. 1, p. 86–87, doi:10.1306/D4267D16-2B26-11D7-8648000102C1865D.

Little, W. W., 1997, Tectonic and eustatic controls on cyclical fluvial patterns, Upper Cretaceous strata of the Kaiparowits Basin, Utah, in L. M. Hill, ed., Learning from the land: Grand Staircase – Escalante National Monument science symposium proceedings: Salt Lake City: Bureau of Land Management, p. 489–504.

Little, W. W., 1995, The influence of tectonics and eustasy on alluvial architecture, Middle Coniacian through Campanian strata of the Kaiparowits Basin, Utah, PhD dissertation, University of Colorado, Boulder, 328 p.

Liu, S., and D. Nummedal, 2004, Late Cretaceous subsidence in Wyoming: quantifying the dynamic component: Geology, v. 32, no. 5, p. 397, doi:10.1130/G20318.1.

Liu, S., D. Nummedal, and L. Liu, 2011, Migration of dynamic subsidence across the Late Cretaceous United States Western Interior Basin in response to Farallon plate subduction: Geology, v. 39, no. 6, p. 555–558, doi:10.1130/G31692.1.

Lunt, I. a., J. S. Bridge, and R. S. Tye, 2004, A quantitative, three-dimensional depositional model of gravelly braided rivers: Sedimentology, v. 51, no. 3, p. 377–414, doi:10.1111/j.1365-3091.2004.00627.x.

Lynds, R. M., 2005, Fine-grained sediment in modern and ancient sandy braided rivers, PhD dissertation, University of Wyoming, Laramie, 163 p.

Martinsen, O. J., A. J. Pulham, P. D. W. Haughton, and M. D. Sullivan, 2011, Outcrops revitalized: tools, techniques and applications: Society for Sedimentary Geology, 267 p.

McHargue, T., M. J. Pyrcz, M. D. Sullivan, J. D. Clark, a. Fildani, B. W. Romans, J. a. Covault, M. Levy, H. W. Posamentier, and N. J. Drinkwater, 2011, Architecture of turbidite channel systems on the continental slope: patterns

and predictions: Marine and Petroleum Geology, v. 28, no. 3, p. 728–743, doi:10.1016/j.marpetgeo.2010.07.008.

Miall, A., 2002, Architecture and sequence stratigraphy of Pleistocene fluvial systems in the Malay Basin, based on seismic time-slice analysis: AAPG Bulletin, v. 86, no. 7, p. 1201–1216.

Miall, A. D., 2000, Principles of sedimentary basin analysis, 3rd Edition: Berlin, Springer Verlag, 616 p.

Miall, A. D., 2006, Reconstructing the architecture and sequence stratigraphy of the preserved fluvial record as a tool for reservoir development: a reality check: AAPG Bulletin, v. 90, no. 7, p. 989–1002, doi:10.1306/02220605065.

Miall, A. D., 1988, Reservoir heterogeneities in fluvial sandstones: lessons from outcrop studies: AAPG Bulletin, v. 72, no. 6, p. 682–697.

Milliken, K., M. Blum, and J. Martin, 2012, Scaling relationships in fluvial depostional systems, in AAPG Annual Convention and Exhibition, Long Beach, California, April 22–25, 2012.

Nittrouer, J. A., J. Shaw, M. P. Lamb, and D. Mohrig, 2011, Spatial and temporal trends for water-flow velocity and bed-material sediment transport in the lower Mississippi River: Geological Society of America Bulletin, v. 124, no. 3-4, p. 400–414, doi:10.1130/B30497.1.

North, C. P., 1996, The prediction and modeling of subsurface fluvial stratigraphy, in P. A. Carling, and M. R. Dawson, eds., Advances in fluvial dynamics and stratigraphy: Chichester, United Kingdom, Wiley, p. 395–508.

Paola, C., and D. Mohrig, 1996, Palaeohydraulics revisited: palaeoslope estimation in coarse-grained braided rivers: Basin Research, v. 8, p. 243–254.

Parker, G., and C. Paola, 1998, Alluvial fans formed by channelized fluvial and sheet flow I: theory: Journal of Hydraulic Engineering, v. 124, no. 10, p. 985–995.

Peterson, F., 1969, Cretaceous sedimentation and tectonism in the Southeastern Kaiparowits Region, Utah: Geological Survey Professional Paper, 259 p.

Peterson, F., and H. A. Waldrop, 1965, Jurassic and Cretaceous stratigraphy of southcentral Kaiparowits Plateau, Utah, in D. Goode, and R. A. Robison, eds., Geology and Resources off South-Central Utah: Guidebook of the Geology of Utah: Utah Geological Society and Intermountain Association of Petroleum Geologists, p. 47–69.

Pettinga, L. A., 2013, Tectonic Controls on Alluvial Architecture in the Upper Cretaceous John Henry Member, Straight Cliffs Formation, Southern Utah, Master's thesis, University of Utah, Salt Lake City, 292 p.

Pyrcz, M. J. et al., 2011, Numerical modeling of deepwater channel stacking pattern from outcrop and the quantification of reservoir significance: Concepts in Sedimentology and Paleontology, no. 10, p. 149–159.

Pyrcz, M. J., J. B. Boisvert, and C. V. Deutsch, 2009, ALLUVSIM: A program for event-based stochastic modeling of fluvial depositional systems: Computers & Geosciences, v. 35, no. 8, p. 1671–1685, doi:10.1016/j.cageo.2008.09.012.

Richards, K., 1982, Rivers - form and process in alluvial channels: New York, Methuen, 358 p.

Rittersbacher, A., S. J. Buckley, J. a. Howell, G. J. Hampson, and J. Vallet, 2013, Helicopter-based laser scanning: a method for quantitative analysis of large-scale sedimentary architecture: Geological Society, London, Special Publications, v. 387, doi:10.1144/SP387.3.

Roberts, L. N. R., and M. A. Kirschbaum, 1995, Paleogeography of the Late Cretaceous of the Western Interior of Middle North America - coal distribution and sediment accumulation: U.S. Geological Survey Professional Paper, no. 1561, p. 115.

Robinson, J. W., and P. J. McCabe, 1997, Sandstone-body and shale-body dimensions in a braided fluvial system: Salt Wash Sandstone Member (Morrison Formation), Garfield County, Utah: AAPG Bulletin, v. 81, p. 1267–1291.

Robison, R. A., 1966, Geology and coal resources of the Tropic area, Garfield County Utah: Utah Geological and Mineralogical Survey Special Studies 18: 47 p.

Rubin, D. M., and D. S. McCulloch, 1980, Single and superimposed bedforms: a synthesis of San Francisco Bay and flume observations: Sedimentary Geology, v. 26, no. 1, p. 207–231.

Schumm, S. A., 1972, Fluvial paleochannels, in J. K. Rigby, and W. K. Hamblin, eds., Recognition of Ancient Sedimentary Environments: SEPM, Special Publication 16, p. 98–107.

Shanley, K. W., and P. J. McCabe, 1993, Alluvial architecture in a sequence stratigraphic framework: a case history from the Upper Cretaceous of

southern Utah, USA, in Special Publication of the International Association of Sedimentologists 15, p. 21–26.

Shanley, K., and P. McCabe, 1991, Predicting facies architecture through sequence stratigraphy - an example from the Kaiparowits Plateau, Utah: Geology, v. 19, p. 742–745.

Shaw, J. B., D. Mohrig, and S. K. Whitman, 2013, The morphology and evolution of channels on the Wax Lake Delta, Louisiana, USA: Journal of Geophysical Research: Earth Surface, v. 118, no. 3, p. 1562–1584, doi:10.1002/jgrf.20123.

Sheets, B. A., C. Paola, and J. M. Kelberer, 2007, Creation and preservation of channel-form sand bodies in an experimental alluvial system, in G. J. Nichols, E. Williams, and C. Paola, eds., Sedimentary Processes, Environments and Basins: International Association of Sedimentologists, Special Publication 38, p. 555–567.

Spencer, J. E., 1996, Uplift of the Colorado Plateau due to lithosphere attenuation during Laramide low-angle subduction: Journal of Geophysical Research: Solid Earth, v. 101, p. 595–609.

Stright, L., A. Bernhardt, and A. Boucher, 2013, DFTopoSim: Modeling topographically-controlled deposition of subseismic scale sandstone packages within a mass transport dominated deep-water channel belt: Mathematical Geosciences, v. 45, no. 3, p. 277–296.

Szwarc, T., 2014, Interactions between axial and transverse drainage systems in the Cordilleran foreland basin: evidence from detrital zircons in the Straight Cliffs Formation (Late Cretaceous), Southern Utah, Master's thesis, University of Utah, Salt Lake City, 209 p.

Vaninetti, G. E., 1979, Coal stratigraphy of the John Henry Member of the Straight Cliffs Formation, Kaiparowits Plateau, Utah, Master's thesis, University of Utah, Salt Lake City, 274 p.

Visser, C. A., and A. G. Chessa, 2000, Estimation of length distributions from outcrop data sets: application to the Upper Permian Cutler Formation: Petroleum Geoscience, v. 6, p. 29–36.

Wang, Y., K. M. Straub, and E. A. Hajek, 2011, Scale-dependent compensational stacking: an estimate of autogenic time scales in channelized sedimentary deposits: Geology, v. 39, no. 9, p. 811–814, doi:10.1130/G32068.1.

Williams, G. P., 1986, River meanders and channel size: Journal of Hydrology, v. 88, p. 147–164.

Wolfe, J. A., and G. R. Upchurch, J., 1987, North American nonmarine climates and vegetation during the Late Cretaceous: Palaeogeography, Palaeoclimatology, Palaeoecology, v. 61, p. 33–77.

Yalin, M. S., 1964, Geometrical properties of sand waves: American Society of Civil Engineers, Journal of the Hydraulics Division, v. 90, p. 105–119.

Yalin, M. S., 1971, On the formation of dunes and meanders, in International Association of Hydraulic Research, Proceedings of the 14th Congress, p. 101–108.

Zeller, J., 1967, Meandering channels in Switzerland, in Symposium on River Morphology, International Association of Hydrological Sciences, General Assembly of Bern, n. 75, p. 174–186.